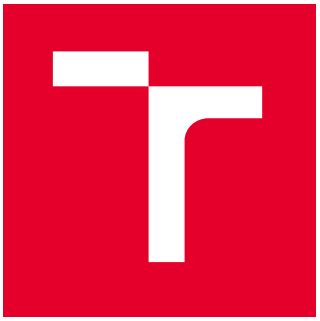

BRNO UNIVERSITY OF TECHNOLOGY

VYSOKÉ UČENÍ TECHNICKÉ V BRNĚ

FACULTY OF MECHANICAL ENGINEERING

FAKULTA STROJNÍHO INŽENÝRSTVÍ

INSTITUTE OF PHYSICAL ENGINEERING

ÚSTAV FYZIKÁLNÍHO INŽENÝRSTVÍ

METHODS FOR DETECTING THE FREQUENCY OF CENTERS OF HYDROGEN-CYANINE (HCN) HYPERFINE TRANSITIONS USING A TUNABLE LASER IN THE RANGE 1527 NM TO 1563 NM

METODY DETEKCE FREKVENCE STŘEDŮ HYPERJEMNÝCH ABSORPČNÍCH ČAR KYANOVODÍKU (HCN) POMOCÍ PŘELADITELNÉHO LASERU V ROZSAHU 1527 NM AŽ 1563 NM

DOCTORAL THESIS

DIZERTAČNÍ PRÁCE

AUTHOR
AUTOR PRÁCE

Ing. Martin Hošek

SUPERVISOR
ŠKOLITEL

Ing. Ondřej Číp, Ph.D.

BRNO 2024

Abstrakt
Kyanovodík (HCN) je médiem, jehož absorpční spektrum pokrývá celé telekomunikační C-pásmo. To dělá z HCN vhodného kandidáta pro použití při frekvenční stabilizaci laserů. Tato práce se zaměřuje na přesné měření středů absorpčních čar HCN, což povede k zvýšení užitečnosti tohoto plynu v praxi. Cíle práce je dosaženo pomocí dvou metod laserové spektroskopie, a to lineární absorpční spektroskopie a saturované absorpční spektroskopie. Je sestavena tabulka absorpčních čar HCN, kde nejistota frekvence středů čar dosahuje čtyřicetinásobného zlepšení oproti doposud neměřené nejistotě.

Summary
Hydrogen cyanide (HCN) is a medium whose absorption spectrum covers the whole telecommunication C-band. This makes HCN a great candidate to use in laser frequency locking. The focus of the thesis is the precise measurement of the HCN absorption lines' centres frequency, improving the usefulness of the gas for the applications. This goal is achieved by utilising two laser spectroscopy techniques: linear absorption spectroscopy and saturation absorption spectroscopy. The table of HCN absorption lines was built, with the uncertainty of their central frequency being about fortyfold better than the state-of-art uncertainty.

Klíčová slova
laserová spetroskopie, lineární absorpční specktroskopie, saturovaná absorpční spektroskopie, kyanovodík, frekvenčně stabilizované lasery

Keywords
laser spectroscopy, linear absorption spectroscopy, saturation absorption spectroscopy, hydrogen cyanide, frequency stabilised lasers

HOSEK, M.*Methods for detecting the frequency of centers of Hydrogen-Cyanine (HCN) hyperfine transitions using a tunable laser in the range 1527 nm to 1563 nm.* Brno: Vysoké učení technické v Brně, Fakulta strojního inženýrství, 2024. 82 s. Vedoucí Ing. Ondřej Číp, Ph.D.

Prohlašuji, že jsem dizertační práci vypracoval samostatně pod vedením Ing. Ondřeje Čípa, Ph.D. Dále prohlašuji, že jsem řádně citoval všechny použité prameny a literaturu. Tato práce nebyla použita v rámci jiného vysokoškolského studia či k získání jiného nebo stejného titulu.

Ing. Martin Hošek

Tímto děkuji svému vedoucímu Ing. Ondřeji Čípovi, Ph.D. za vedení této práce a za četné rady a náměty vedoucí k její lepší kvalitě. Rád bych také poděkoval celému týmu Koherenční optiky Ústavu přístrojové techniky AV ČR, v.v.i za pomoc při řešení mnohých experimentálních problémů. V neposlední řadě bych poděkoval své rodině, a především pak mé ženě. Bez jejich psychické podpory by sepsání této práce nebylo možné.

Ing. Martin Hošek

Contents

1. Introduction and structure of the work

In the past, the length units mainly related to the dimensions of the human body, e.g. fathom (the distance between outstretched arms), span (the distance between the tip of the thumb and the tip of the little finger) or the surrounding environment, e.g. grain, mining fathom (the height of the mine corridor reachable with the bead). The size of the units was sometimes different in different regions, e.g. Prussian lachter 2.092 m, Silesian lachter 1.9202 m.

The breakthrough came in the 18^{th} century thanks to the development of the industry. In 1791, the need for unified units led to the definition of meter as 10^{-7} of the earth's quadrant passing through Paris. Between 1793 and 1799, the astronomers Pierre Méchain and Jean-Baptiste Delambre performed a distance measurement, resulting then in embodiment in three platinum standards and seven iron copies. The first prototype of a meter is called *Métre des archives* and was deposited in the French national archive in 1799.

On 20^{th} May 1875, seventeen states signed the Treaty of the Meter, which, among others, established the General Conference on Weights Measures (CPGM from *Conférence Général des Poids et Mésures*, CGPM) responsible for maintenance of the international system of units. At the first meeting of CPGM, the new meter prototype was established Fig. 1.1. It was made of platinum and iridium, making it more durable. Additionally, the difference from the formal standard was the length of the bar. It was longer than 1 meter, and the meter was defined as the distance between two lines inscribed at the bar surface.

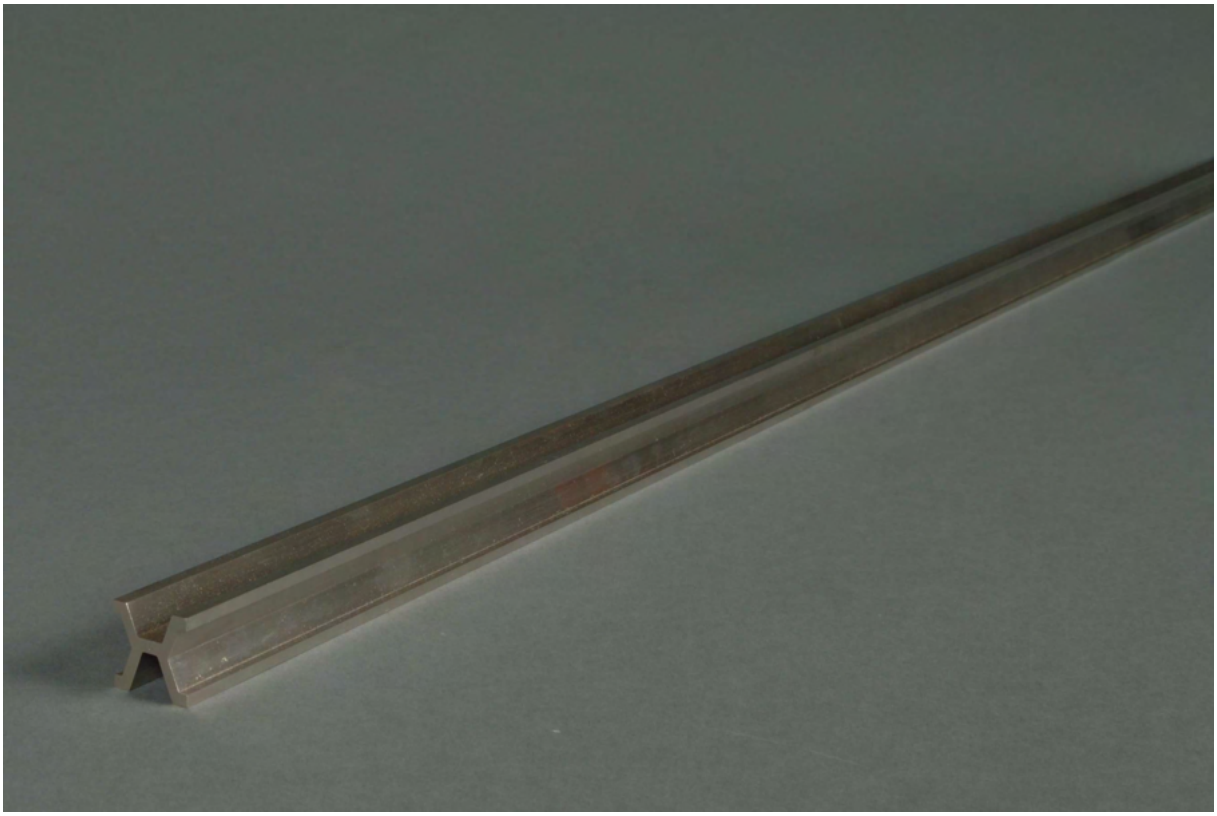

Figure 1.1: The formal standard of the meter [1].

At the 11^{th} CGPM in 1960, the international system of units (SI from *Système International*) was created. The SI system consists of seven base units (second, metre, kilogram, ampere, kelvin, mole, candela). The rest of the units are derived from the SI system. This system aims to define both the units and the methods for realising units.

At the same conference, the definition of meter changed to the "length equal to 1 650 763.73 wavelengths in vacuum of the radiation corresponding to the transition between the levels $2p^{10}$ and $5d^5$ of the krypton-86 atom" [2]. It was the first time the length was measured using the light, and this has not changed since then.

The current definition of the meter is: "The metre, symbol m, is the SI unit of length. It is defined by taking the fixed numerical value of the speed of light in vacuum c to be 299 792 458 when expressed in the unit $\mathrm{m} \cdot \mathrm{s}^{-1}$, where the second is defined in terms of the caesium frequency $\Delta\nu_{Cs}$" [3].

In practice, not every laboratory or industrial company can have such experimental devices to realise the unit according to its definition. For this purpose, the International Bureau of Weights and Measures (BIPM from *Bureau International des Poids et Mesures*) publishes the Mise en Pratique, giving the recommended approach to realise a particular unit with the given uncertainty.

Regarding one meter [4], frequency-locking the laser to the minimum of a specific absorption line is a valuable way of realising it. A laser of this kind possesses a very stable frequency or wavelength with the unit of 1 m, which can also be transferred to the period of oscillation with the unit of 1 s. The list of such suitable absorption lines is called the "Recommended values of standard frequencies" [5].

In the visible part of the spectrum, the list of "Recommended values of standard frequencies" includes eight iodine absorption lines. This makes iodine the cornerstone in frequency metrology and associated laser spectroscopy [6], [7], [8]. On the other hand, in the near-infrared spectrum, the only absorption line presented on the list is P16 ($\nu_1 + \nu_3$) band of acetylene $^{13}C_2H_2$. The central frequency of this line is known with the uncertainty of 1 kHz. As the accessibility of isotopically pure acetylene is getting limited, the demand for alternative absorption medium in the near-infrared spectrum is increasing.

$H^{13}C^{14}N$ is an absorption medium with an advantage over acetylene, having a wider absorption spectrum Fig. 1.2. The absorption spectrum of $H^{13}C^{14}N$ covers well the telecommunication C-band (1530 - 1560 nm), making it the ideal candidate for use in optical fibre communication. The absorption lines of $H^{13}C^{14}N$ were studied in the past (more on this is reviewed in Chapter 5). Due to the use of not-so-precise techniques, the positions of line centres are known a thousand times less precisely than those of $^{13}C_2H_2$. Moreover, the authors in [9] observe discrepancies in results using $H^{13}C^{14}N$ for laser frequency stabilisation in frequency scanning interferometry (FSI).

The $H^{13}C^{14}N$ absorption lines measurement became one of the work packages of the Large Volume Metrology Applications (LaVA) project (funded by EC/EURAMET, project number l EMPIR 17IND03). The project consortium included leading European National Metrology Institutes (e.g. National Physical Laboratory (NPL) from the United Kingdom, National Metrology Institute of Italy (INRIM from *L'Istituto Nazionale di Ricerca Metrologica*) and National Laboratory of Metrology and Testing (LNE from *Laboratoire national de métrologie et d'essais*) from France), their research partners (e.g. the Institute of Scientific Instruments (ISI from *Ústav přístrojové techniky*) from the Czech Republic and the National Conservatory of Arts and Crafts (CNAM from *Conservatoire*

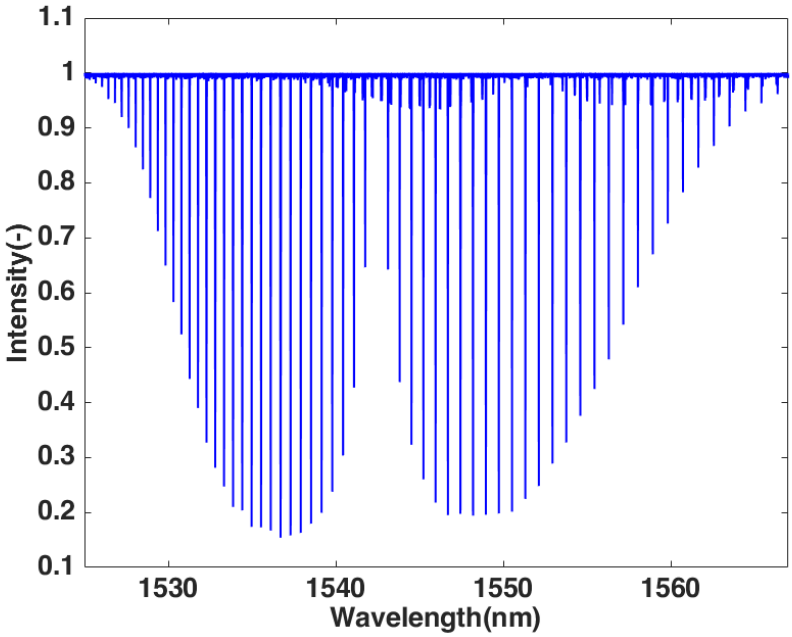

Figure 1.2: Absorption spectrum of $H^{13}C^{14}N$ $2\nu_3$ absorption band.

national des arts et métiers) from France) and industrial partners (e.g. SAAB AKTIEBOLAG from Sweden, Oy Mapvision from Finland).

Structure of the work: Chapter 2 describes the goals of the thesis that are to be met. The objectives are structured in five points. Together with a brief explanation, they provide crucial insights on the content and focus of the thesis' experimental path.

The major themes of the Chapter 3 are the highly-tunable laser sources and optical frequency combs. The principle of laser and optical frequency comb is described there, and particular lasers used in the experimental part of the thesis are mentioned too.

In this work, two laser spectroscopy methods are used: specifically the linear absorption spectroscopy and the saturation absorption spectroscopy. Both methods are explained in the Chapter 4. The principle of the methods and the limitations of their use are included in this chapter.

The current state of scientific knowledge in measurement of $H^{13}C^{14}N$ absorption lines is the topic of Chapter 5. The chapter is focusing on the analysis of the most up-to-date articles as well as the assessment of the measured results.

In Chapter 6, the linear spectroscopy experiments are explained. The results obtained using the experimental setups are shown. Furthermore, their precision and accuracy are commented on.

The Chapter 7 is focusing on the saturation absorption spectroscopy. The gradual progress described in this chapter led to the publication of the article [10], that is also analysed in this chapter.

2. Thesis objectives

The objectives of my thesis can be summarised in several points (see below). Those are heading towards the ultimate goal of writing down the table of $H^{13}C^{14}N$ absorption lines centre in the $2\nu_3$ band with corresponding optical frequencies. The new table will be helpful for many areas, especially for the metrology of length.

1. **Select a laser source allowing fast tuning of the optical frequency with narrow linewidth of the spectral line.**

   The spectrum of $H^{13}C^{14}N$ covers range from from 1527 nm to 1563 nm, which is approx. 36 nm. It is one of the advantages of $H^{13}C^{14}N$ as an absorption medium over the conventionally used C_2H_2. At the same time it is also necessary to find a laser, that allows to scan over the whole spectrum within reasonable timeframe without any optical frequency mode-hops. The important objective is to acquire such a laser and get familiar with controlling it.

2. **Design and implement the experimental equipment to realise the linear absorption spectroscopy with laser optical frequency traceable to optical frequency comb.**

   The linear absorption spectroscopy, as described in section 4.1, is a relatively simple method which allows the measurement of absorption lines centre. The authors in [11] used to measure $H^{13}C^{14}N$ absorption lines with the uncertainty of about 1 MHz. The improvement of the laser optical frequency precision by using the optical frequency comb will lead to a better evaluation of frequencies of $H^{13}C^{14}N$ spectral line centres.

3. **Design and set up a modulation-free saturation absorption spectroscopy method and develop a vacuum apparatus for a low-pressure spectroscopy of $H^{13}C^{14}N$ gas.**

   The saturation absorption spectroscopy is a method allowing for Doppler-free spectroscopical measurement. Compared to the linear absorption spectroscopy, it enables about three orders of magnitude more precise absorption lines centre determination. On the other hand, it is a more sophisticated method. It has been used for $H^{13}C^{14}N$ measurement in the past, as discussed in the section 5.2, but no systematical measurement of absorption lines position has been performed so far. Besides, it was also necessary to develop a vacuum apparatus for filling the cell with $H^{13}C^{14}N$ gas allowing for precise control of the $H^{13}C^{14}N$ gas pressure.

4. **Measure precisely the optical frequency of hyperfine line centres of $H^{13}C^{14}N$.**

   The knowledge of $H^{13}C^{14}N$ absorption lines centre is helpful not only from the fundamental research point of view. In the frequency scanning interferometry, the uncertainty u_{f1}, u_{f2} of the centre's frequency f_1, f_2 has a direct impact on the uncertainty of length measurement u_c. These uncertainties relate as $u_c = (u_{f1} - u_{f2})/(f_1 - f_2)$. Further improvement of $H^{13}C^{14}N$ data can have a positive impact on this method's precision.

5. **Assemble the resultant table of optical frequencies of the measurement of the individual hyperfine $H^{13}C^{14}N$ transition centres in the band from**

1527 nm **to** 1563 nm**. Compare that table with the data obtained in the past by less accurate linear absorption spectroscopy.**

The precise measurement of the $H^{13}C^{14}N$ absorption lines centre has the potential to establish $H^{13}C^{14}N$ on the list of *Recommended values of standard frequencies* [5] and be included in *Mise en pratique for the definition of the metre in the SI* [12].

3. Highly-coherent tunable laser sources and optical frequency combs

The first predecessor of the laser was the maser (Microwave Amplification by Stimulated Emission of Radiation). The maser acronym itself well describes the function of it. It is a device using stimulated emission to amplify the microwave radiation. The first maser was built in 1953 by C. H. Townes, J. P. Gordon and H. J. Zeiger at Columbia University, USA.

Further research following the invention of the maser led to the construction of the first optical maser or laser (Light Amplification by Stimulated Emission of Radiation) in 1960 by T.H. Mainman. C. H. Townes, N. Basov, and A. Prokhorov shared the Nobel Prize in Physics *for fundamental work in the field of quantum electronics, which has led to the construction of oscillators and amplifiers based on the maser–laser principle* [13] in 1964.

Assuming, to simplify, the two energy levels model. In the case of radiation, with energy corresponding to the difference in energy levels, three processes occur. The electrons in the lower energy level can absorb the radiation and they can be excited to the higher energy level. This process is called induced absorption. Meanwhile, the electrons in the higher absorption level can deexcite to the lower energy level and convert their excitation energy to photons.

The third process, enabled by the radiation, is stimulated emission. As the electrons on the higher energy level "sense" the presence of the radiation field, they can deexcite to the lower energy level. The excitation energy transforms into photons with precisely the same phase, polarisation and direction of propagation as the photons in the presented radiation field.

As the absorption and the emission effects occur simultaneously, conditions for the emission dominating the absorption need to be established. It means that the number of electrons in the higher energy level has to prevail over those in the lower energy level. The so-called population inversion can be achieved in several ways, e.g. external laser pumping and arc lamp pumping.

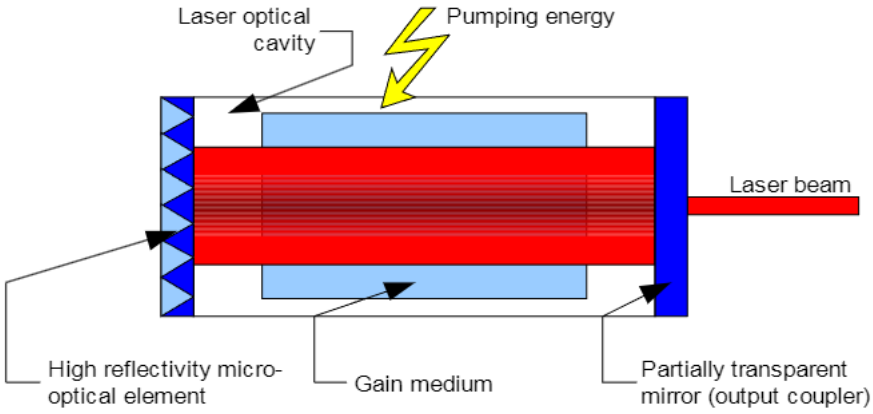

Figure 3.1: Laser resonator. Adapted from [14].

To express the point more rigorously, the threshold condition expressing the difference in the population densities of the energy levels needed for the lasing ΔN can be written as:

$$N_2 \frac{g_1}{g_2} - N_1 > \frac{\gamma_l}{2\sigma_{cross.}(f)l}, \tag{3.1}$$

where $N_{1,2}$ are the population density of lower and higher energy levels, $g_{1,2}$ are the statistical weight of lower and higher energy levels, γ_l is a loss coefficient including all the losses in the interaction cavity, $\sigma_{cross.}(f)$ is the absorption cross section for the particular energy transition, and l is the length of the active laser medium Fig. 3.1.

3.1. External cavity laser

One of the convenient ways to build the broadly-tunable laser is to use an external cavity [15]. The laser itself has a broad gain profile. It means that the radiation coming from the laser without an external cavity would have a broad continuous frequency spectrum. The inclusion of an external frequency filter (typically diffraction grating) allows to filter out only a narrow part of the frequency spectrum. Subsequently, by tilting the grating, it allows for a change in the frequency of the outcoming laser radiation. Depending on the construction of the external cavity laser, we distinguish two types: Littrow configuration and Littman-Metcalf configuration.

3.1.1. Littrow configuration

In the Littrow configuration of external cavity laser Fig. 3.2, the design includes a laser diode with an anti-reflective (AR) coated front facet, a collimating lens and a diffraction grating. The zero-order refracted beam is used as an output, while the first-order refracted beam serves as an optical feedback for the laser diode. The frequency of the laser is tuned by rotating the diffraction grating.

The disadvantage of the Littrow configuration is in the change of direction of the output beam caused by the rotation of the diffraction grating. It makes the arrangement inconvenient for specific applications, e.g. laser interferometry.

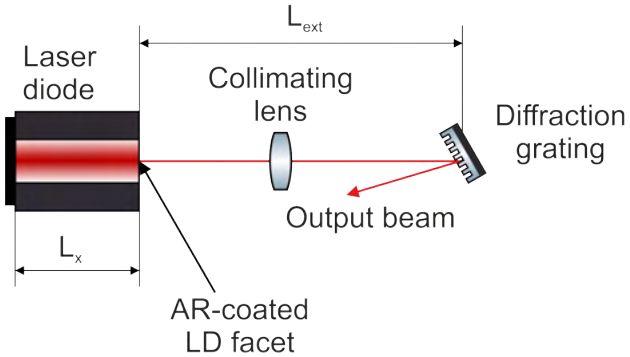

Figure 3.2: Littrow configuration of external cavity laser. Adapted from [16].

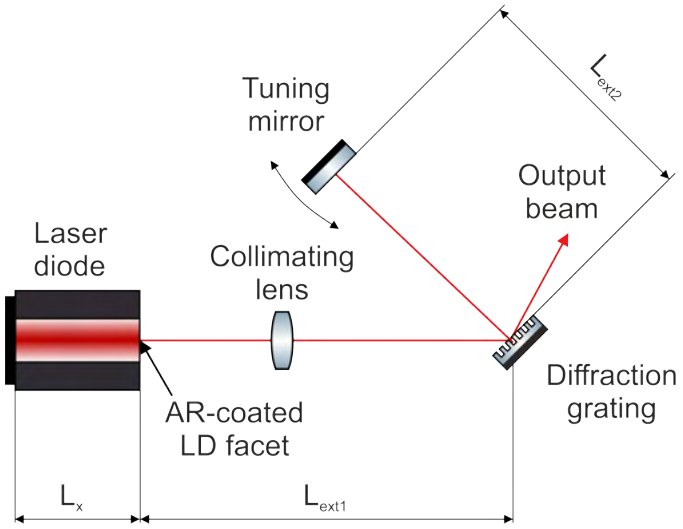

Figure 3.3: Littman-Metcalf configuration of external cavity laser. Adapted from [16].

3.1.2. Littman-Metcalf configuration

The Littman-Metcalf configuration, compared to the Littrow configuration, includes an additional tuning mirror Fig. 3.3. In this case, the diffraction grating is stationary, and the frequency tuning is instead caused by rotating the mirror. The output beam is a zero-order diffraction. The first-order diffraction serves as the feedback to the laser diode. Compared to the Littrow configuration, it configuration produces a narrower linewidth due to frequency-dependent diffraction occurring twice. The disadvantage of the Littman-Metcalf configuration compared to the Littrow configuration is the narrower grating pass band and additinally a more sophisticated aligning process as described in [16].

3.2. Lasers used in the experimental setups

In the experiments described in this thesis, two lasers were mostly used. Koheras Adjustik E15 and CTL 1550. The main features of both of them are described in the upcoming sections.

3.2.1. Koheras Adjustik E15

In the preliminary experiments, applying to both linear absorption spectroscopy and saturation absorption spectroscopy, the Koheras Adjustik E15 was used. It is a DFB (distributed feedback) fibre laser allowing the laser frequency scan in the range from ≈1539.8 nm to ≈1541.0 nm. The laser frequency can be tuned by changing the laser diode temperature or the piezo crystal voltage. Moreover, the piezo crystal allows for laser frequency modulation up to 20 kHz with the modulation width up to 8 GHz. The frequency linewidth of the laser is below 0.1 kHz, and the maximum optical output power is 40 mW. The laser is controllable through USB and ethernet interfaces.

The Koheras Adjustik E15 allows to measure one $H^{13}C^{14}N$ absorption line. At the same time, it was the ideal solution for the preliminary measurement thanks to its availability and accessibility at the Institute of Scientific Instruments (ISI) of the Czech Academy of Sciences (where the experimental part of my studies took place).

In the latter experiments, the CTL 1550 laser was used. Utilising the CTL 1550 allowed to measure the whole absorption spectrum of $H^{13}C^{14}N$.

3.2.2. CTL 1550

Continuously-tunable laser (CTL 1550, TOPTICA Photonics AG) is an external cavity semiconductor laser (ECSL) with a tuning range from 1510 nm to 1630 nm. The wide frequency (wavelength) scan is enabled by motor. It allows to scan with the speed up to 10 nm/s. The fine tuning can be performed by a piezo actuator with the range of 35 GHz and a resolution of a few kHz.

The laser current can be modulated using a DC input with the bandwidth limit at 100 MHz, the sensitivity of 0.73 mA/V and an input range ±5 V. The alternative for laser current modulation is an AC input, which allows a modulation above 100 kHz. The sensitivity of the input is 2.2 mA/V with the input range of ±1.8 V.

The laser has an integrated isolator and the FiberDock collimator with a focal length of 11 mm. The maximum optical output power behind the fibre collimator is 39 mW. The frequency linewidth of the laser beam is bellow 10 kHz.

The mode-hope free operation of the CTL is ensured by synchronous tuning of all of the frequency-sensitive elements. It is guaranteed by SMILE (Single Mode Intelligent Loop engine). The communication with the laser can be facilitated in multiple ways, either using a DLC pro controller, USB, or Ethernet interface.

3.3. Optical frequency comb

An optical frequency comb (OFC) is a unique laser device whose frequency spectrum consists of many equally spaced spikes (teeth). As the frequency spectrum of the OFC can cover a significantly broad part of the spectrum (in order of 100 THz), it allows us to compare the stability of lasers at different frequencies. We can observe its influence in many fields, such as a frequency metrology and a distance measurement. It led to the awarding of the Nobel Prize in Physics to J. L. Hall and T. W. Hänsch *for their contributions to the development of laser-based precision spectroscopy, including the optical frequency comb technique* [17] in 2005.

A frequently used device for OFC generating is a mode-locked laser [18]. This laser allows for picosecond or femtosecond pulse generation. A series of such pulses is then sent through a photonic fibre to broaden the spectrum further.

The frequency of the OFC f_n can be expressed as:

$$f_n = nf_r + f_0, \tag{3.2}$$

where n is the integer signing the order of the OFC tooth, f_r is the repetition frequency, and f_0 is the offset frequency. The offset frequency is caused by the offset between the electric field and the pulse envelope (sometimes called carrier envelope offset). To minimise the uncertainty of the f_0, it is stabilised. One of the convenient ways to do so is to suppress the fluctuation of laser cavity length using a piezoelectric crystal.

The repetition rate of the OFC is equal to the inverted value of the pulse repetition rate in the time domain Fig. 3.4. The stabilisation of the whole OFC spectrum can be done by stabilisation of f_r and f_0. By doing that, we can get a broad-spectrum device

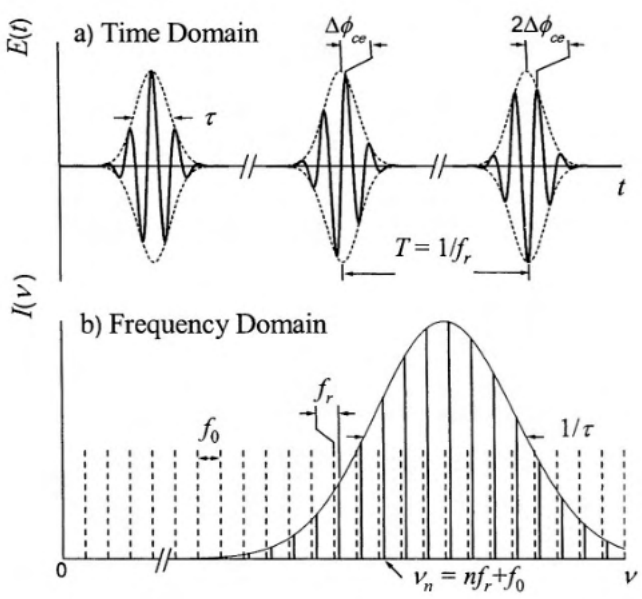

Figure 3.4: Time (a) and frequency (b) domain of optical frequency comb. Adapted from [18].

that permits us to compare the stability of the laser source. Another application of OFC is measuring the precise frequency of the laser by beating it against OFC, as will be discussed later in this work.

4. Laser spectroscopy

A laser spectroscopy includes many methods and techniques for investigating atoms and molecules as well as their characteristics [15]. It can be derived from the absorption or emission spectrum, that provides the information about the atomic structure and the composition of unknown matter. The intensity of the line is proportional to transition probability, which tells how strongly are the two levels of the transitions coupled. All these pieces of information enable to better understand the world around us and to better describe it.

From all of the methods in the laser spectroscopy family, I decided to invest in studying in detail linear absorption spectroscopy and saturation absorption spectroscopy. The first one has the advantage of being relatively simple and, simultaneously, allowing to study the absorption lines with high accuracy [19], [20]. The latter permits overcoming the principal limitation of linear absorption spectroscopy by removing the Doppler broadening.

Worth mentioning is the fact that both methods were deeply studied and used for I_2 absorption lines' measurement [21],[22] at the Institute of Scientific Instruments (ISI) of the Czech Academy of Sciences in the past. Besides, the experimental part of my studies took place at ISI.

4.1. Linear absorption spectroscopy

4.1.1. Principle of the method

In the linear absorption spectroscopy, the laser beam passes through the absorption medium. As the frequency of the laser source is tuned over the absorption line profile, the transmitted optical power is recorded on the photodetector Fig. 4.1. The signal from the photodetector is then combined with the information about laser source frequency. Afterwards, the position of the absorption line centre can be retrieved.

Given that each spectral line absorbs differently, the less it absorbs, the more challenging (less accurate) is the absorption line centre determination. The absorption can be maximised by extending the length of the absorption gas cell, using the multi-pass arrangement or by increasing the gas pressure. While growing pressure in the gas cell leads to the significant pressure broadening of the absorption lines, cell's widening has practical limitations. Another option is to modulate the laser beam frequency [23], [24].

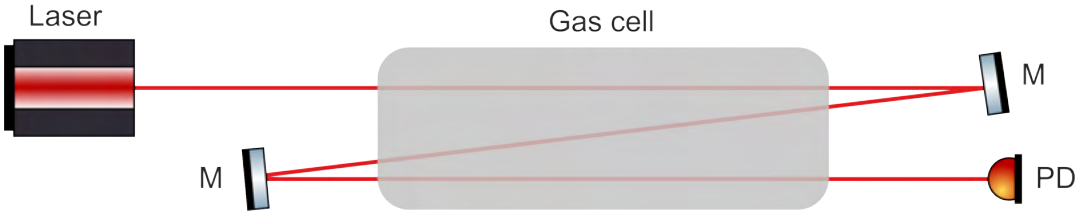

Figure 4.1: Principle of linear absorption spectroscopy: mirrors (M), and photodetector (PD).

4.1.2. Modulation of the laser optical frequency

Laser's optical frequency modulation improves the signal-to-noise (S/N) ratio of the detected absorption signal thanks to the background noise suppression. It allows to cancel the low-frequency noise while detecting the optical signal on higher harmonic frequencies. Modulation of the laser optical frequency has applications not only in laser spectroscopy but also in encoding, telecommunication, and other technical disciplines.

The frequency of the wave, in our case, light f_L, is periodically changed with the amplitude Δf. The resulting frequency f_{modul} can be described as:

$$f_{modul} = f_L + \Delta f \cos \omega t, \tag{4.1}$$

where ω is the angular modulation frequency and t is time. Using the Fourier series, the equation can be modified to:

$$f_{modul} = \frac{A_0}{2} + \sum_{m=1}^{\infty} (A_m \cos m\omega t + B_m \sin m\omega t). \tag{4.2}$$

The A_m coefficient for $m \geq 0$ can be calculated from:

$$A_m = \frac{\pi}{2} \int_0^{\pi} f_{modul} \cos mt \, dt \ . \tag{4.3}$$

As described in [25], the B_m coefficients are not equal to zero if the unharmonic distortions of modulation take place. The B_m coefficient plays an important role, when m is an odd number. This is due to the odd harmonic signals having zero crossing precisely at the minimum of the absorption line. The odd harmonic signals are ideal candidates for practical use since the zero crossing is easily sustainable by feedback loops.

The enhancement of modulation amplitude improves the S/N ratio of the detected signal. The limit of this effect is different depending on the demodulation frequency, and it increases with the m. For the first harmonic detection, it is 0.7 times half width at half maximum (HWHM) of the absorption line, and for the third harmonic, 1.6 times HWHM. The amplitude of lower harmonic signals generally possesses higher amplitude. The need for lower modulation amplitude, makes them better for practical use. On the other hand, the detection on higher harmonics allows suppressing the residual amplitude modulation.

The modulated signal is subsequently detected on the photodetector and demodulated. In the case of Lorentz profile of absorption line, the calculation of demodulated signal follows the equation [26]:

$$\int_T^{T+N/\omega} \frac{2\gamma}{\gamma^2 - (\omega_0 - at + \sin(\omega t))^2} \sin(\omega t + \phi) \, dt \ , \tag{4.4}$$

where T is the start time of the integration, N is the number of modulation periods after the start time, γ is HWHM of Lorentz profile, ω_0 is the angular frequency of the absorption line minimum, a is the slope of the frequency scan, and ϕ is the phase difference between the modulation and the demodulation frequency. The crucial for the integral result is the value of ϕ, as for the $\phi = 90°$, the integral is equal to zero for all the frequencies. The maximum of the integral occurs for $\phi = 0°, 180°, 360°, ...$ When using a lock-in amplifier, all of the calculations are performed by the device, and the only important task left for the operator is to set the phases.

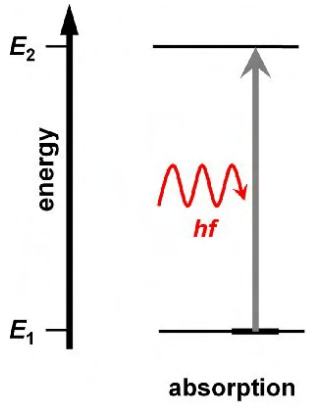

Figure 4.2: Photon absorption in a two-level system. Adapted from [27].

The photodetector signal in linear absorption spectroscopy is usually demodulated on the first harmonic frequency. The disadvantage of higher harmonic frequencies demodulation is that it requires higher modulation amplitude to maximise the S/N ratio. Due to Doppler broadened lines, the need for the modulation amplitude is too high, and the negative effects (e.g. residual amplitude modulation (RAM)) would dominate the signal of lower harmonics.

4.1.3. Limitation of the linear absorption spectroscopy

The linear absorption spectroscopy is relatively simple method with all advantages and disadvantages it broughts. The principal limitation is the HWHM of the measured absorption line. I will be dedicating the following lines to the dominant broadening mechanism in linear absorption spectroscopy.

If the frequency of the incoming light corresponds to the energy of any of the energy transitions in the absorption medium atoms (molecules), the photon can be absorbed Fig. 4.2. Mathematically, it could be written as follows:

$$hf = E_2 - E_1, \tag{4.5}$$

where f is the frequency of the light, E_2 is the energy of the higher energy level, E_1 is the energy of the lower energy level, and h is the Planck constant.

As a matter of fact, there is never only one energy corresponding to a certain transition, but there is an interval of energies the medium could absorb. In principle, each energy level is broadened ΔE due to the electrons' finite lifetime on each energy level Δt. These two quantities are related through the uncertainty principle:

$$\Delta E * \Delta t \geq \frac{\hbar}{2}, \tag{4.6}$$

where $\hbar$ stands for reduced Planck constant. This broadening mechanism is called natural broadening.

As natural broadening represents the limit of how narrow the absorption line can be, there are many other sources of line broadening (pressure broadening, collisional broadening, transit time broadening, and others). The broadening source can be divided into two groups depending on which absorption line profiles they create, Gauss (G) or Lorentz (L). Equations of both profiles are as follows:

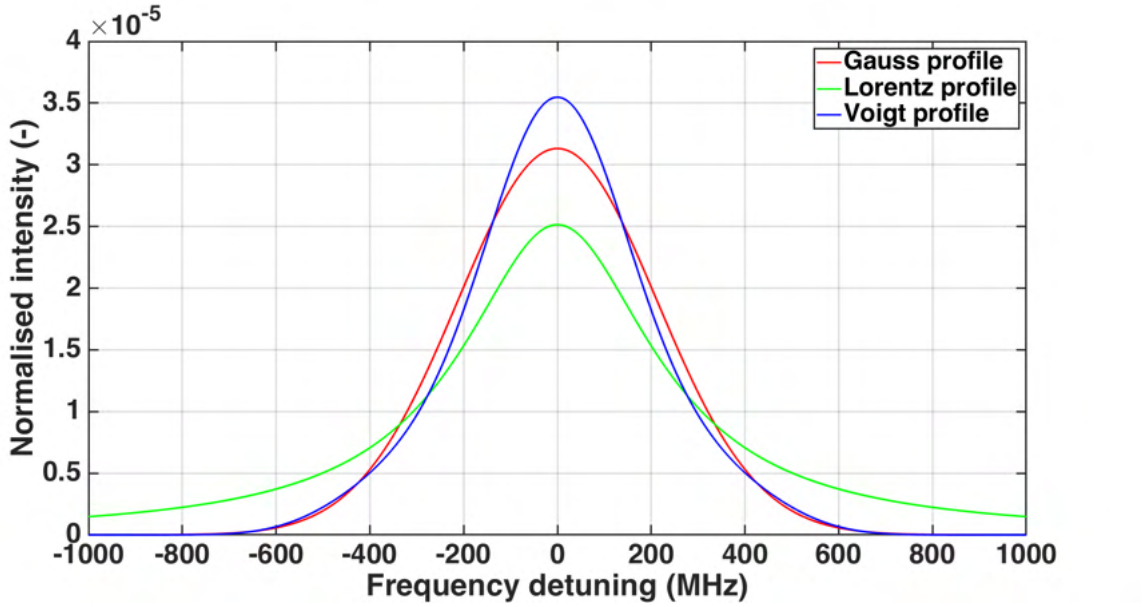

Figure 4.3: Example of Gauss, Lorentz and Voigt profile.

$$G(\omega,\sigma) \equiv \frac{1}{\sigma\sqrt{2\pi}} e^{-\frac{\omega^2}{2\sigma^2}}; L(\omega,\gamma) \equiv \frac{\gamma}{\pi(\omega^2+\gamma^2)}, \tag{4.7}$$

The absorption lines' profile is then obtained as the convolution of Gauss profile (with HWHM σ) and Lorentz profile (with HWHM γ):

$$V_g(\omega,\sigma,\gamma) \equiv \int_{-\infty}^{\infty} G(\omega',\sigma) * L(\omega-\omega',\gamma) d\omega'. \tag{4.8}$$

The example of the Voigt profile (V_g) calculated as the convolution of Gauss and Lorentz profiles (both with 250 MHz HWHM) can be seen in Fig. 4.3.

The Doppler broadening is the dominant broadening mechanism of the absorption lines in linear absorption spectroscopy. It is caused by molecules in the gas cell moving randomly. The molecules having the non-zero velocity component in the direction parallel to the laser beam "feel" the laser frequency as different from the actual frequency of the laser source. This makes molecules to absorb the laser radiation on different laser source frequencies, and the absorption lines are broadened. Doppler broadening (having a Gaussian profile) dominant mechanism limiting the accuracy of the linear absorption spectroscopy. Several methods allow Doppler-free measurement [28]. Out of those methods, in my experiments I used the saturation absorption spectroscopy.

The saturation absorption spectroscopy is the content of the following section.

4.2. Saturation absorption spectroscopy

4.2.1. Principle of the method

Quantitatively, the optical power/intensity needed for the absorption line saturation was described in [28]. It is derived from Beer's law, which is an equation describing the interaction between light and the absorptive environment:

$$I = I_0 e^{-\alpha(\omega)z}, \tag{4.9}$$

where I stands for the light intensity lowered by crossing the distance z in the absorptive medium. I_0 stands for the light intensity before the absorptive medium, and $\alpha(\omega)$ is the absorptive coefficient dependent on the light source's angular frequency ω.

For sufficiently low I_0, the absorptive coefficient can be assumed as independent of I_0. It means that the intensity of absorbed light is directly proportional to the incoming intensity. As the I_0 increases, this assumption is not valid. It is caused by the insufficient number of electrons in the lower state of the energy transition. If the number of absorbing electrons exceeds the number of electrons getting back by relaxation processes, there are no other electrons left to absorb the incoming light. The transition reaches the saturation, and the absorbed light is no longer directly proportional to the incoming light Fig. 4.4.

The saturation of the energy transition can be used in the saturation absorption spectroscopy for measuring the Doppler-free absorption lines. The example of the experimental setup Fig. 4.5 consists of two counter-propagating laser beams. The laser beam goes through the half-wave plate, which, in combination with the polarising beams splitter (PBS), allows for the division of the beam power in a variable ratio. The high-power pump beam then transmits through the PBS and the gas cell, and it is absorbed at the beam-dumb. The low-power probe beam is reflected at PBS, then it goes all the way around the gas cell, and after reflecting on the other PBS, it passes through the gas cell in precisely opposite direction than the pump beam. The probe beam measures the line profile saturated by the pump beam, and thus, it is monitored by the photodetector.

The profile of the saturated absorption line Fig. 4.6 has the so-called Lamb dip at the centre, caused by the frequency-selective saturation of molecular transition. The optical power has to be optimised to maximise the depth of the dip.

The saturation coefficient S describes quantitatively the degree of a certain energy transition saturation. The formula for S derived in [28] goes as follows:

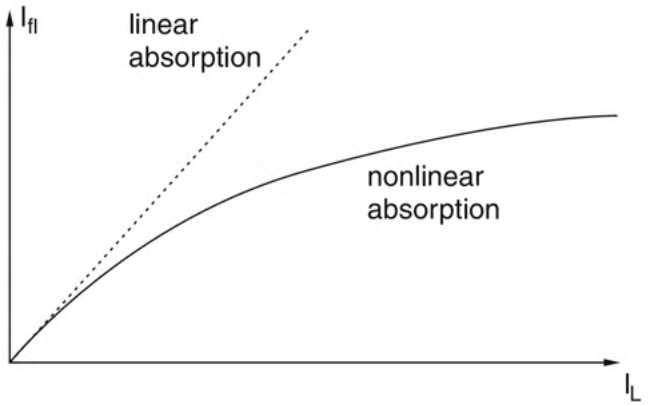

Figure 4.4: Graph of the fluorescence intensity I_{fl} radiated by electrons escaping the higher energy level as a function of incident laser intensity I_L. Adapted from [28].

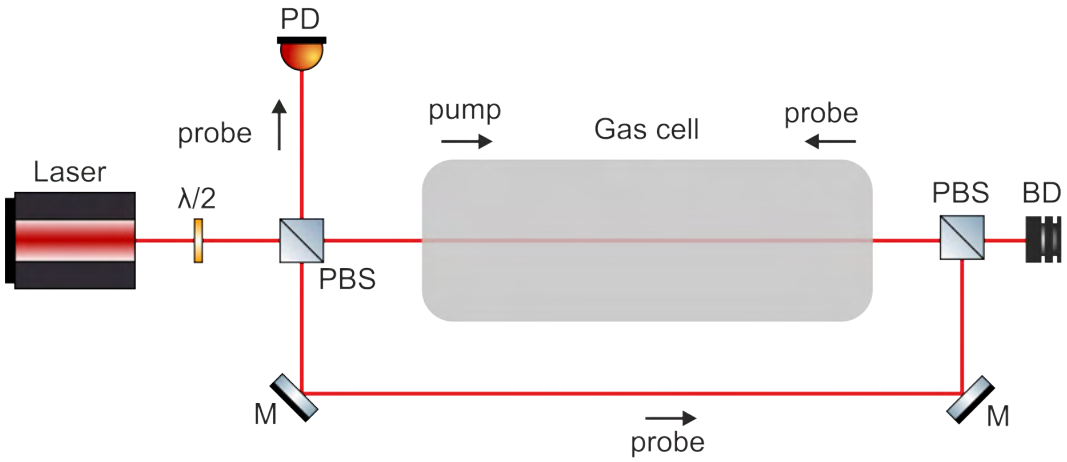

Figure 4.5: Principle of saturation absorption spectroscopy: beam-dump (BD), half-wave plate ($\lambda/2$), mirrors (M), polarising beam splitters (PBS), photodetector (PD).

$$S = \frac{P}{A}\frac{B_{12}}{cR^*}, \tag{4.10}$$

where P stands for the pump beam power, A stands for the area of the pump beam, c stands for the speed of light in vacuum, B_{12} stands for Einstein coefficient of induced absorption, and R^* stands for an effective relaxation rate. The intensity for which the $S = 1$ is called the saturation intensity. It corresponds to the difference in population of higher and lower energy levels being half of the unsaturated value. The optimum of Lamb-dip S/N ratio is reached for $S \approx 1.4$. Further increase of the radiation intensity leads to the Lamb-dip broadening instead of improving the S/N ratio.

The Einstein coefficients express probabilities of the absorption/emission of light at a concrete energy transition per second. The Einstein coefficient of induced absorption can be expressed as:

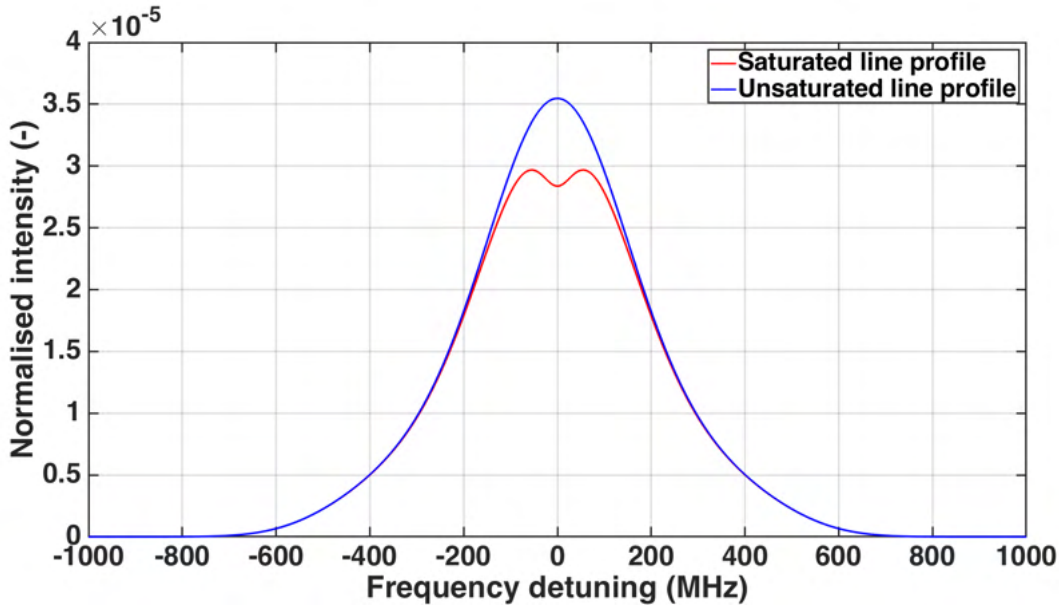

Figure 4.6: Comparison of the unsaturated and the saturated line profile.

$$B_{12} = -\frac{c}{hf\Delta N}\frac{\ln I/I_0}{z}, \tag{4.11}$$

where h stands for Planck constant, f stands for a frequency corresponding to the frequency of photon absorbed at a specific energy transition, ΔN stands for a difference in the occupation of lower and higher energy level, I/I_0 stands for the ratio of the pump beam intensity in front of the gas cell and behind the gas cell, and z stands for the interaction length of the light and the absorption medium.

The relaxation rates R_1 and R_2 inform us about how much the electrons on lower and higher energy level are inclined to transit to a different energy level. The effective relaxation rate R^* then corresponds to the probability of electrons' relaxation at both, the lower and the higher energy level. It can be expressed as:

$$R^* = \frac{R_1 R_2}{R_1 + R_2}, \tag{4.12}$$

where $R_1 = \frac{1}{t_T}$. t_T stands for the transit time of molecules through the laser beam area. $R_2 = k\frac{N}{V}$, where k is the Boltzmann constant and $\frac{N_m}{V}$ is a number of molecules per unit of the volume.

4.2.2. Limitation of the saturation absorption spectroscopy

While the saturation absorption spectroscopy overcomes the main limitation of the linear absorption spectroscopy precision, which is the Doppler broadening, another sources of the absorption line broadening can still be presente. Examples of such broadening can include: the time-of-flight broadening [29], the Stark broadening (caused by an external electric field), the Zeeman broadening (caused by a magnetic field), the collisional broadening, and many others.

The experimental setup overcoming these limits is becoming increasingly complex as the most accurate method for the absorption lines central frequency determination is to use the atomic (ion) clock [30], [31]. The ultimate restriction is the natural broadening caused by the finite time of life of electrons on energy levels.

5. State of art of $H^{13}C^{14}N$ precision spectroscopy

5.1. Linear absorption spectroscopy

5.1.1. Experimental arrangement of Sasada et al.

The first thorough study of $H^{13}C^{14}N$ $2\nu_3$ band to be mentioned was published by Sasada et al. [32] from Keio University in Japan in 1990. Authors studied HCN in the natural abundance and also enriched $H^{13}C^{14}N$ sample. Samples were prepared by reaction of H_2SO_4 and NaCN.

The laser used in the Sasada's article was a distributed feedback semiconductor laser (Hitachi HL1541A). Its radiation was split into several parts Fig. 5.1. The first part went through the 1 m long, 8 Torr CO reference cell. The second part went through 1 m, 1.3 Torr HCN absorption cell and the last part was sent to the Fabry-Perot (FP) interferometer (Tec-Optics SA-300). Photodiodes followed by lock-in amplifiers detected the beams transmitted through the absorption cells.

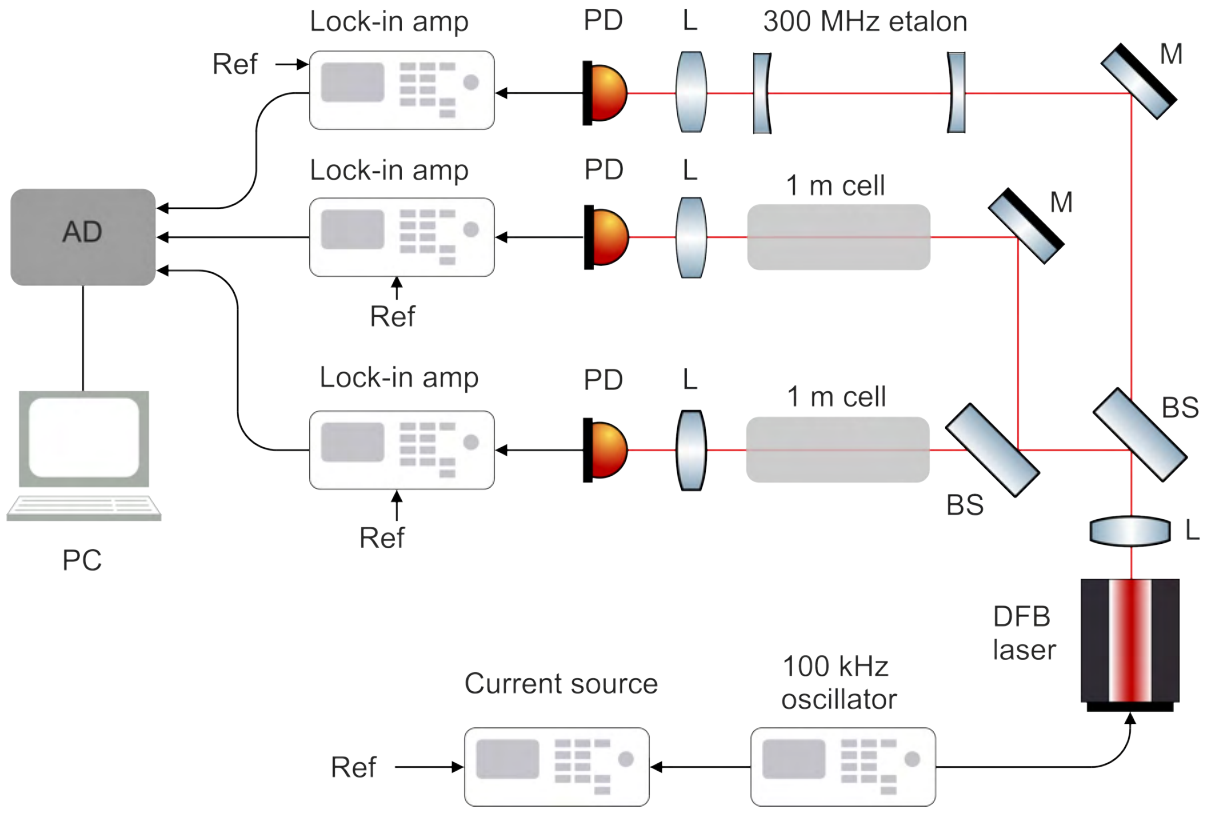

Figure 5.1: Experimental setup used in [32] for spectroscopy in HCN: amplifiers (AMP), analogue-digital (AD) converter, beam splitters (BS), computer (PC), distributed feedback (DFB) laser, lenses (L), mirrors (M), references (Ref).

Authors measured the band from 6380 to 6410 cm^{-1} ($\approx$ from 1567 to 1560 nm) with the absolute accuracy of 0.0005 cm^{-1} ($\approx$ 15 MHz) and the band from 6410 to 6570 cm^{-1} ($\approx$ from 1560 to 1522 nm) with the absolute accuracy of 0.0033 cm^{-1}. The lower accuracy was caused by using a less precise Michelson interferometer type of wavelength meter (Advantest TQ8325). The data were then combined with the data from [33] and [34] to perform least-square analysis to calculate molecular constant. These constants then served for the calculation of the absorption lines position for $2\nu_3$ and $2\nu_3 + \nu_2$ bands of $H^{12}C^{14}N$ and $H^{13}C^{14}N$ with the accuracy of 0.0005 cm^{-1} ($\approx$ 15 MHz) for the intense lines and lower accuracy up to 0.0021 cm^{-1} ($\approx$ 63 MHz) for less intense lines. The pressure shift effect was estimated to be lesser than the presented accuracy of the wavenumber measurement.

5.1.2. Experimental arrangement of Gilbert et al.

The Standard Reference Material (SRM) is a document certified by the National Institute of Standards and Technology (NIST). It is used to ensure the reproducibility of the results across all scientific fields. The SRM 2519 is a wavelength reference absorption cell filled with hydrogen cyanide. The special publication [35] (1998) is dealing with measurement of $H^{13}C^{14}N$ $2\nu_3$ band.

Authors used a tunable diode laser, which was sent through two $H^{13}C^{14}N$ absorption cells Fig. 5.2. Both cells were 15 cm long. The low-pressure cell was $(1.3 \pm 0.1)kPa$, the high-pressure cell $(12.6 \pm 0.7)kPa$. Laser wavelength was measured by a wavelength meter with the uncertainty of $\pm 0.000\,16$ nm. To check the wavelength meter accuracy, the diode laser light was frequency doubled and used for the saturation absorption spectroscopy on the $5S_{1/2} \rightarrow 5P_{3/2}$ transitions of rubidium isotopes ^{85}Rb and ^{87}Rb. The laser was stabilised for certain absorption lines, and the wavelength meter reading was within 0.000 10 nm of the literature values [36].

Twenty-one measured absorption lines were fitted by the Voigt profile. The data measured in the high-pressure cell were fitted by the Lorentzian profile, as the dominant broadening mechanism was the pressure broadening. Authors discussed and then included several sources of uncertainty in their uncertainty budget. The uncertainty sources while

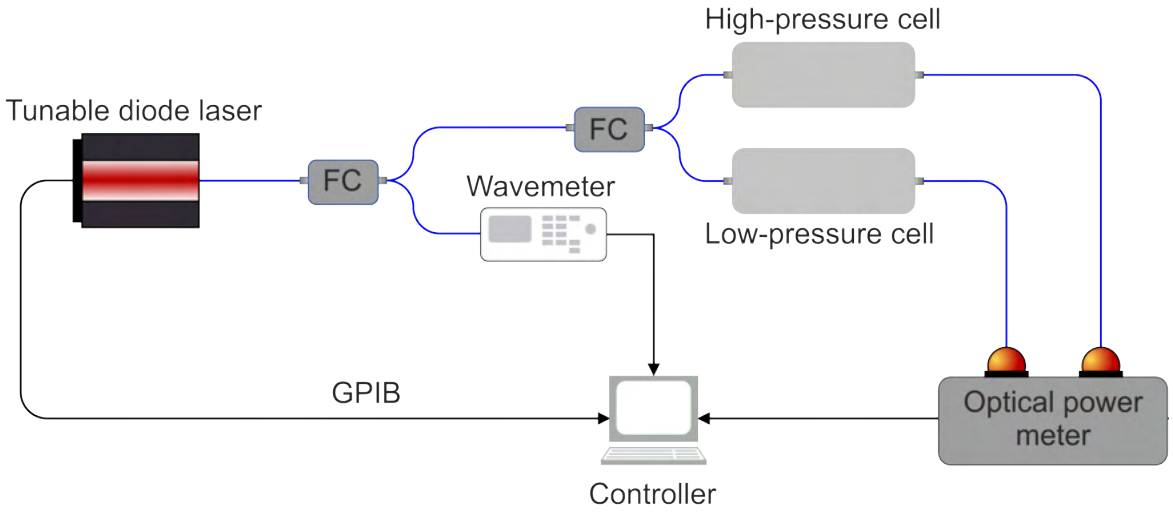

Figure 5.2: Experimental setup used for $H^{13}C^{14}N$ absorption lines measurement: fibre couplers (FC), general purpose interface bus (GPIB). Adapted from [35].

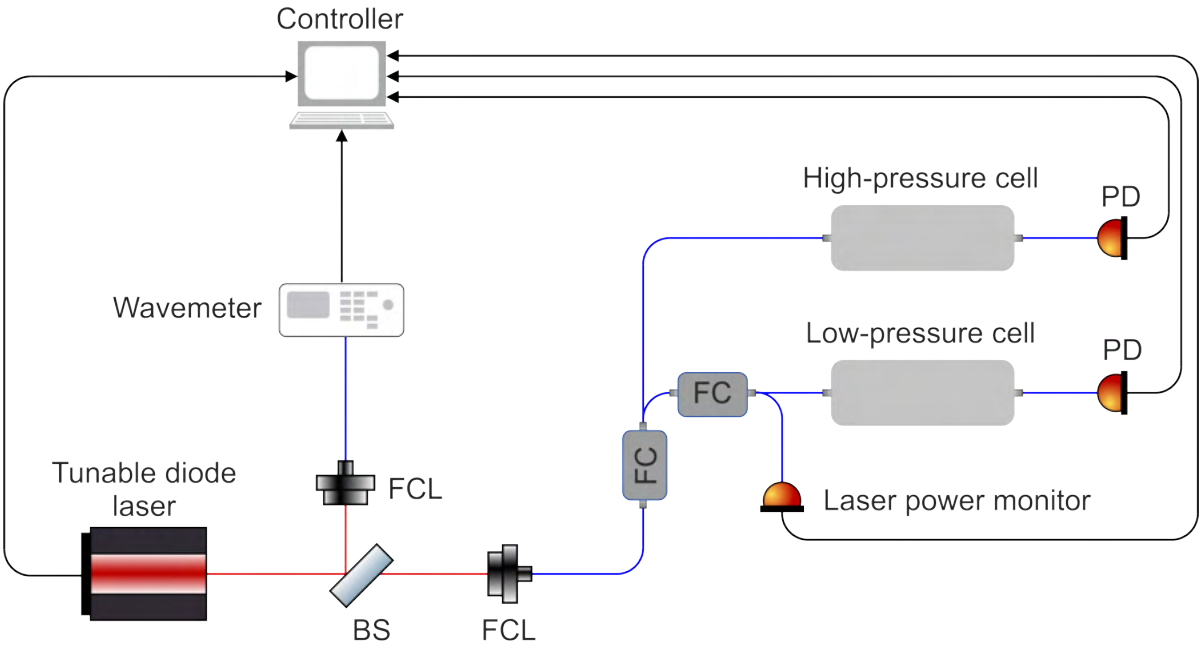

Figure 5.3: The experimental apparatus for the linear absorption spectroscopy measurement: beam splitter (BS), fibre collimators (FCL), fibre couplers (FC), photodetectors (PD). Adapted from [11].

determining the line centre's relative position were the nearby line contribution, the background slope, the removal of outlier point, the statistical uncertainty of the fit, the and the reproducibility of the fit. In the absolute line centre determination, the wavelength meter uncertainty and the pressure uncertainty were also added. By doing that, authors certified the position of twenty-one lines measured by them (including the pressure shift coefficients) with the uncertainty of 0.0006 nm (≈ 75 MHz @ 1550 nm) and thirty lines measured in [32] with the uncertainty of 0.003 nm (≈ 374 MHz @ 1550 nm)

5.1.3. Experimental arrangement of Swann et al.

The most up-to-date study of $H^{13}C^{14}N$ $2\nu_3$ band was done by Swann and Gilbert in [11]. They used a very similar setup Fig. 5.3 to the one they used in [35] with the addition of a FP filter (cavity), narrowing the scanning laser frequency line. The absorption cells were 0.13 kPa and either 3.3 kPa or 6.0 kPa. All of the cells were 15 cm long with windows attached to the cell by a glass frit method. The windows were mounted at an angle of 11° and wedged by ≈ 2° to prevent the interference fringes in the transmitted signal. The cells were filled with the $H^{13}C^{14}N$ produced by the reduction of 99 % isotopically pure potassium cyanide with a stearic acid under the vacuum and a mild heat (≈ 80 °C).

The wavelength meter accuracy was tested by measuring rubidium hyperfine components as mentioned earlier in the [35] article description (section 5.1.2). The laser frequency stabilised to the rubidium line was measured by a comparison with the optical frequency comb [37]. The uncertainty combined as the calibration uncertainty and the uncertainty of the wavelength meter drifting between particular calibrations was 0.004 pm (≈ 0.5 MHz @ 1560 nm).

The linearity of the wavelength meter was verified by measuring $^{12}C_2H_2$ lines between 1528 nm and 1538 nm. The lines were measured the same way as the HCN lines described

in the [35], and the results were compared with those in [38], with the average results being in 0.002 pm agreement.

The pressure monitoring in the absorption cells was allowed by the previous measurement of the P16 absorption line pressure broadening dependence on the pressure. In the case of a low-pressure cell, authors reported an exponential decay in the pressure from 0.133 kPa to 0.106 kPa over the nine-day duration of the measurement. They mention as the likely reason the adsorption of HCN on the cell surface.

Twenty-five absorption lines were measured and extrapolated to zero pressure with the uncertainty varying from 0.000 01 nm ($\approx$ 1.2 MHz) to 0.000 027 nm ($\approx$ 3.4 MHz). Authors also determined the pressure shift coefficients and the pressure broadening coefficients of these twenty-five lines. The measured line centres corresponded well with the data measured in [32].

The position of twenty-five measured lines was used for the calculation of the molecular constants for ground and excited states and served for the calculation of the position of fifty-six $H^{13}C^{14}N$ absorption lines. The uncertainty was from 0.000 008 nm ($\approx$ 1.0 MHz) to 0.000 025 nm ($\approx$ 3.1 MHz).

5.1.4. Practical use of the linear absorption data

Authors in [9] used $H^{13}C^{14}N$ absorption cells as the length reference in their frequency scanning interferometer. During the gas cell calibration procedure, they found out the correlated term in the uncertainty of the $H^{13}C^{14}N$ absorption lines' centre at different pressures. It indicates that certain shifts might be present in the data published in [11].

In the article [39], authors used $H^{13}C^{14}N$ and $^{12}C^{16}O$ absorption cells as an inexpensive traceable method for the calibration of the ladar system. They stated that the "conservative" systematic uncertainties of the absorption lines positions represented limitations for their calibration's accuracy.

The $H^{13}C^{14}N$ was also used in [40] and [41] as wavelength reference for the fibre Brag grating demodulation. It shows that the linear absorption spectroscopy of $H^{13}C^{14}N$ represents a useful tool for many applications, even though more accurate data would help further improve its benefits for the scientific as well as the industrial community.

5.2. Saturation absorption spectroscopy

5.2.1. Experimental arrangement of Labachelerie et al.

The first experiment (up to my best knowledge) regarding the saturation absorption spectroscopy in $H^{13}C^{14}N$ was described in [42]. Authors used an external cavity semiconductor laser (Littrow configuration) Fig. 5.4, allowing the initial 120 nm tuning range. The tuning range was limited by the glueing of mechanical supports restricting the range to 1.51-1.58 μm. The absorption cell was a 20 cm long FP cavity with 99 % reflectivity of the input and the output mirror. The laser current was frequency modulated at 1 kHz with the modulation depth of 6 MHz. While the laser frequency was locked to FP cavity resonance, it could be tuned by $\approx$ 1 GHz using the piezo-crystal.

The experiments were conducted with $^{12}C_2H_2$, $^{13}C_2H_2$ and HCN (what hydrogen cyanide isotope was used authors do not mention). The cavity was filled with the 10-20 mTorr of acetylene (the pressure used in HCN experiments is not noted), and "many"

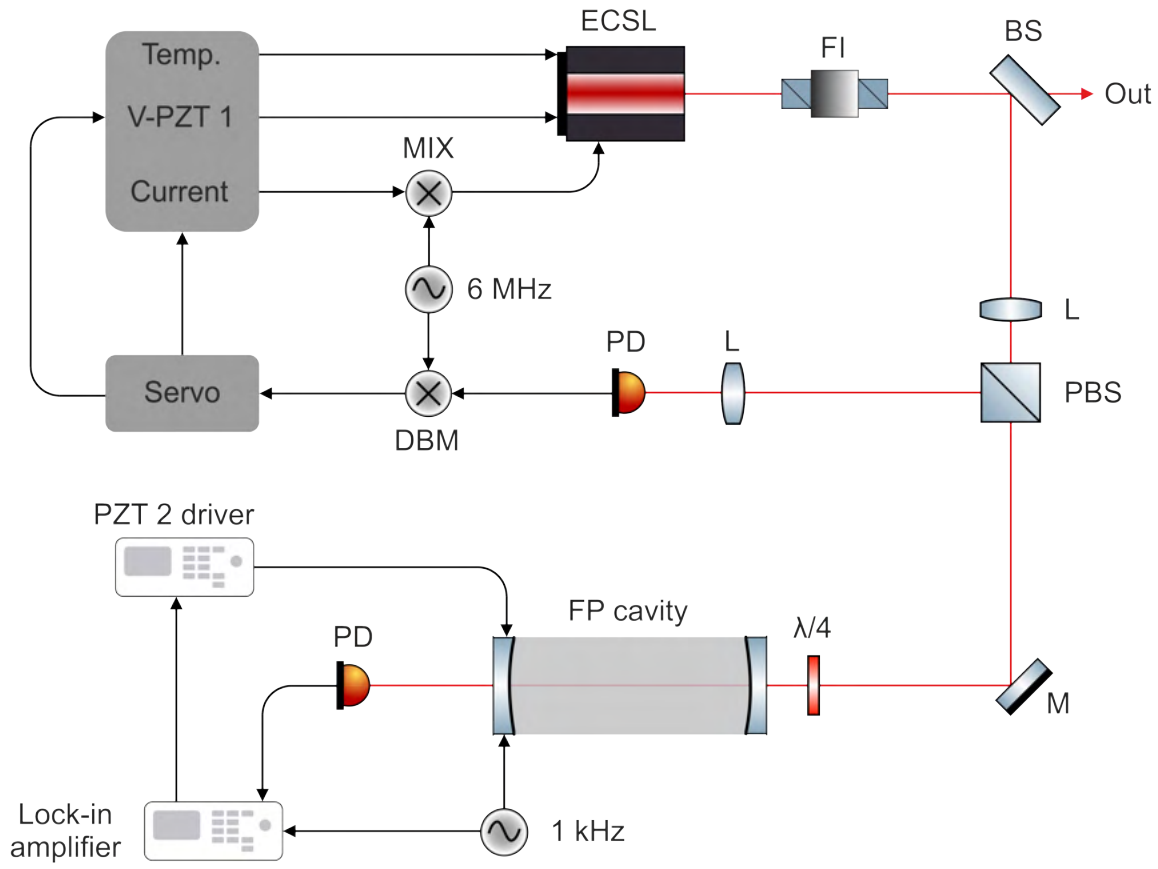

Figure 5.4: Experimental setup for saturation absorption spectroscopy in acetylene and hydrogen cyanide: beam splitter (BS), double-balanced mixer (DBM), external cavity semiconductor laser (ECSL), Fabry-Perot (FP) cavity, Faraday isolator (FI), piezo crystals (PZT), polarising beam splitter (PBS), quarter-wave plate ($\lambda/4$). Adapted from [42].

sub-Doppler lines were recorded. The successful saturation of P27 $^{13}C_2H_2$ and P27 HCN absorption lines serves as an example. Authors also calculated the relative stability of the laser locked to a minimum of P13 $^{12}C_2H_2$ with the best stability of 10^{-12} reached at an integration time of $\approx 1\,\mathrm{s}$.

5.2.2. Experimental arrangement of Awaji et al.

Additional research by the [42] authors led to another publication [43]. They further improved the experimental setup Fig. 5.5. They used the external cavity semiconductor laser (ECSL) locked to $H^{12}C^{14}N$ absorption line as an input to injection lock a high-power laser. This laser was frequency doubled using a Potassium titanyl phosphate (KTP) crystal.

In the other branch of the experimental setup Fig. 5.5, the 778 nm semiconductor laser was sent through the glass cell containing natural Rb. Then it was reflected back by 100 % reflectivity mirror. The laser frequency was locked to Rb ($F_g = 1 \rightarrow F_e = 3$) line f_{Rb}. Afterwards, the other part of the 778 nm laser was mixed at the acousto-optic modulator (AOM) with the frequency-doubled 1556 nm laser. The resulting frequency of the $H^{12}C^{14}N$ absorption line centre f_{HCN} was then:

$$f_{HCN} = (f_{Rb} - f_{AOM} + f_B)/2, \tag{5.1}$$

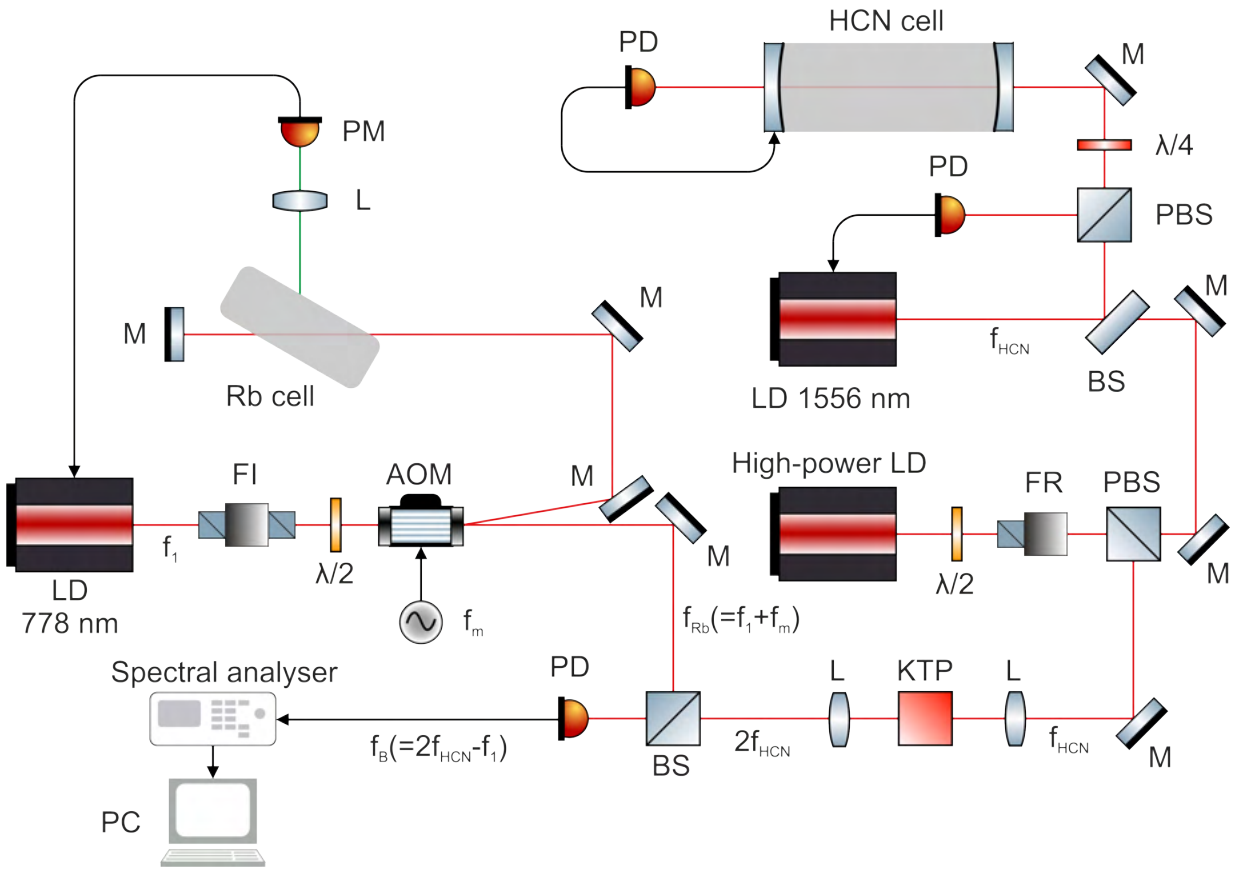

Figure 5.5: Experimental setup for the saturation absorption spectroscopy measurement of $H^{12}C^{14}N$ absorption line: acousto-optic modulator (AOM), beam sampler (BSF), beam splitter (BS), computer (PC), Faraday isolator (FI), Faraday rotator (FR), half-wave plates ($\lambda/2$), laser diodes (LD), lenses (L), mirrors (M), photodetector (PD), photomultiplier (PM), polarising beam splitters (PBS), Potassium titanyl phosphate (KTP), quarter-wave plate ($\lambda/4$). Adapted from [43].

where f_{AOM} was the 80 MHz frequency introduced at the AOM first order of the diffraction and $f_B = 1418.7$MHz was the beat-note centre frequency. The frequency of P27 $H^{12}C^{14}N$ absorption lines centre was determined as $f_{HCN} = (192622446.9 \pm 0.1)$MHz.

5.2.3. Experimental arrangement of Henningsen et al.

Authors from the Danish Fundamental Metrology (DFM) were dealing with the saturation spectroscopy of the acetylene and the hydrogen cyanide in photonic bandgap fibres [44]. They used an external cavity laser amplified by an erbium-doped fibre amplifier (EDFA) to 60 mW. The radiation went through the hollow-core photonic bandgap fibre (HC-PBG) with the 7-cell core of 10 μm diameter located in a vacuum box.

Three different detection schemes were used. In the first case, the transmitted signal through the hollow-core fibre was detected close to the window W2 by 5x5 mm^2 Ge detector. The second configuration included an aspherical lens with 13 mm focal length focusing the exit beam and a mirror placed in the focal plane reflecting the beam back into the fibre. The mechanical chopper (CH) was placed in front of the mirror. The Ge

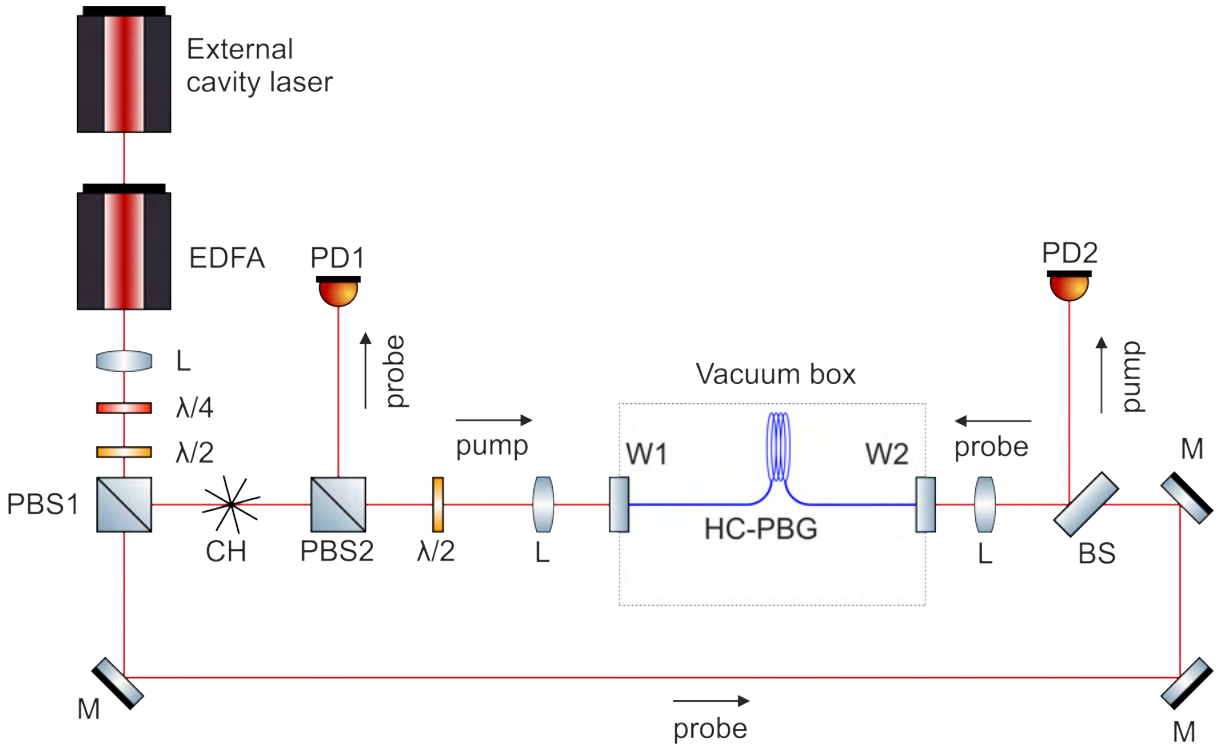

Figure 5.6: Experimental setup for the saturation absorption spectroscopy in the hollow-core fibre: beam splitter (BS), chopper (CH), erbium-doped fibre amplifier (EDFA), half-wave plates ($\lambda/2$), hollow-core photonic bandgap fibre (HC-PBG), lenses (L), mirrors (M), photodetectors (PD), polarising beam splitters (PBS), quarter-wave plate ($\lambda/4$), sapphire windows (W)). Adapted from [44].

detector monitored the signal chopped at 670 Hz frequency. The signal from the detector was subsequently demodulated in a lock-in amplifier.

The third version of the experimental setup is shown in Fig. 5.6. The laser beam transmitted by PBS1 (polarising beam splitter) served as a counter-propagating beam through the hollow-core fibre. The described laser beam is called probe beam and it was measured at the PD1 (photodetector). The PD2 monitored the pump beam.

The experiments with the 6.35 m long HC-PBG filled with $H^{13}C^{14}N$ showed different results to those of acetylene. In the case of hydrogen cyanide, after filling the fibre, the pressure started to drop exponentially. Authors attributed the exponential drop to the permanent dipole moment of the $H^{13}C^{14}N$ molecule, that causes the tendency of the gas to "stick" to the fibre wall.

Authors successfully measured the saturation absorption signal for the P9 C_2H_2 (however, they do not mention the used isotope) and R7 $H^{13}C^{14}N$. The dominating broadening mechanism in their measurement was transit-time broadening, causing the measured lines to have HWHM of ≈ 20 MHz.

Presented article illustrates authors' effort to use the saturation absorption spectroscopy for $H^{13}C^{14}N$ absorption lines measurement. The restricting factor seems to be the permanent dipole moment of the molecule. It causes the decrease of an "effective" pressure in the absorption cell (the hollow-core fibre) given that molecules "stick" to the fibre walls [45]. Therefore, this might be the reason why no systematic measurement

of $H^{13}C^{14}N$ absorption lines centre using the saturation absorption spectroscopy has not been performed so far.

6. Linear absorption spectroscopy

6.1. First harmonic detection method

6.1.1. Preliminary experiment with the Koheras Adjustik laser

At the first stage of my research on the measurement of $H^{13}C^{14}N$ absorption lines, I used a simple linear absorption setup Fig. 6.1. The laser beam (Koheras Adjustik E15) went through a Faraday isolator (FI), ensuring no reflected light returned to the laser source. The beam was then split into numerous parts, one passing through the absorption cell three times and afterwards hitting the photodetector (PD). The reference signal was monitored on the other PD. This allows the use of the technique, that eliminates the residual amplitude modulation (RAM) [46]. The RAM was subtracted by the in-house custom-built hardware, simultaneously enabling the frequency modulation technique. The laser frequency was locked to the minimum of a particular absorption line. The second part of the experimental setup allowed us to measure the frequency of the laser precisely.

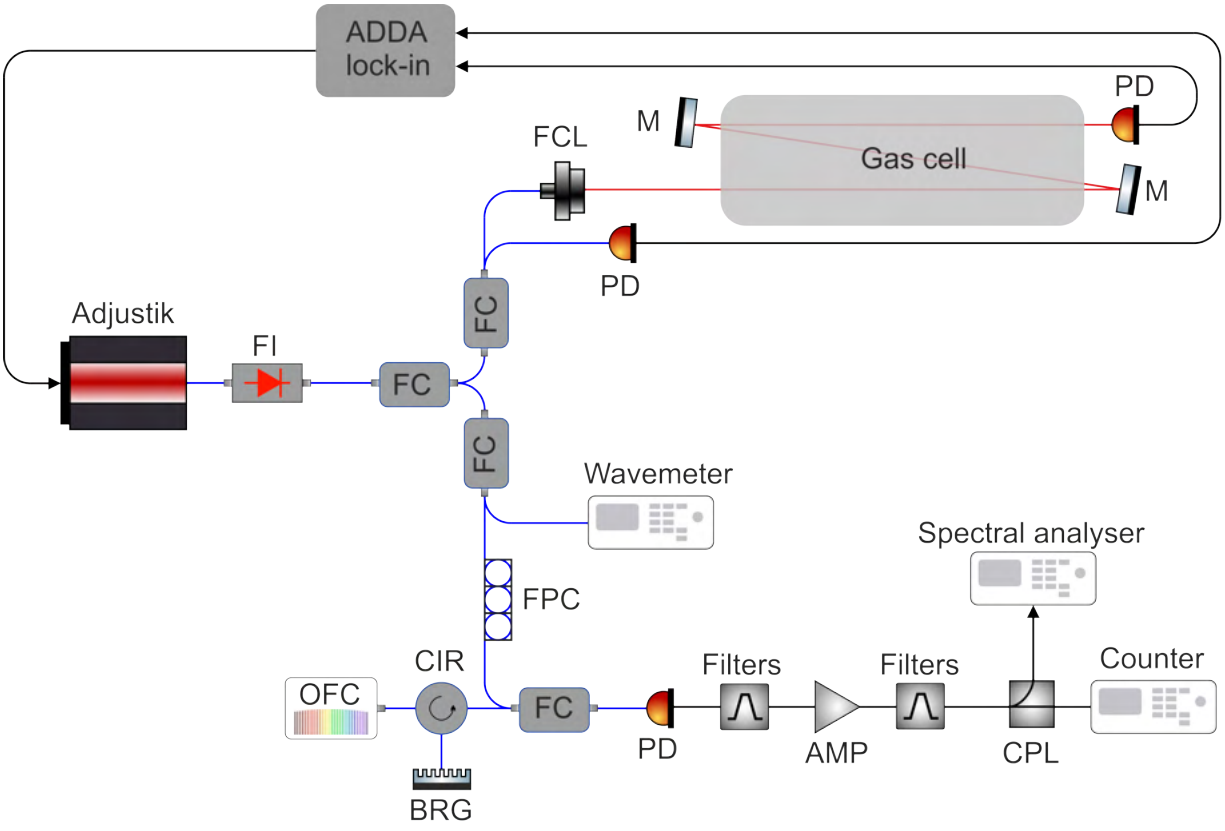

Figure 6.1: The scheme of the experimental setup for the preliminary linear absorption spectroscopy measurement: amplifier (AMP), analogue-digital digital-analogue (ADDA) lock-in, Bragg grating (BRG), circulator (CIR), Faraday isolator (FI), fibre collimator (FCL), fibre couplers (FC), fibre polarisation controller (FPC), Koheras Adjustik E15 (Adjustik), mirrors (M), optical frequency comb (OFC), photodetectors (PD), and radio frequency coupler (CPL). Adapted from [50].

The optical frequency comb (OFC) [47] was filtered through the Brag grating, reflecting only a specific part of the OFC spectrum. The OFC is then combined with the laser beam. The combined beam then hit the PD, and after being frequency filtered, the beat-note frequency was measured by the counter. The laser was locked to the absorption line minimum, and the frequency of the absorption line minimum was calculated from the beat-note record.

To optimise the experimental setup, I used $^{13}C_2H_2$ absorption cell (100 Pa nominal pressure, 30 cm length, Institute of Scientific Instruments [7], [48]) and compared the measured values of the absorption lines centre with those published in [49]. The measured lines P12 and P13 were from $\nu_1+\nu_3$ band and P18 was from $\nu_1+\nu_2+\nu_4+\nu_5$ band. The differences between my measurement [50] and [49] were ≈ 700 kHz for P12 and P13 lines and ≈ 6.5 MHz for P18 line. The big difference in the case of P18 was caused by relatively low absorption and worse stability of the laser locked to the line minimum.

Used Adjustik laser's tuning range is approx. from 1539.8 nm to 1541.0 nm. That permitted me to measure a single absorption line of $H^{13}C^{14}N$ (the following gas cell was used: 67 Pa nominal pressure, 20 cm length, Wavelength References, Inc.), concretely R2. The difference between my measurement [50] and the results published in [11] was about 0.9 MHz, while the relative stability of a laser locked to the minimum of R2 line was 10^{-8} at 8 hours integration time.

6.1.2. Experiments with the CTL 1550

Further improvements in the experimental configuration in Fig. 6.1 led to the setup Fig. 6.2. The Koheras Adjustik E15 laser was replaced by a newly acquired continuously-tunable laser (CTL 1550, TOPTICA Photonics AG) with built-in Faraday isolator. The CTL 1550 allows for a mode-hop free frequency tuning in the range from 1510 nm to 1630 nm. This range is covering the whole absorption spectrum of $H^{13}C^{14}N$. The optical power of the CTL was stabilised by a variable optical attenuator (VOA). The VOA is getting an error signal from the proportional–integral–derivative (PID) controller. In order to create an error signal, the signal from the reference output of the double-balanced photodetector (DBPD) (Nirvana 2017, Newport) is used. The combination of the Glan-Taylor crystal (GT) and a half-wave plate ($\lambda/2$) ensured the polarisation stability of the laser beam entering the experimental setup.

I used the absorption cell (0.4 Torr nominal pressure, 40 cm length, Wavelength References, Inc.), with the wedged windows. The windows had an anti-reflective (AR) coating and were fitted to the tube at a slight tilt to minimise the interference effects. The cell was covered in a custom-made temperature-controlling device, minimising the pressure changes in the cell caused by temperature changes Fig. 6.3. The PID controller regulated the temperature through four Peltier heaters attached to an aluminium cover. The cover was in thermal contact with the glass cell. The temperature-controlling sensor was located inside the aluminium cover. The sensor measured the temperature stability in the order of 10 mK, ensuring that the temperature-induced pressure effect on the gas was negligible.

In this measurement, I used the double-balanced photodetector to minimise the noise introduced to an optical signal. The laser frequency was modulated at 10 kHz with the 6 MHz modulation depth. The lock-in amplifier referenced by active hydrogen maser [51] demodulated the signal at the first harmonic frequency.

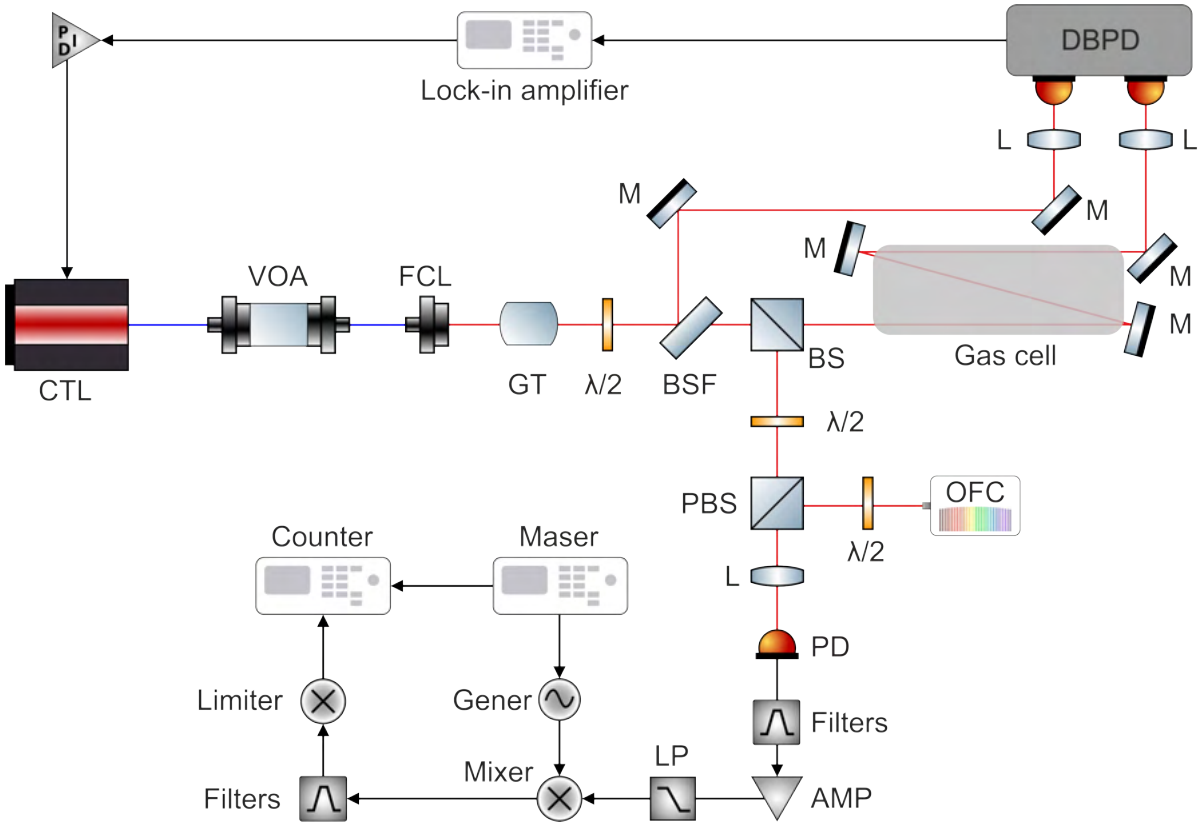

Figure 6.2: The experimental setup for the linear spectroscopy measurement: band pass filter (BP), beam sampler (BSF), beam splitter (BS), continuously-tunable laser (CTL), double-balanced photodetector (DBPD), fibre collimator (FCL), Glan-Taylor crystal (GT), half-wave plates ($\lambda/2$), lens (L), low pass filter (LP), mirrors (M), photodetector (PD), polarising beam splitter (PBS), and variable optical attenuator (VOA). Adapted from [53].

A part of the laser beam was combined with an optical frequency comb [47], and the resulting beat-note frequency was filtered and measured by counter. The counter was referenced to an active hydrogen maser [51]. The whole experimental setup was covered in a thermal insulation box (MIRELON), minimising the temperature changes in the optical part of the setup.

The CTL frequency was locked to the minimum of a certain absorption line and kept in lock typically for about 8 hours. A representative example Fig. 6.4 of the Allan deviation [52] shows the stability of about $9{*}10^{-12}$ at 1 min integration time. It represents three orders of improvement compared to the results presented in [50].

Thanks to the experimental configuration described above, I was able to measure twenty-six absorption lines with the 2σ standard deviation between 40 kHz and 70 kHz [53]. While I reached the limit of the linear absorption method regarding the laser frequency stability, the crucial task to improve was the repeatability of the results. The repeated measurement of the same line within a long-term interval ($\approx$ week) between each measurement showed the absolute frequency of a line centre fluctuation in 1 MHz order.

The polarisation fluctuation was considered to be the potential source of the repeatability issues. As the polarisation of the laser beam was changing, it was causing differences in the split ratio of the beam splitters (even if they were the non-polarising beam split-

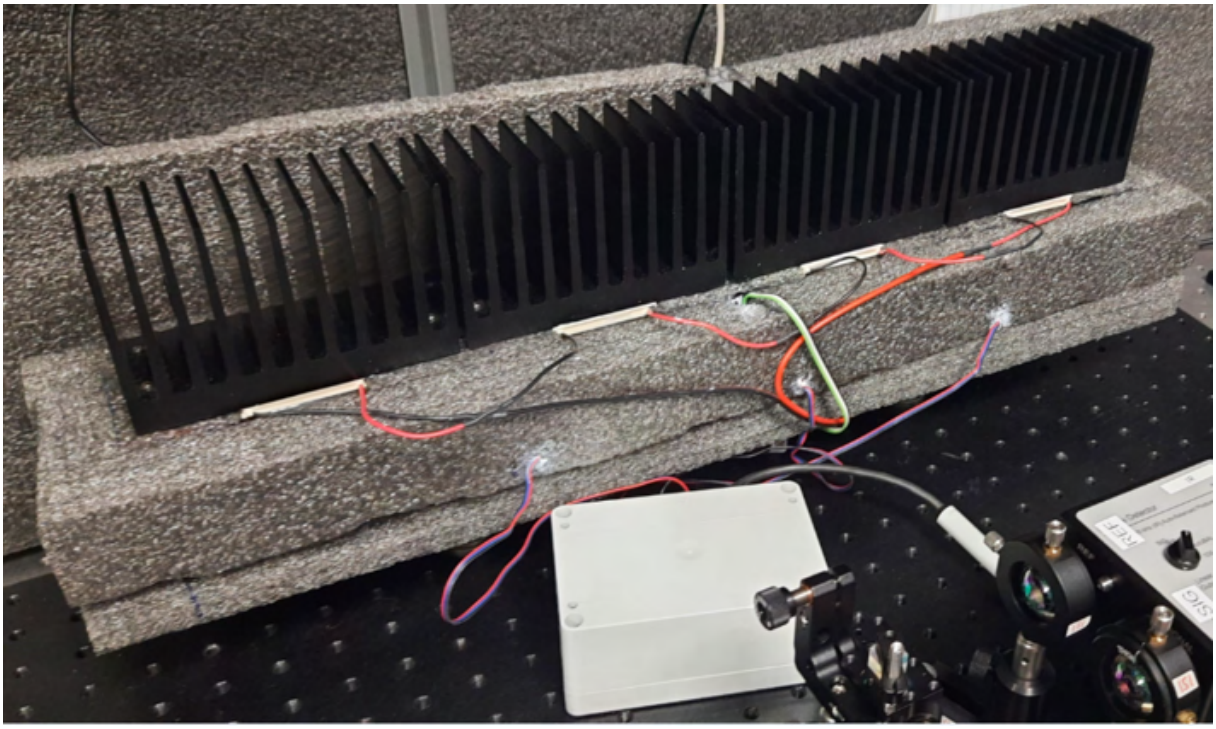

Figure 6.3: The device serving for a temperature control of the gas cell.

ters). In principle, the power stabilisation cannot fix the power fluctuation. Hence, I used a polarimeter to study the effect and minimise it Fig. 6.5.

The CTL included a pre-installed Toptica FiberDock collimator, which should be optimally adjusted to minimise the polarisation fluctuation in the fibre. As this was not

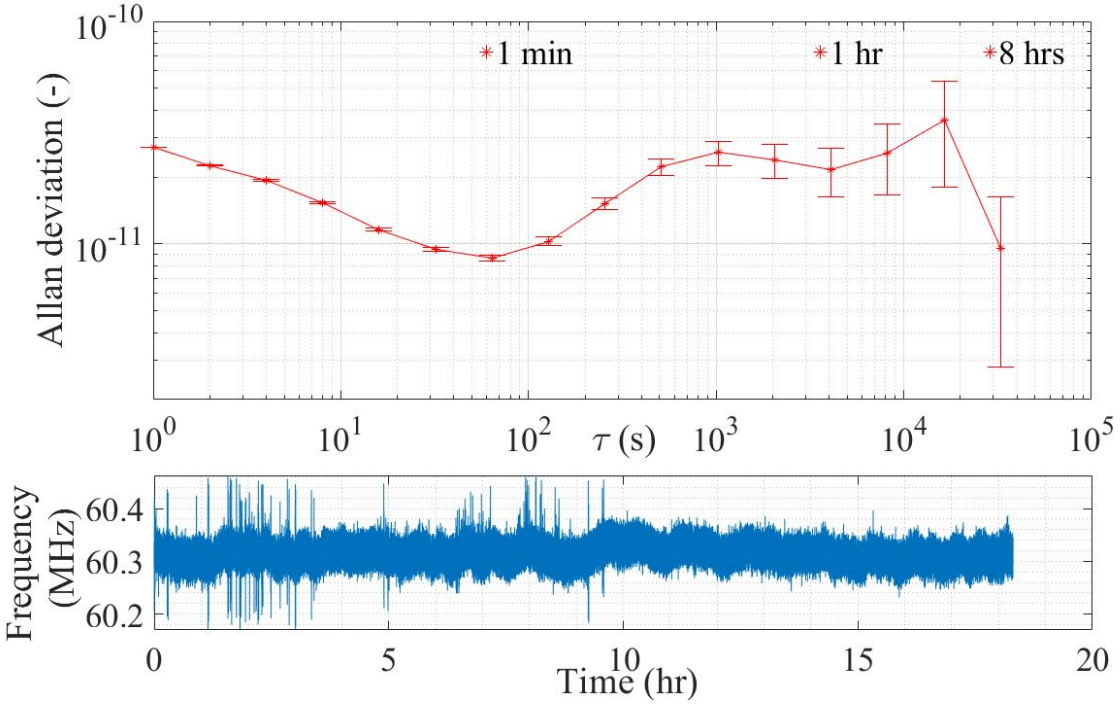

Figure 6.4: The Allan deviation (upper figure) calculated from the time evolution of laser frequency locked to the minimum of $H^{13}C^{14}N$ R6 absorption line. Adapted from [53].

the case, the easiest way to optimise the coupling of the laser beam into optical fibre was to insert a half-wave plate between the optical isolator and the collimator inside the laser box. The plate was rotated, so the fluctuations of the laser beam polarisation were minimal.

The following step was to insert GT crystal (GT5-C, Thorlabs) into the optical path. It produced a pure linear polarisation with an extinction ratio of 100000:1 and had the AR coating for 1050 - 1700 nm. Then, I inserted the half-wave plate and measured the polarisation behind the 50/50 non-polarising cube (BS012, Thorlabs). The improvement achieved by inserting the half-wave plate and GT crystal compared to the configuration without them can be seen in Fig. 6.5.

Further linear absorption spectroscopy research led to the modulation-free absorption technique, which will be described in the next section.

6.2. Modulation-free spectroscopy

Only the tiny surrounding of the absorption lines minimum is monitored while using the modulation techniques for the determination of the absorption lines centre (the modulation depth in [53] was 6 MHz). As further enlargement of modulation depth brings more disadvantages (e.g. the modulation broadening of the absorption lines, the residual amplitude modulation), the idea of using a modulation-free spectroscopy came to light. The monitored part of the line can be easily changed, this makes a clear advantage over techniques using a frequency modulation. To determine the absorption line centre, wider part of the absorption line was involved.

The modified setup for modulation-free absorption lines measurement can be seen in Fig. 6.6. The frequency of the CTL was locked to the particular tooth of OFC using a phase locked loop (PLL), as described in [54]. The OFC absolute frequency was maintained by continuously tracking a global navigation satellite system (GNSS). Thanks to that, the frequency of the CTL was known with fractional uncertainty at 10^{-13} order

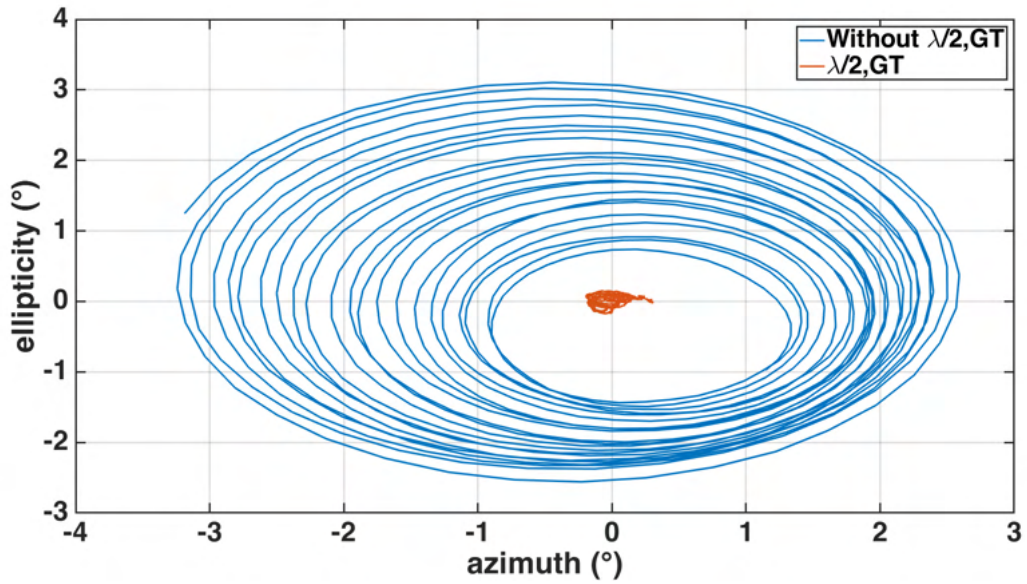

Figure 6.5: The polarisation stability during the wavelength tuning.

Table 6.1: The pressure shift coefficients determined by the linear absorption spectroscopy compared to the results published in [11].

Line	k_{ISI} (MHz/Torr)	dk_{ISI} (MHz/Torr)	k_{SW} [11] (MHz/Torr)	dk_{SW} [11] (MHz/Torr)
R23	- 1.31	1.34	- 1.02	0.03
R18	- 1.44	0.26	- 1.45	0.03
R12	- 1.05	0.16	- 0.98	0.03
R10	- 0.45	0.10	- 0.45	0.03
R9	- 0.06	0.12	- 0.09	0.02
R8	0.08	0.10	0.35	0.09
R7	0.48	0.16	0.58	0.12
R5	1.28	0.21	1.39	0.03
R3	1.64	0.28	1.87	0.04
P4	- 1.44	0.26	- 1.52	0.03
P5	- 1.30	0.20	- 1.40	0.03
P10	0.27	0.09	0.40	0.02
P16	1.93	0.29	2.30	0.06
P20	2.09	0.57	2.49	0.09
P24	1.48	1.23	2.06	0.03

and controllable down to 10^{-15} order. Given that it is possible to control the offset between the CTL and the OFC tooth frequency, the CTL frequency can be constantly scanned over the absorption line profile.

A feedback loop maintained the power stability of the laser, and the PD detected and monitored the power fluctuation. The acousto-optic modulator (AOM) served as the active element. The setup included two absorption cells (0.4 Torr nominal pressure, 40 cm length, Wavelength References, Inc. and 2 Torr nominal pressure, 40 cm length, Wavelength References, Inc). The use of two absorption cells simultaneously allowed me to calculate the pressure shift coefficient for each measured absorption line.

The profiles of fifteen absorption lines were scanned with the step of 1 MHz (50 kHz around the central part of the profile). The measured absorption line profile was then fitted, and the position of the absorption lines minimum was recovered with an uncertainty in the order of 100 kHz. Despite all of the attempts to improve the repeatability of the measurement, the problems with the (time-dependent) background in the measured spectrum remained. It shifted the absorption lines' positions by order of 100 kHz. The pressure shift coefficients, that were measured using two absorption lines Tab.6.1 corresponded to the coefficients presented in [11] Fig. 6.7.

Compared to [11], higher uncertainty is caused by the use of only two absorption cells to determine the pressure shift coefficients. Authors employed about ten cells and the least-square method to obtain coefficients. Furthermore, the relative pressure uncertainty in our cells was 10 %, limiting the measurement precision.

The subsequent step in improving the repeatability of the results was to reduce the background in the spectrum by optimising the beam splitters used in the experimental setup. The laser beam was sent through a selected beam splitter, and the signal from the reflective part helped to maintain the power stabilisation. Measured signal in the transmission branch can be seen in Fig. 6.8. The beam splitters used in the comparison were a non-polarising beam splitter cube (50:50 reflection: transmission), polka dot plate

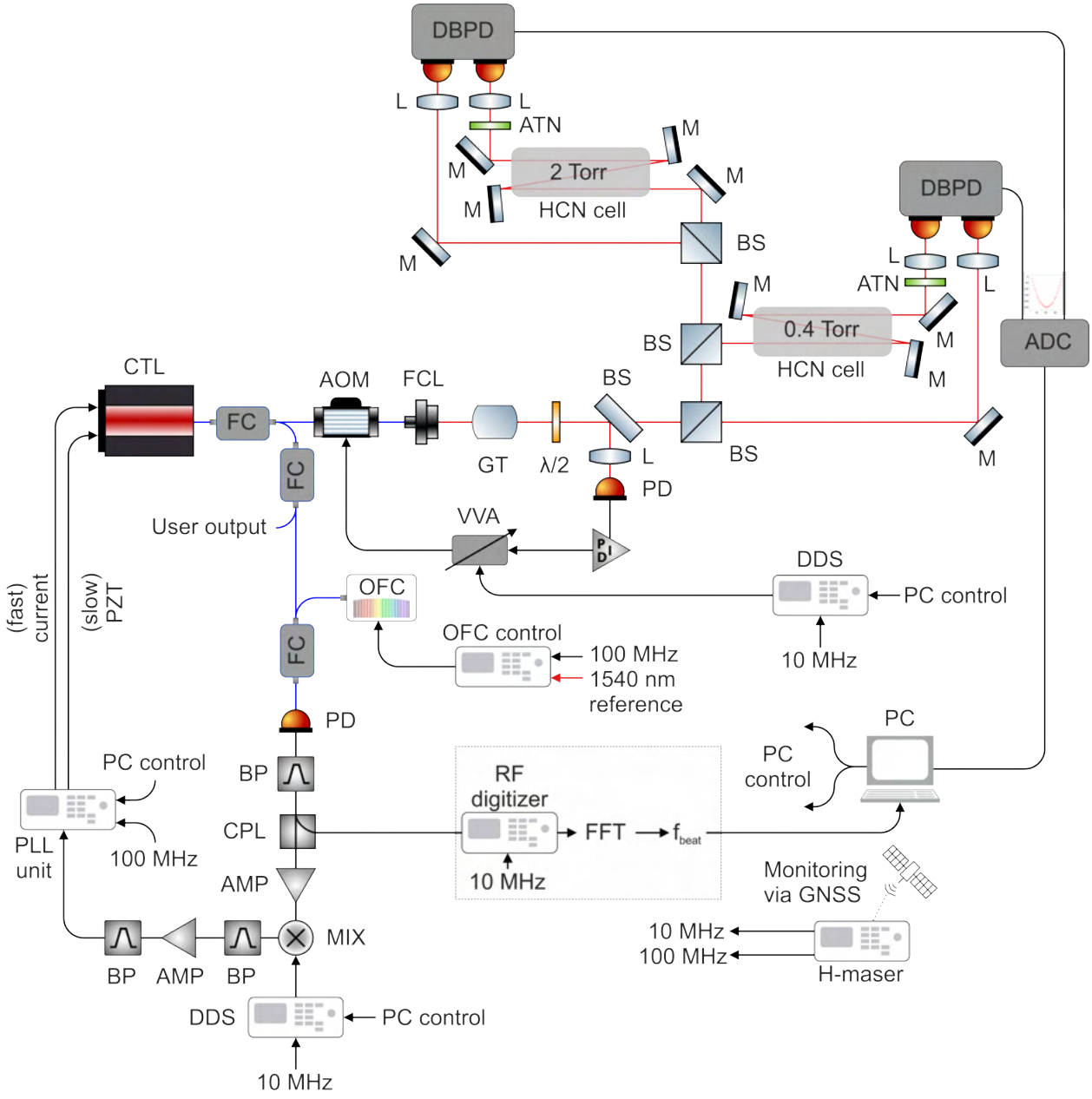

Figure 6.6: An experimental setup for modulation-free $H^{13}C^{14}N$ absorption lines centre measurement: acousto-optic modulator (AOM), amplifiers (AMP), analogue-digital converter (A/D), attenuators (ATN), band pass filters (BP), beam splitters (BS), continuously-tunable laser (CTL), direct digital synthesiser (DDS), double-balanced photodetector (DBPD), fast Fourier transform (FFT), Glan-Taylor crystal (GT), half-wave plates ($\lambda/2$), lenses (L), mirrors (M), optical frequency comb (OFC), phase locked loop (PLL) unit, photodetector (PD), polarising beam splitter (PBS), proportional–integral–derivative (PID) controller, radio frequency (RF) digitiser card, radio frequency coupler (CPL), radio frequency mixer (MIX), and voltage variable attenuator (VVA). Adapted from [54].

beam splitters (50:50 and 30:70 reflection: transmission) and Al coated custom-made plate (3 nm and 6 nm thick layer) beam splitters. Post testing, it turned out, that previously

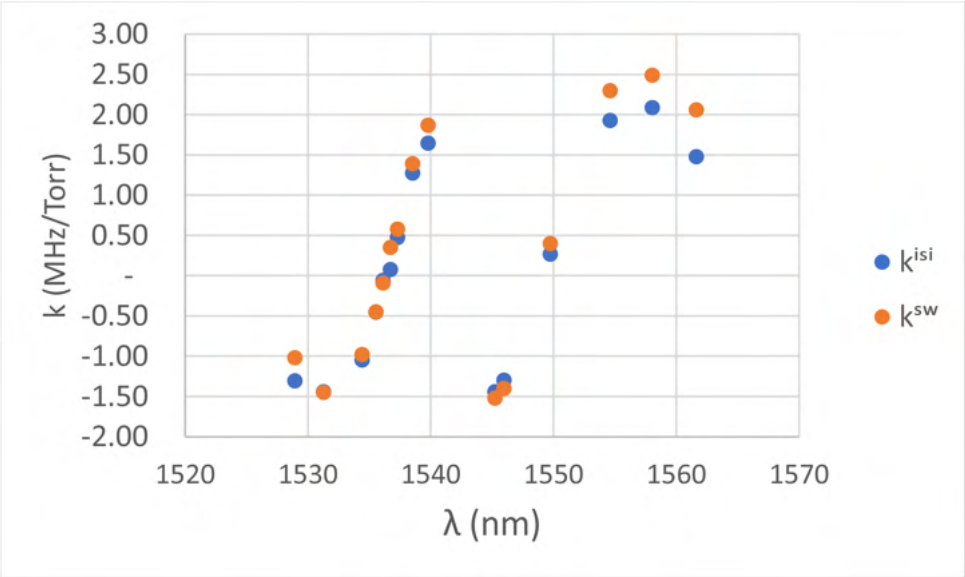

Figure 6.7: A comparison of the pressure shift coefficients measured by an experimental setup described previously k^{ISI} and those measured in [11] k^{SW}.

employed non-polarising beam splitter cube was the best choice. It proved as the best thanks to the lowest intensity of the parasitic background signal.

Even after testing different beam splitters, the described problem in the absorption spectrum background remained. The background was causing troubles by shifting the measured position of $H^{13}C^{14}N$ absorption lines centres. The theoretical calculations, in which I compared the fitting of the Gauss profile with and without a modelled background, showed that the background should not be more than 0.01 % of signal for high absorptive lines and 0.001 % for low absorptive lines. My conclusion corresponds with the [55], where authors say: "Expending only reasonable effort, the line centre of a pressure broadened

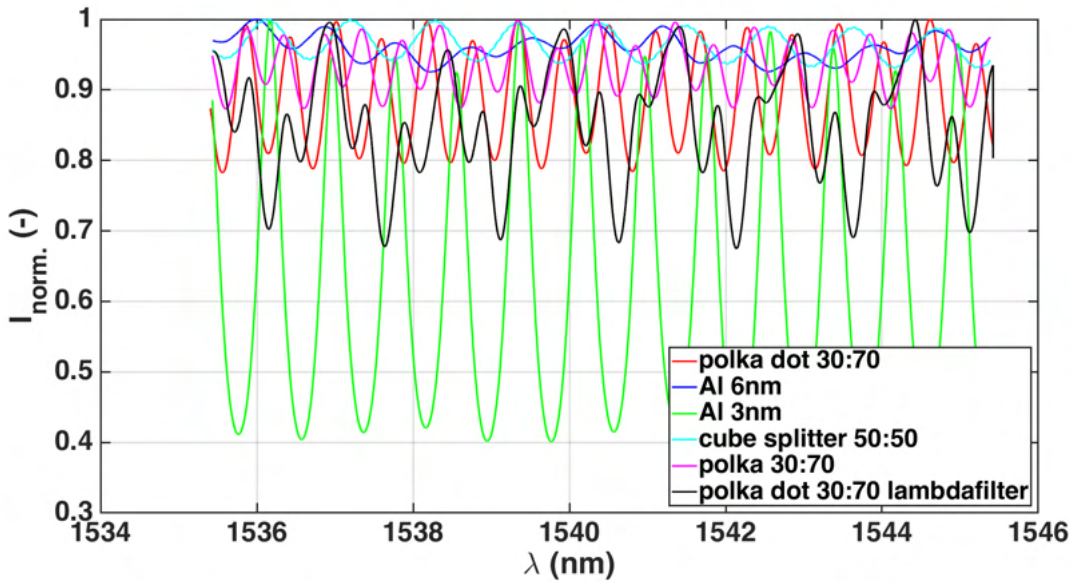

Figure 6.8: A comparison of the transmission signal from beam splitters. The CTL wavelength was tuned from 1535 nm to 1545 nm.

line typical of a molecular absorption wavelength reference cannot be defined to better than about $\pm 0.01\,\mathrm{pm}$". It corresponds to $\approx 1\,\mathrm{MHz}$ at $\lambda = 1550\,\mathrm{nm}$.

Further research was focused on the saturation absorption spectroscopy, permitting a high background suppression [16], as well as Doppler-free profile measurement.

7. Saturation absorption spectroscopy

Before the first attempts for the saturation absorption spectroscopy measurements in $H^{13}C^{14}N$, I calculated a saturation coefficient S (described in the section 4.2.1). The needed relaxation coefficient was taken from [56] and HCN partition function from [57]. The results showed two options, either to use high optical power to saturate the energy transitions in $H^{13}C^{14}N$ or to use low pressure of $H^{13}C^{14}N$. As the low-pressure absorption cells of HCN are not commercially available, the first attempts were performed with a high optical power.

7.1. High optical power approach

The instrumental equipment at the Institute of Scientific Instruments (ISI) includes a Koheras Boostik amplifier, that produces enough optical power for my experiment. The amplifier was seeded by the Koheras Adjustik E15 diode laser, which permitted to measure a single absorption line of $H^{13}C^{14}N$ (R2 line) at 1540.431 20 nm. The sketch of the experimental setup can be seen in Fig. 7.1.

To optimise the optical power propagating into the experimental setup, the half-wave plate ($\lambda/2$) and the polarising beam splitter (PBS) were combined to easily lower and to absorb the excessive optical power by a beam-dump (BD). The laser beam then went through the telescope. The telescope lowered the diameter of the beam to 2.5 mm. The beam with a lowered diameter could then pass through the Faraday isolator (FI). The FI afterwards protected the laser from the back-scattered light. The R2 absorption line of $H^{13}C^{14}N$ was saturated by 492 mW pump beam and then measured by 61 mW probe beam. After crossing the gas cell, the pump beam was absorbed by the BD. The probe beam hit the double-balanced photodetector (DBPD) (Nirvana 2017, Newport), subtracting the noise in the signal branch using the reference branch signal. The 0.5 m long gas cell was filled with 0.4 Torr (about 53 Pa) $H^{13}C^{14}N$. The laser frequency was modulated at 1.26 kHz modulation frequency with modulation depth $\approx$ 7.5 MHz. The detection was done by a lock-in amplifier at the third harmonic frequency.

The signal monitored on the oscilloscope can be seen in Fig. 7.2. It is important to highlight that the recorded signal is only illustrative and can not be under any circumstances used to determine the position of the absorption line centre. Due to a high pump power, the absorption line was power-broadened ($\approx$ 20 MHz full width at half maximum). For that reason, the high modulation depth was needed to optimise the signal-to-noise (S/N) ratio. The third harmonic signal at the crossing with the scanning signal shows an s-shape curve, that corresponds to the saturated line profile. This result confirmed that it is possible to measure the saturated absorption in $H^{13}C^{14}N$. However, it was necessary to decrease the gas pressure so that the pump beam optical power could be lowered too.

7.2. Low gas pressure approach

7.2.1. Preliminary experiments

The absorption cell used in the high optical power approach (0.4 Torr pressure) is a cell with the lowest pressure available on the market (up to my knowledge). The lowest

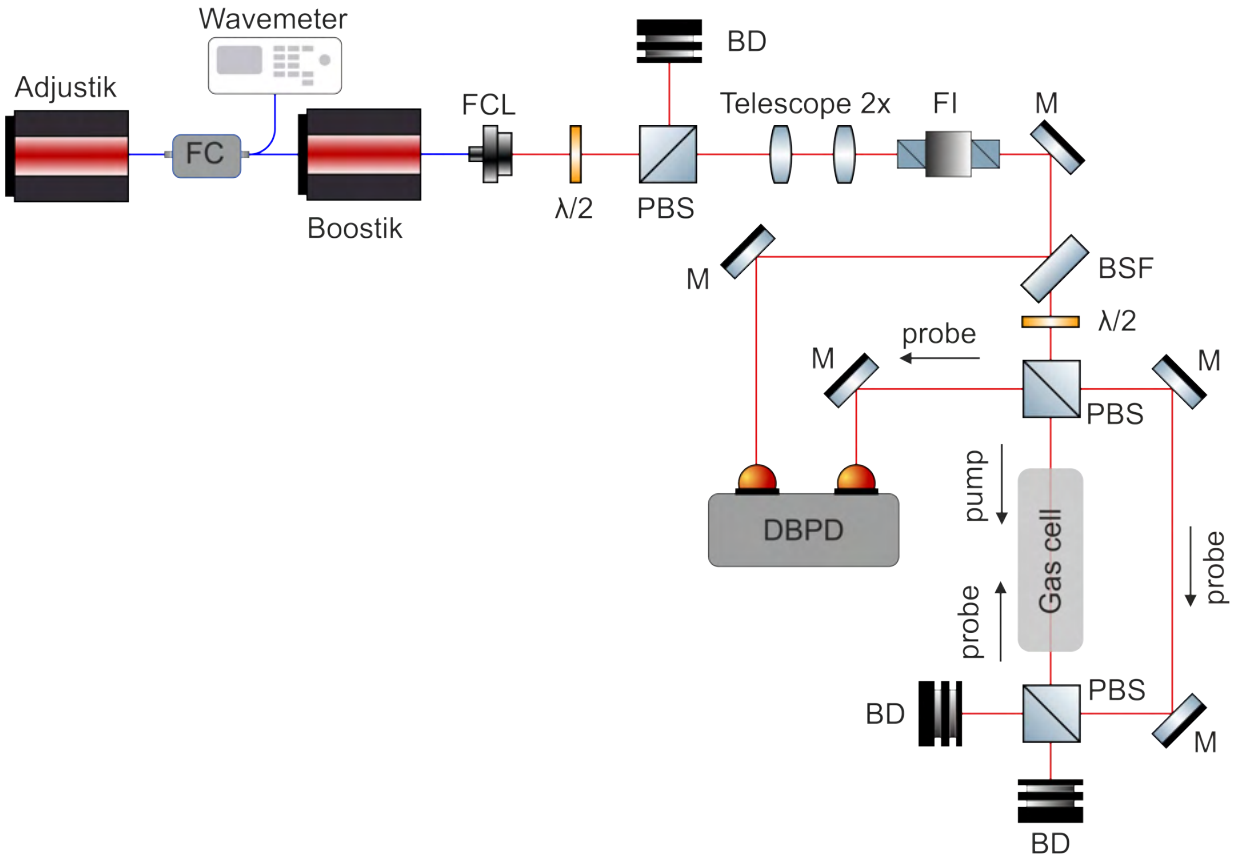

Figure 7.1: A saturation absorption spectroscopy setup based on the Koheras Boostik amplifier: beam-dumbs (BD), beam sampler (BSF), double-balanced photodetector (DBPD), Faraday isolator (FI), fibre collimator (FCL), fibre coupler (FC), half-wave plates ($\lambda/2$), mirrors (M), polarising beam splitters (PBS).

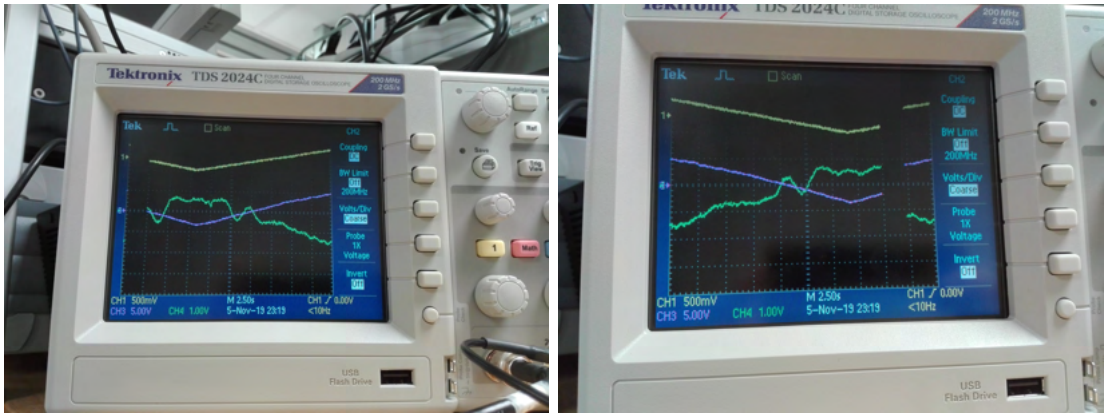

(a) (b)

Figure 7.2: The third harmonic detection signal (green) from scanning (violet) the saturated profile of $H^{13}C^{14}N$ R2 absorption lines.

pressure cell possesses a still too high pressure to be applied for the saturation absorption spectroscopy in order to determine the absorption lines' centre. After a detailed analysis of the possible solutions, a high-pressure vessel connected to a vacuum setup Fig. 7.3 seemed to fix the issue.

The gas reservoir was connected to the rest of the setup through a needle valve, allowing fine dosing of the absorption cell. I was able to monitor the gas pressure filled in the cell with the uncertainty of about 3 % thanks to the combination of the low precision wide-range vacuum gauge and the precise low-range capacitance vacuum gauge. Before filling the cell, it was evacuated by the turbomolecular vacuum pump. The cell was connected to the rest of the setup through a below, that protected the cell from being stretched or strained.

When the vacuum part of the experimental setup was built, I focused on building the optical part Fig. 7.4. The experimental configuration was similar to that presented in Fig. 7.1. The main difference was that the erbium-doped fibre amplifier (EDFA) replaced the Boostik as the needed optical power was lower (≈100 mW). The fibre cell was filled to 25 Torr (Wavelength References, Inc.) and served as reference to ensure that the wavelength of the laser corresponded to the wavelength of the absorption line centre.

The absorption cell during the first experiments (described in [58]) was filled to pressure 1-5 Pa, and the laser was modulated through the piezo with 1 kHz modulation frequency and 6 MHz modulation width. The pump power was about 130 mW and the probe beam power about 3.5 mW. I used the synchronous demodulation technique to obtain the third harmonic signal of the absorption line Fig. 7.5.

As I managed to record the first third harmonic signal, the problems with the S/N ratio degrading in time occurred. Up to my best knowledge, the reason behind this is the permanent dipole moment of HCN molecules, which makes them adsorb to the absorption cell walls. The effect is briefly mentioned in [44] but was not systematically studied. At first, the adsorption effect was pretty fast, as the S/N ratio of the third harmonic signal dropped to 50 % in about 45 minutes Fig. 7.6. It made the signal hardly usable for the absorption line centre determination, as the "effective" pressure in the cell was rapidly changing through the measurement.

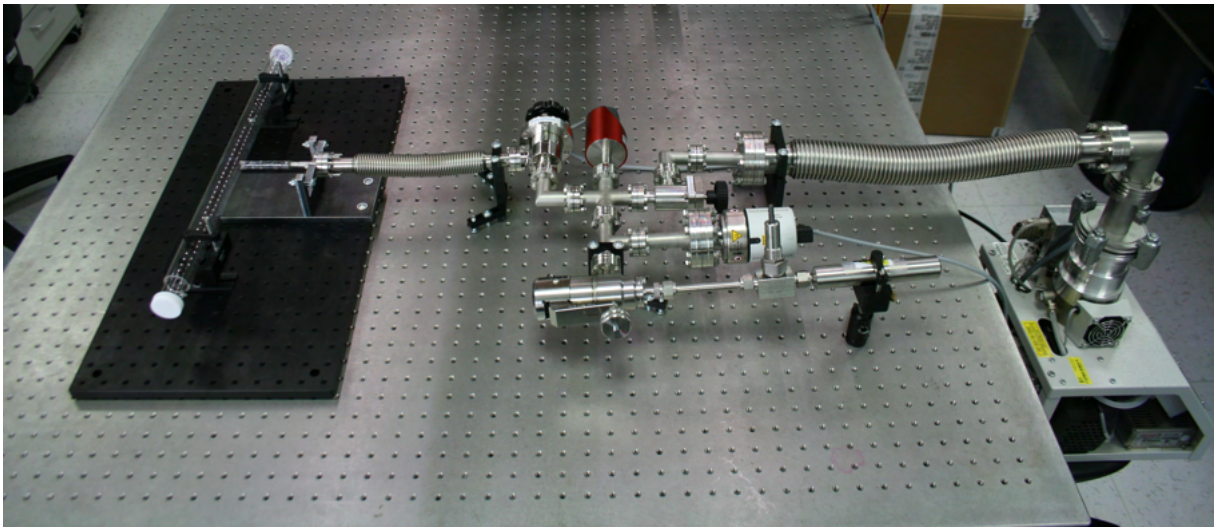

Figure 7.3: The vacuum setup for controllable filling of absorption cell.

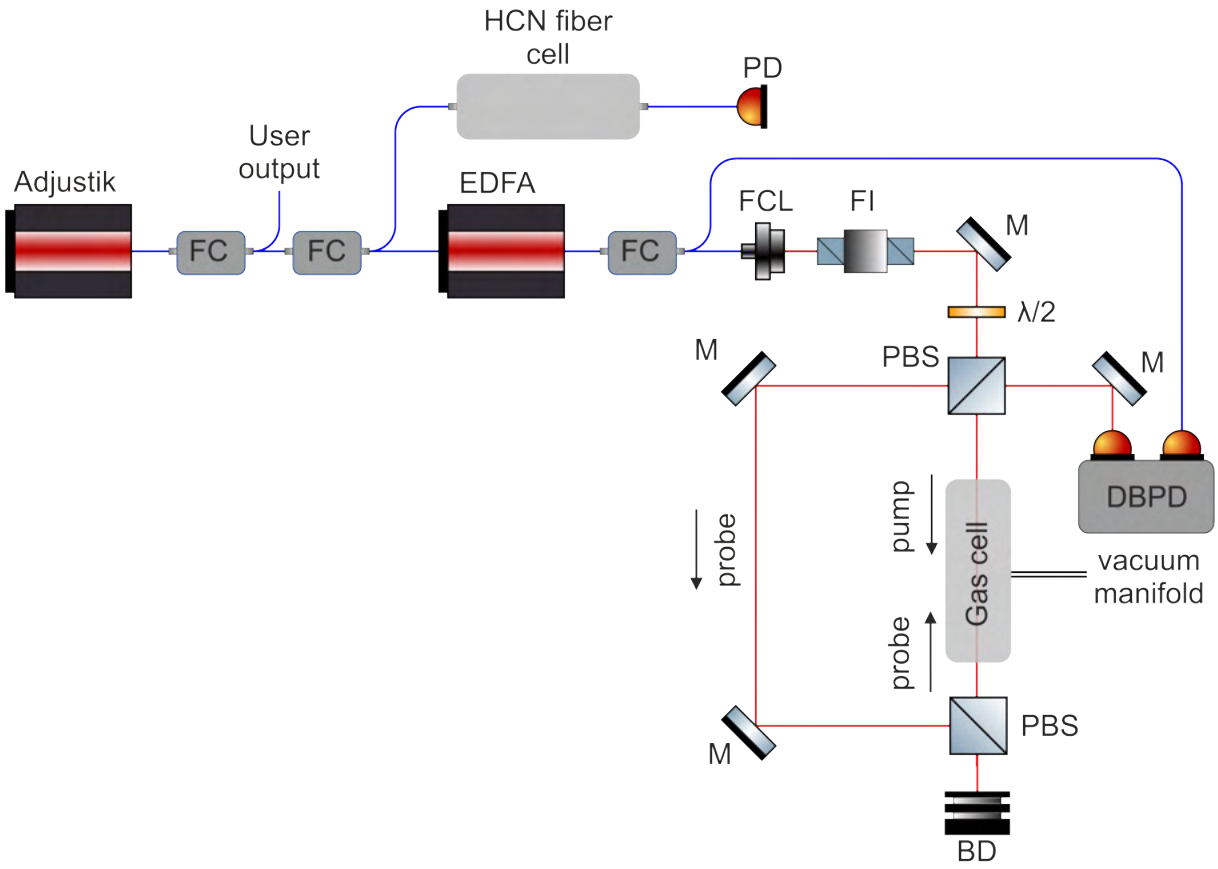

Figure 7.4: The optical part of the experimental setup for the saturation absorption spectroscopy in $H^{13}C^{14}N$: beam-dump (BD), double-balanced photodetector (DBPD), erbium-doped fibre amplifier (EDFA), Faraday isolator (FI), fibre collimator (FCL), fibre couplers (FC), half-wave plate ($\lambda/2$), mirrors (M), polarising beam splitters (PBS), photodetector (PD). Adapted from [58].

7.2.2. Molecule adsorption suppression

Saturating the gas cell wall by filling the cell with $\approx 10\,\mathrm{Pa}$ constituted the first attempt to remove the adsorption effect. After being filled up, the cell remained still for several days, and then the pressure was reduced to $\approx 2.5\,\mathrm{Pa}$. The error signal was then monitored, but unfortunately, no "presaturation" effect was observed.

The following attempt was to activate the inner walls of the cell by perfusion with an ozonised air for 90 minutes, with $\approx 50\,\mathrm{mg/h}$ of ozone. Then, the cell was filled with 1 % solution of chlorotrimethylsilane (Aldrich, >98 % by GC) in methanol (Penta chemicals, p.a.). Thereafter, the cell was incubated for 90 minutes at a room temperature. The solution was then discarded. The cell was thoroughly washed with pure methanol, blow-dried with a filtered air, and simultaneously heated to about 50 °C with a hot air gun (as described in [10]). It led to decline of the adsorption effect, so the S/N ratio of the third harmonic signal dropped to 50 % in about 6.5 hours Fig. 7.7. Anyway, further investigation on minimising the adsorption effect would be beneficial. However, given the lenght of my doctoral studies, I was not able to dedicate to this.

7.2.3. Table of $H^{13}C^{14}N$ absorption lines

Finally, further optimisation of the experimental conditions led to publication [10]. I utilised a continuously-tunable laser (CTL 1550, TOPTICA Photonics AG) with the build-in Faraday isolator as the laser source Fig. 7.8, which allows for mode-hop free tuning across the range from 1510 nm to 1630 nm. The CTL's optical frequency was locked to the particular tooth of the optical frequency comb (OFC) with the desired frequency offset. As the frequency offset was tunable, it permitted to tune the CTL

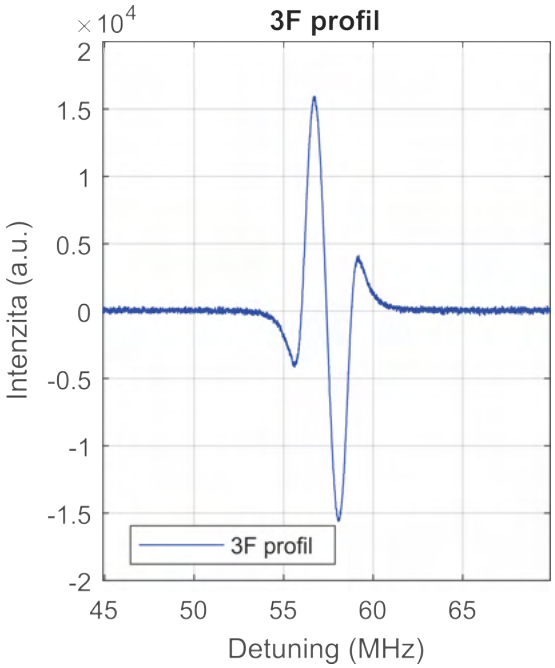

Figure 7.5: A saturated absorption profile. Adapted from [10].

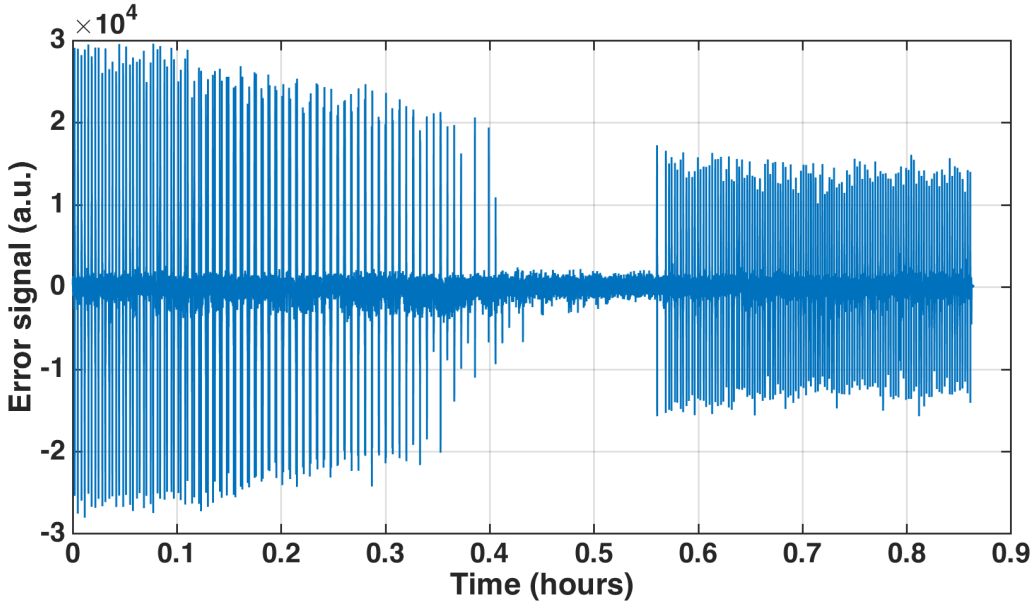

Figure 7.6: The decay of the third harmonic detection signal in time. The gap in the middle of the figure is caused by the absorption line profile getting out of the scanning interval.

frequency and to scan the absorption line profile (the offset lock was described in detail in [54]). The CTL's frequency was known with a relative accuracy of 10^{-13} and could be controlled down to the 10^{-15} level. The repetition frequency of the OFC (250 MHz) was referenced by H-maser (described in [51]). The absolute frequency of the H-maser was continuously tracked to a global navigation satellite system (GNSS) time. The GNSS tracing was enabled by the time transfer receiver instrument. Furthermore, the absolute frequency of the H-maser was non-periodically compared to the frequency of a $^{40}Ca^{+}$ ion optical clock [59].

The optical power coming from the CTL was frequency-modulated using AOM. The modulation frequency was 5 kHz, the modulation depth 3 MHz. The laser beam was then amplified by EDFA and power stabilised using the variable optical attenuator (VOA, V1550PA, Thorlabs). The pump beam power was kept at ≈120 mW and the probe beam power at ≈10 mW with a beam diameter of about 2.3 mm. The absorption cell was 40 cm long stainless steel tube with fused silica optical windows glued to the cell body by vacuum-compatible glue. Its inner surface was treated as described in the section 7.2.2. The pressure in the cell was kept between 1.45 Pa and 1.8 Pa, and the cell was refilled once every ≈ 0.5 hour.

The probe signal was synchronously demodulated using a digital lock-in amplifier (SRS 865, Standford Research Systems) and the third harmonic signal was detected. Each absorption line scan was performed in the range of ± 12.5 MHz around the absorption line centre with the step of 1 kHz around the centre and 5 kHz at the rest of the scan. The points around the central part of the profile were then interpolated by linear function to detect the zero-crossing, which corresponds to the absorption line centre. This way, I was able to measure fifty-six absorption lines of the $H^{13}C^{14}N$. The position of seventeen lines out of the total of fifty-six was already published in [10]. Those lines are marked by $^{+}$ in the Tab. 7.1 and Tab. 7.2. The rest of the lines are yet to be published.

The position of the absorption line centre was calculated to zero pressure using pressure shift coefficients measured in [11]. As authors did not measure pressure shift coefficients

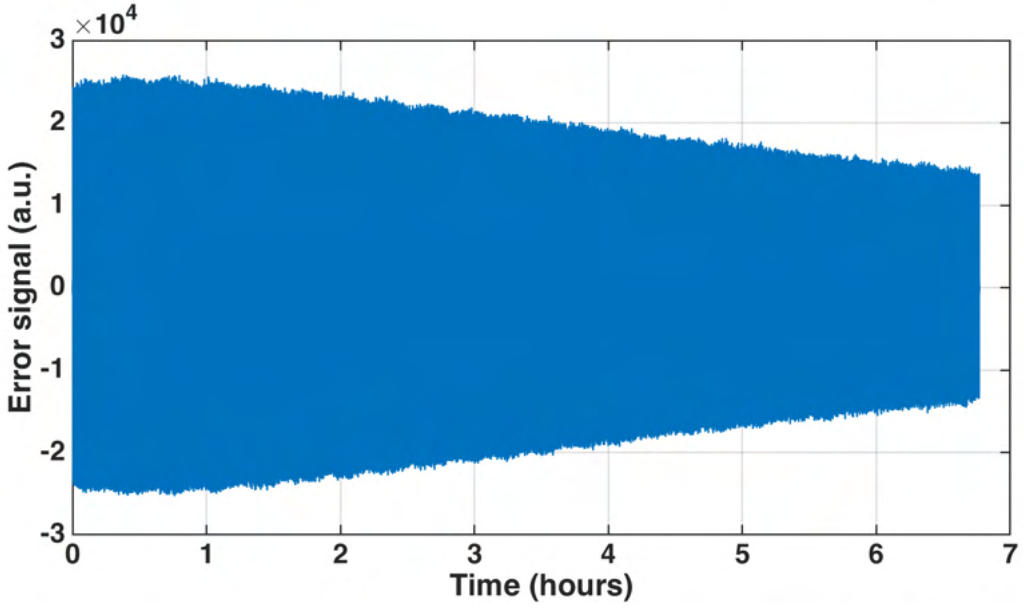

Figure 7.7: The decay of the third harmonic detection signal in time after passivisation of inner walls of the gas cell. Adapted from [58].

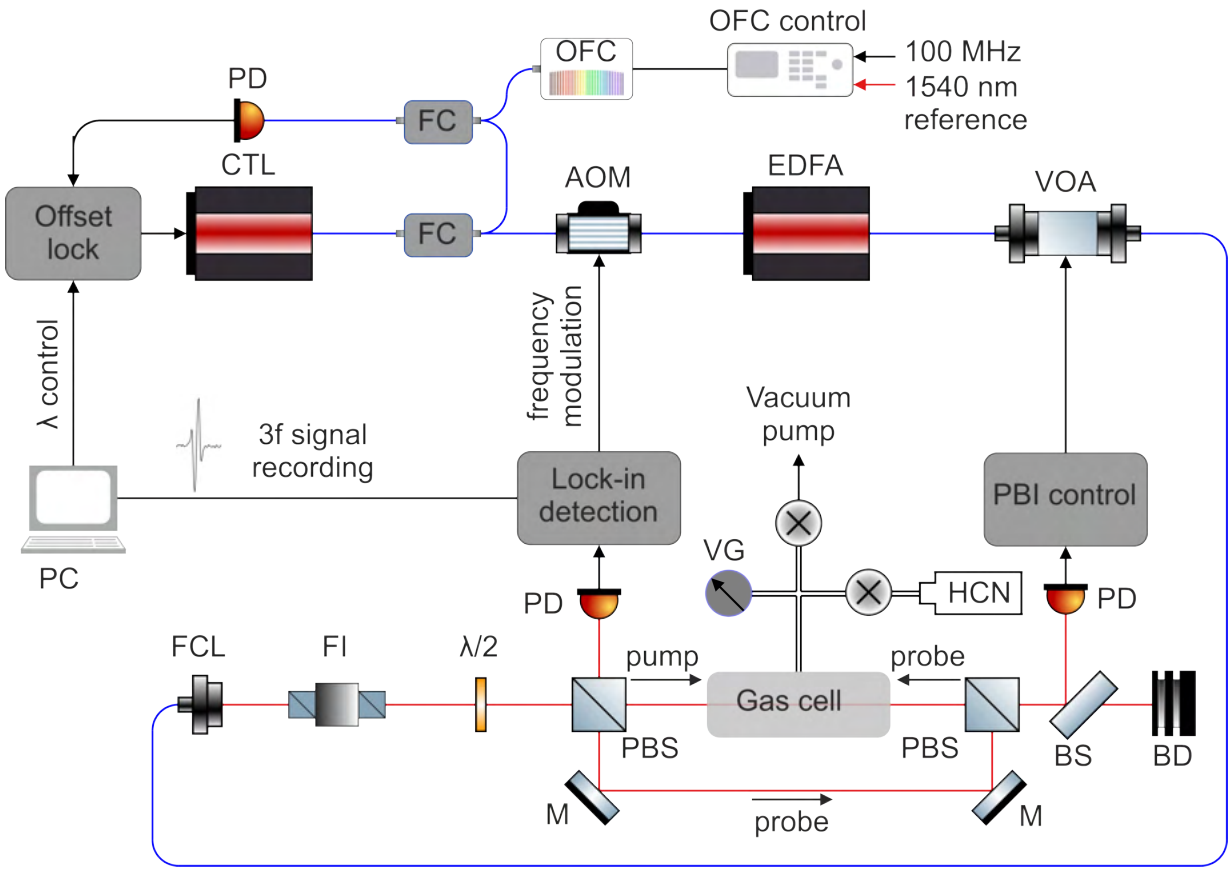

Figure 7.8: The experimental arrangement for the saturation absorption spectroscopy: acousto-optical modulator (AOM), beam-dump (BD), beam sampler (BS), computer (PC), continuously-tuneable laser (CTL), erbium-doped fibre amplifier (EDFA), Faraday isolator (FI), fibre collimator (FCL), fibre coupler (FC), mirrors (M), optical frequency comb (OFC), photodetectors (PD), polarising beam splitters (PBS), probe beam intensity (PBI), vacuum gauge (VG), variable optical attenuator (VOA). Adapted from [10].

of all of the absorption lines, a non-linear interpolation/extrapolation was used to obtain missing coefficients (these are marked in the Tab. 7.1 and Tab. 7.2 by *).

In the uncertainty of each measured line, these effects were considered (as mentioned in [10]): the uncertainty of the pressure shift coefficients and the pressure shift ($\approx 10\,\mathrm{kHz}$), the spread of measured absorption lines centre ($\approx 5\,\mathrm{kHz}$), the uncertainty of a fitting linear function ($\approx 3\,\mathrm{kHz}$), the residual zero offset and background profile ($\approx 3\,\mathrm{kHz}$), the residual offsets and drifts in the harmonic detection analogue control ($\approx 3\,\mathrm{kHz}$), and the additional safety margin for potential systematic shift effects. The safety margin was increased for the R2 and the R3 absorption lines due to the observed line profile distortion. The safety margin was also increased for the R27-R24 and the P25-P28 lines due to potential non-linear extrapolation error.

The measured absorption lines' centre position was compared with a position published in [11]. The difference between those positions was calculated in Tab. 7.1 and Tab. 7.2 and were graphically shown in the Fig. 7.9. Both results corresponded at $\lambda = 1560\,\mathrm{nm}$, where the wavelength meter in the [11] was referenced. At the wavelengths other than 1560 nm, the difference between data varies. On the other hand, with few exceptions, the

Table 7.1: Centre frequencies of R branch of the $2\nu_3$ band of $H^{13}C^{14}N$ interpolated to zero pressure.

Line	This work f_{ISI} (MHz)	Ref.[11] f_{SW} (MHz)	Difference δf (MHz)
R27	196299247.932 (40)*	196299247.943 (3213)	- 0.011
R26	196246352.984 (40)*	196246352.641 (2312)	0.343
R25	196192245.155 (40)*	196192244.523 (1669)	0.632
R24	196136925.519 (40)*	196136924.719 (1283)	0.800
R23	196080395.145 (25)$^+$	196080394.150 (1154)	0.995
R22	196022655.178 (25)*	196022654.167 (1025)	1.011
R21	195963706.778 (25)	195963705.654 (1025)	1.124
R20	195903551.125 (25)*	195903550.056 (1024)	1.069
R19	195842189.486 (25)*	195842188.474 (1023)	1.012
R18	195779623.109 (25)$^+$	195779622.061 (1023)	1.048
R17	195715853.317 (25)*	195715852.394 (1022)	0.923
R16	195650881.446 (25)*	195650880.461 (1021)	0.985
R15	195584708.867 (25)	195584708.057 (1021)	0.810
R14	195517337.014 (25)*	195517336.133 (1020)	0.881
R13	195448767.320 (25)*	195448766.576 (1019)	0.744
R12	195379001.274 (25)$^+$	195379000.555 (1019)	0.719
R11	195308040.399 (25)$^{+*}$	195308039.664 (1018)	0.735
R10	195235886.247 (25)	195235885.672 (1017)	0.575
R9	195162540.395 (25)$^+$	195162539.755 (1016)	0.640
R8	195088004.481 (25)$^+$	195088003.897 (1016)	0.584
R7	195012280.156 (25)$^+$	195012279.620 (1015)	0.536
R6	194935369.109 (25)*	194935368.616 (1014)	0.493
R5	194857273.056 (25)$^+$	194857272.495 (1013)	0.561
R4	194777993.774 (25)*	194777993.293 (1012)	0.481
R3	194697533.032 (40)$^+$	194697532.583 (1012)	0.449
R2	194615892.657 (40)$^{+*}$	194615892.235 (1011)	0.422
R1	194533074.564 (25)	194533074.164 (1010)	0.400
R0	194449080.484 (25)	194449080.077 (1009)	0.407

$^+$ Absorption lines centres published in [10].

* Absorption lines, for which the pressure shift coefficient was not measured in [11]. The pressure shift coefficient for these lines was obtained by a non-linear interpolation/extrapolation.

difference never gets higher than the uncertainty stated by authors in [11]. We assume that the differences between the data were the reason behind the discrepancies in the calibration using $H^{13}C^{14}N$ absorption cells [9].

The presented measurements of $2\nu_3$ band of $H^{13}C^{14}N$ constitute about fortyfold improvement to data published to date. Hopefully, this could significantly help to accept $H^{13}C^{14}N$ as a suitable spectroscopic medium. Moreover, it would lead to inclusion of $H^{13}C^{14}N$ on the list of *Recommended values of standard frequencies* [5] and *Mise en pratique for the definition of the metre in the SI* [12].

Table 7.2: Centre frequencies of P branch of the $2\nu_3$ band of $H^{13}C^{14}N$ interpolated to zero pressure.

Line	This work f_{ISI} (MHz)	Ref.[11] f_{SW} (MHz)	Difference δf (MHz)
P1	194277572.890 (25)	194277572.286 (1007)	0.604
P2	194190062.885 (25)*	194190062.342 (1006)	0.543
P3	194101385.001 (25)*	194101384.529 (1005)	0.472
P4	194011541.171 (25)$^+$	194011540.774 (1004)	0.397
P5	193920533.536 (25)$^+$	193920533.046 (1003)	0.490
P6	193828364.208 (25)*	193828363.735 (1003)	0.473
P7	193735035.335 (25)$^{+*}$	193735034.897 (1002)	0.438
P8	193640549.115 (25)*	193640548.757 (1001)	0.358
P9	193544907.760 (25)	193544907.333 (1000)	0.427
P10	193448113.529 (25)$^+$	193448113.185 (999)	0.344
P11	193350168.716 (25)	193350168.417 (998)	0.299
P12	193251075.636 (25)*	193251075.300 (997)	0.336
P13	193150836.645 (25)*	193150836.272 (996)	0.373
P14	193049454.131 (25)	193049453.813 (995)	0.318
P15	192946930.515 (25)*	192946930.197 (993)	0.318
P16	192843268.251 (25)$^+$	192843267.988 (992)	0.263
P17	192738469.822 (25)	192738469.544 (991)	0.278
P18	192632537.753 (25)*	192632537.513 (990)	0.240
P19	192525474.593 (25)*	192525474.335 (989)	0.258
P20	192417282.929 (25)$^+$	192417282.740 (988)	0.189
P21	192307965.380 (25)*	192307965.253 (987)	0.127
P22	192197524.596 (25)*	192197524.562 (986)	0.034
P23	192085963.269 (25)	192085963.273 (985)	- 0.004
P24	191973284.118 (25)$^+$	191973284.280 (1106)	- 0.162
P25	191859489.898 (40)*	191859490.268 (1228)	- 0.370
P26	191744583.389 (40)*	191744583.966 (1594)	- 0.577
P27	191628567.416 (40)*	191628568.387 (2205)	- 0.971
P28	191511444.841 (40)*	191511446.216 (3059)	- 1.375

$^+$ Absorption lines centres published in [10].

* Absorption lines, for which the pressure shift coefficient was not measured in [11]. The pressure shift coefficient for these lines was obtained by a non-linear interpolation/extrapolation.

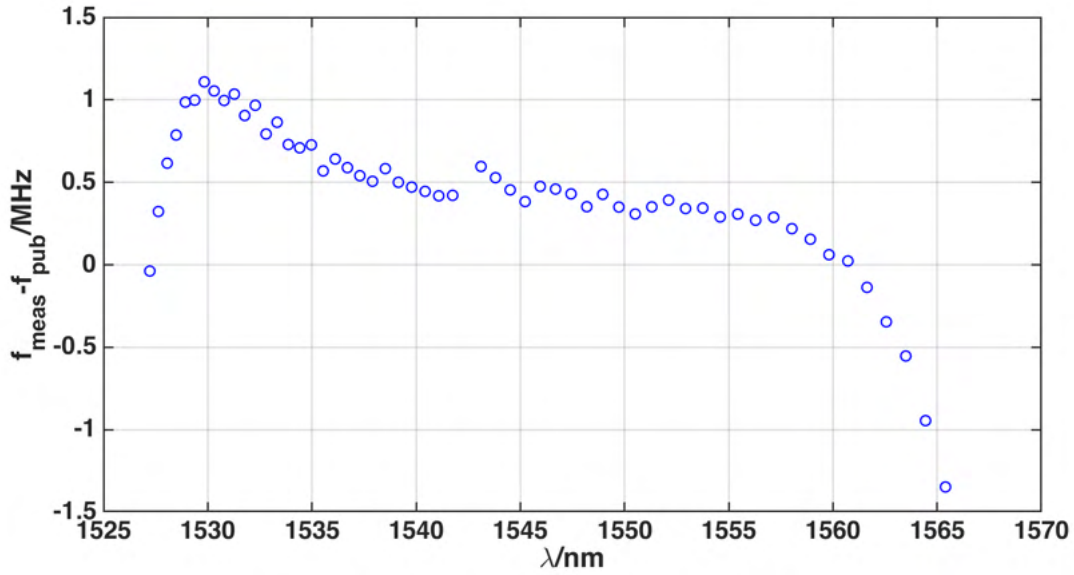

Figure 7.9: The differences between my data and data published in [11]. Adapted from [60].

8. Conclusion

In this doctoral thesis, I concentrated on the precise measurement of $H^{13}C^{14}N$ $2\nu_3$ band absorption lines position. To reach the objectives, I worked with an external cavity laser that scans the whole $H^{13}C^{14}N$ spectrum (1527 nm - 1565 nm). The laser frequency was measured using the beat note against the optical frequency comb. These two devices' operation principles are described in the Chapter 3.

The linear absorption spectroscopy is a relatively simple method allowing the study of absorption gases. This method is described in section 4.1. In the past, the linear absorption spectroscopy was applied for the $H^{13}C^{14}N$ absorption lines measurement already. In the most recent article [11], authors calculated the position of $H^{13}C^{14}N$ absorption lines with the uncertainty of 1 MHz. They also measured the pressure shift coefficients, permitting them to compare measurements at different gas pressures. In addition, they were able to subtract the pressure shift and to calculate the absorption line position at zero pressure.

The first experiments on the linear absorption spectroscopy were carried out with the Koheras Adjustik E15 laser. As the laser scanning range was only about 1 nm, it enabled me to measure a single absorption line (R2). The laser was frequency-locked to the minimum of the absorption line and kept as such for 8 hours. The achieved fractional frequency stability was in 10^{-8} order. These results were printed in [50].

Further experiments were done with the external cavity laser CTL 1550, that covers the whole absorption spectrum of the $H^{13}C^{14}N$. The position of twenty-six absorption lines [53] (reprint added at the end of this thesis), with the 2σ standard deviation of the frequency between 40 kHz and 70 kHz was measured. It corresponded to the relative stability of a laser locked to the absorption line minimum of about $9 * 10^{-12}$ at 1 s integration time. The repeatability of the measurement was the issue, as the absolute frequency after relocking to the absorption line minimum was varying in the 1 MHz order.

Moreover, a modulation-free approach was focused on, as that allowed us to measure the whole profile of the absorption line. The troubles with the background in the absorption spectrum were not successfully solved, even though the maximum effort was invested. The polarisation fluctuation was minimised using the Glan-Taylor crystal, and the temperature fluctuation of the absorption cell was decreased by building the temperature-controlling device.

The pressure coefficients were measured (see Tab. 6.1). As only two absorption cells were used, the uncertainty of the coefficients was higher than compared to the [11]. On the other hand, the coefficient trend Fig. 6.7 corresponds well with [11].

The Doppler broadening represents the principal limitation of the linear absorption spectroscopy measurements. The saturation absorption spectroscopy is overcoming the limitation by selectively saturating the absorption gas molecules moving perpendicular to the laser beam, as discussed in the section 4.2. The saturation of $H^{13}C^{14}N$ absorption lines was successfully performed in [42], [44]. On the contrary, no one measured the position of absorption lines or created a table of these absorption lines' centres.

Prior to the saturation absorption experiments, the optimal optical power vs. gas pressure was calculated. The calculation showed two possibilities, either to use the high optical power or the low gas pressure. Given the conditions at the time, it was decided to start with the high optical power approach. The Koheras Adjustik E15 laser seeded

the Koheras Boostik amplifier. Even though the saturation of the R2 absorption line was observed, the results were hardly publishable and inconclusive.

Following saturation spectroscopy experiments involved building the vacuum setup. Its purpose was to refill the absorption cell with sufficiently low $H^{13}C^{14}N$ pressure. It was necessary due to the lack of low-pressure cells on the market. The experiments involved external cavity laser CTL 1550 seeded to the erbium-doped fibre amplifier (EDFA). The experimental configuration Fig. 7.4 led to the observation of the saturated absorption line profile. The repeated scanning of the profile showed the degradation of the S/N ratio as reported in [58].

The issue with the S/N ratio degradation was successfully fixed. As a solution, the S/N ratio degradation was suppressed to the level where the systematic study of the absorption lines was possible. It allowed to use the experimental configuration Fig. 7.8 and to measure the position of fifty-six absorption lines' centre with the precision of 25 kHz. This represents the very first measurement of the $H^{13}C^{14}N$ absorption lines' centre position using the saturation absorption spectroscopy. This result also improves the precision of the prior data on $H^{13}C^{14}N$ [11] of about fortyfold [10] (reprint added at the end of this thesis). Besides, this improvement in the precision could lead to the wider application of $H^{13}C^{14}N$, as the reachable accuracy could improve.

The ultimate goal is to is to get included some of the $H^{13}C^{14}N$ lines in the list of *Recommended values of standard frequencies* [5]. To achieve this it is crucial that other experimental groups from all over the world further devote to the study of the saturated absorption data to demonstrate the repeatability of the measurement. To conclude, the following important step would be to improve the precision of the pressure shift coefficient published in [11].

9. Bibliography

[1] National Institute of Standards and Technology. Meter Bar 27. Online. Available from: https://www.nist.gov/sites/default/files/styles/960_x_960_limit/public/images/2016/09/22/meter27.jpg?itok=mYiPOq6W. [visited on 14-07-2023].

[2] Bureau International des Poids et Mesures. Resolution 6 of the 11th CGPM (1960). Online. Available from: https://www.bipm.org/en/committees/cg/cgpm/11-1960/resolution-6. [visited on 22-01-2024].

[3] Bureau International des Poids et Mesures. Resolution 1 of the 26th CGPM (2018). Online. Available from: https://www.bipm.org/en/committees/cg/cgpm/26-2018/resolution-1. [visited on 22-01-2024].

[4] A. J. Lewis, A. Yacoot, M. J. T. Milton, and A. J. Lancaster. A digital framework for realising the SI—a proposal for the metre. *Metrologia* 59 (4), 044004 (2022). doi: 10.1088/1681-7575/ac7fce.

[5] F. Riehle, P. Gill, F. Arias, and L. Robertsson. The CIPM list of recommended frequency standard values: guidelines and procedures. *Metrologia* 55 (2), 188–200 (2018). doi: 10.1088/1681-7575/aaa302.

[6] T.H. Yoon, J. Ye, J.L. Hall, and J.M. Chartier. Absolute frequency measurement of the iodine-stabilized He-Ne laser At 633 nm. *Applied Physics B* 72 (2), 221-226 (2001). doi: 10.1007/s003400000473.

[7] J. Lazar, J. Hrabina, P. Jedlicka, and O. Cip. Absolute Frequency Shifts Of Iodine Cells For Laser Stabilization. *Metrologia* 46 (5), 450-456 (2009). doi: 10.1088/0026-1394/46/5/008.

[8] T.W. Hänsch, M. D. Levenson, and A. L. Schawlow. Complete Hyperfine Structure Of A Molecular Iodine Line. *Physical Review Letters* 26 (16), 946-949 (1971). doi: 10.1103/PhysRevLett.26.946.

[9] J. Dale, B. Hughes, A. J. Lancaster, A. J. Lewis, A. J. H. Reichold. and M. S. Warden. Multi-channel absolute distance measurement system with sub ppm-accuracy and 20 m range using frequency scanning interferometry and gas absorption cells. *Optics Express* 22 (20), 24869–24893 (2014). doi: 10.1364/OE.22.024869.

[10] J. Hrabina, M. Hosek, S. Rerucha, M. Cizek, Z. Pilat, M. Zucco, J. Lazar, and O. Cip. Absolute frequencies of $H^{13}C^{14}N$ hydrogen cyanide transitions in the 1.5-μm region with the saturated spectroscopy and a sub-kHz scanning laser. *Optics Letters* 47 (21), 5704-5707 (2022). doi: 10.1364/OL.467633.

[11] W. C. Swann, and S. L. Gilbert. Line centers, pressure shift, and pressure broadening of 1530-1560 nm hydrogen cyanide wavelength calibration lines. *Journal of the Optical Society of America B* 22 (8), 1749-1756 (2005). doi: 10.1364/JOSAB.22.001749.

[12] R. Schödel, A. Yacoot, and A. Lewis. The new mise en pratique for the metre - a review of approaches for the practical realization of traceable length metrology from 10^{-11} m to 10^{13} m. *Metrologia* 58 (5), 052002 (2021). doi: 10.1088/1681-7575/ac1456.

[13] The Nobel Prize in Physics 1964, NobelPrize.org, Online. Available from: https://www.nobelprize.org/prizes/physics/1964/summary/. [visited on 20-10-2023].

[14] C. S. Long, P. W. Loveday, and A. Forbes. A piezoelectric deformable mirror for intracavity laser adaptive optics. *Proceedings Volume 6930, Industrial and Commercial Applications of Smart Structures Technologies 2008*. 2008. doi: 10.1117/12.776178.

[15] W. Demtröder. *Laser Spectroscopy: Vol. 1: Basic Principles*. 4 edition. Berlin: Springer. 2008. ISBN: 10.1007/978-3-540-73418-5.

[16] O. Cip, *Frequency stabilization of laser diodes and high precision laser interferometry*. Ph.D. thesis. Brno University of Technology, Faculty of Electrical Engineering and Computer Sciences. 2001.

[17] The Nobel Prize in Physics 2005. NobelPrize.org. Online, Available from: https://www.nobelprize.org/prizes/physics/2005/summary/ [visited on 20-10-2023].

[18] J. Ye, S. T. Cundiff, *Femtosecond Optical Frequency Comb: Principle, Operation, and Applications*. 1 edition. Boston: Kluwer Academic Publishers. 2005. ISBN: 978-0-387-23790-9.

[19] W. C. Swann and S. L. Gilbert, *Acetylene* $^{12}C_2H_2$ *absorption reference for* 1510 nm *to* 1540 nm *wavelength calibration - SRM 2517*. Standard Reference Materials. National Institute of Standards and Technology. 2001.

[20] S. L. Gilbert, W. C. Swann, *Carbon monoxide absorption references for* 1560 nm *to* 1630 nm *wavelength calibration - SRM 2514*. Standard Reference Materials. National Institute of Standards and Technology. 2002.

[21] J. Hrabina, M. Hola, J. Lazar, M. Sarbort, and O. Cip. Spectral Properties of Saturation Pressure Filled Iodine Absorption Cells. *Applied Optics* 53 (31), 839-842 (2014). doi: 10.1007/978-3-642-36359-7_153.

[22] J. Hrabina, O. Acef, F. du Burck, N. Chiodo, Y. Candela, M. Sarbort, M. Hola, and J. Lazar. Comparison of Molecular Iodine Spectral Properties at 514.7 and 532 nm Wavelengths. *Measurement Science Review* 14(4), 213-218 (2014). doi: 10.2478/msr-2014-0029.

[23] S. Schilt, L. Thevenaz, and P. Robert. Wavelength modulation spectroscopy: combined frequency and intensity laser modulation. *Applied Optics* 42 (33), 6728-6738 (2003). doi: 10.1364/AO.42.006728.

[24] Y. Du, Z. Peng, and Y. Ding. Wavelength modulation spectroscopy for recovering absolute absorbance. *Optics Express* 26(7), 9263-9272 (2018). doi: 10.1364/OE.26.009263.

[25] F. Bayer-Helmes, and J. Helmcke. *Modulation broadening of spectral profiles*. PTB-Me-17, PTB-Bericht. 1977.

[26] M. Weel, and A. Kumarakrishnan. Laser-frequency stabilization using a lock-in amplifier. *Canadian Journal of Physics* 80(12), 1449-1458 (2002). doi: 10.1139/p02-084.

[27] N. D. Gomes, M. A. Caracahnas, K. M. Farias, V. S. Bagnato. Laser cooling techniques: standard and alternated optical molasses. *Revista Brasileira de Ensino de Física* 39 (4), (2017). doi: 10.1590/1806-9126-RBEF-2017-0102.

[28] W. Demtröder. *Laser Spectroscopy: Vol. 2: Experimental Techniques*. 4 edition Berlin: Springer. 2008. ISBN: 978-3-540-74952-3

[29] O. Firstenberg, M. Shuker, R. Pugatch, D. R. Fredkin, N. Davidson, and A. Ron. Theory of thermal motion in electromagnetically induced transparency: Effects of diffusion, Doppler broadening, and Dicke and Ramsey narrowing. *Physical Review A* 77 (8), 043830 (2008). doi: 10.1103/PhysRevA.77.043830.

[30] A. Lesundak, T. M. Pham, M. Cizek, O. Obsil, L. Slodicka, O. Cip. Optical frequency analysis on dark state of a single trapped ion. *Optics Express* 28(9), 13091-13103 (2020). doi: 10.1364/OE.389411.

[31] A. D. Ludlow, M. M. Boyd, J. Ye, E. Peik, P.O. Schmidt. Optical atomic clocks. *Reviews of Modern Physics* 87(2), 637-701 (2015). doi: 10.1103/RevModPhys.87.637.

[32] H. Sasada, and K. Yamada. Calibration lines of HCN in the 1.5 μm region. *Applied Optics* 29 (24), 3535-3547 (1990). doi: 10.1364/AO.29.003535.

[33] M. Schneider, K. M. Evenson, M. D. Vanek, D. A. Jennings, and J. S. Wells. Heterodyne frequency measurements of $^{12}C^{16}O$ laser transitions. *Journal of Molecular Spectroscopy* 135 (2), 197-206 (1989). doi: 10.1016/0022-2852(89)90150-1.

[34] A. M. Smith, S. L. Coy, W. Klemperer, and K. K. Lehmann. Fourier transform spectra of overtone bands of HCN from 5400 to 15100 cm^{-1}. *Journal of Molecular Spectroscopy* 134 (1), 134-153 (1989). doi: 10.1016/0022-2852(89)90136-7.

[35] S.L. Gilbert, W. C. Swann, and C. M. Wang. Hydrogen cyanide $H^{13}C^{14}N$ absorption reference for 1530-1560 nm wavelength calibration - SRM 2519. *Standard Reference Materials*. National Institute of Standards and Technology. 1998.

[36] G. P. Barwood, P. Gill, and W. R. C. Rowley. Frequency measurements on optically narrowed Rb-stabilised laser diodes at 780 nm and 795 nm. *Applied Physics B* 53 (3), 142–147 (1991). doi: 10.1007/BF00330229.

[37] K. L. Corwin, I. Thomann, T. Dennis, R. W. Fox, W. Swann, E. A. Curtis, C. W. Oates, G. Wilpers, A. Bartels, S. L. Gilbert, L. Hollberg, N. R. Newbury, S. A. Diddams, J. W. Nicholson, and M. F. Yan. Absolute frequency measurements with a stabilized near-infrared optical frequency comb from a Cr:forsterite laser. *Optics Letters* 29 (4), 397–399 (2004). doi: 10.1364/ol.29.000397

[38] K. Nakagawa, M. de Labachelerie, Y. Awaji, and M. Kourogi. Accurate optical frequency atlas of the 1.5-μm bands of acetylene. *Journal of the Optical Society of America B* 13 (12), 2708–2714 (1996). doi: 10.1364/JOSAB.13.002708.

[39] A. B. Mateo, and Z. W. Barber. Precision and accuracy testing of FMCW ladar-based length metrology. *Applied Optics* 54 (19), 6019-6024 (2015). doi: 10.1364/AO.54.006019.

[40] X. Fan, J. Jiang, X. Zhang, K. Liu, S. Wang, Y. Yang, F. Sun, J. Zhang, C. Guo, J. Shen, S. Wu, and T. Liu. Self-marked HCN gas based FBG demodulation in thermal cycling process for aerospace environment. *Optics Express* 26 (18), 22944-22953 (2018). doi: 10.1364/OE.26.022944.

[41] X. Zhang, Y. Li, H. Hu, J. Jiang, K. Liu, X. Fan, M. Feng and T. Liu. Recovered HCN absorption spectrum-based FBG demodulation method covering the whole C-band for temperature changing environment. *IEEE Access* 8, 15039-15046 (2020). doi: 10.1109/ACCESS.2020.2966084.

[42] M. D. Labachelerie, K. Nakagawa, Y. Awaji, and M. Ohtsu. High-frequency-stability laser at 1.5 μm using Doppler-free molecular lines. *Optics Letters* 20 (6), 572–574 (1995). doi: 10.1364/ol.20.000572.

[43] Y. Awaji, K. Nakagawa, M. de Labachelerie, M. Ohtsu, and H. Sasada. Optical frequency measurement of the $H^{12}C^{14}N$ Lamb-dip-stabilized 1.5 μm diode laser. *Optics Letters* 20 (19), 2024–2026 (1995). doi: 10.1364/ol.20.002024.

[44] J. Henningsen, J. Hald, and J. C. Peterson. Saturated absorption in acetylene and hydrogen cyanide in hollow-core photonic bandgap fibers. *Optics Express* 13 (26), 10475-10482 (2005). doi: 10.1364/OPEX.13.010475.

[45] M. J. D. Low, N. Ramasubramanian, P. Ramamurthy, A. V. Deo. Infrared spectrum, surface reaction, and polymerization of adsorbed hydrogen cyanide on porous glass. *The Journal of Physical Chemistry* 72(7), 2371-2378 (1968). doi: 10.1021/j100853a016.

[46] K. Ruxton, A.L. Chakraborty, W. Johnstone, M. Lengden, G. Stewart, and K. Duffin. Tunable diode laser spectroscopy with wavelength modulation: Elimination of residual amplitude modulation in a phasor decomposition approach. *Sensors and Actuators B: Chemical* 150(1), 367-375 (2010). doi: 10.1016/j.snb.2010.06.058.

[47] M. Cızek, V. Hucl, J. Hrabina, R. Smıd, B. Mikel, J. Lazar, O. Cıp. Two-stage system based on a software-defined radio for stabilizing of optical frequency combs in long-term experiments. *Sensors* 14 (1), 1757-1770 (2014). doi: 10.3390/s140101757.

[48] J. Hrabina, M. Sarbort, O. Acef, F. Du Bruck, N. Chiodo, M. Hola, O. Cıp, and J. Lazar. Spectral properties of molecular iodine in absorption cells filled to specified saturation pressure. *Applied Optics* 53(31), 7435-7441 (2014). doi: 10.1364/AO.53.007435.

[49] C. S. Edwards, H. S. Margolis, G. P. Barwood, S. N. Lea, P. Gill, and W.R.C. Rowley. High-accuracy frequency atlas of $^{13}C_2H_2$ in the 1.5 μm region. *Applied Physics B: Lasers and Optics* 80 (8), 977–983 (2005). doi: 10.1007/s00340-005-1851-0.

[50] M. Hosek, S. Rerucha, L. Pravdova, M. Cizek, J. Hrabina, and O. Cip. Investigating the use of the hydrogen cyanide (HCN) as an absorption media for laser spectroscopy. *Proceedings Volume 10976, 21st Czech-Polish-Slovak Optical Conference on Wave and Quantum Aspects of Contemporary Optics*. 2018. doi: 10.1117/12.2517761.

[51] M. Cizek, L. Pravdova, T. Minh Pham, A. Lesundak, J. Hrabina, J. Lazar, T. Pronebner, E. Aeikens, J. Premper, O. Havlis, R. Velc, V. Smotlacha, L. Altmannova, T. Schumm, J. Vojtech, A. Niessner, and O. Cip. Coherent fibre link for synchronization of delocalized atomic clocks. *Optics Express* 30 (4), 5450-5464 (2022). doi: 10.1364/OE.447498.

[52] W. Riley, and D. Howe, *Handbook of Frequency Stability Analysis*. Special Publication. National Institute of Standards and Technology. 2008.

[53] M. Hosek, S. Rerucha, J. Hrabina, M. Cizek, and O. Cip. Measurement of the Hydrogen Cyanide Absorption Lines' Centers with the Potential for Mise en Pratique. *2021 Joint Conference of the European Frequency and Time Forum and IEEE International Frequency Control Symposium (EFTF/IFCS)*. 2021. doi: 10.1109/EFTF/IFCS52194.2021.9604261.

[54] M. Hosek, S. Rerucha, J. Hrabina, M. Cizek, L. Pravdova, and O. Cip. High-precision measurement of the center frequencies of the hydrogen cyanide (HCN) hyperfine transitions in the 1.5 μm wavelength band. *Proceedings Volume 12502, 22nd Polish-Slovak-Czech Optical Conference on Wave and Quantum Aspects of Contemporary Optics*. 2022. doi: 10.1117/12.2664209.

[55] W.C. Swann, and S.L. Gilbert. Accuracy limits for simple molecular absorption based wavelength references. *Technical Digest: Symposium on Optical Fiber Measurements*, 15-18 (2004). doi: 10.1109/SOFM.2004.183465.

[56] P.W. Hastings, M. K. Osborn, C. M. Sadowski, and I. W. M. Smith. Vibrational relaxation of HCN(002). *The Journal Of Chemical Physics* 78 (6), 3893-3898 (1983). doi: 10.1063/1.445111.

[57] R.J. Barber, G. J. Harris, and J. Tennyson. 2002. Temperature dependent partition functions and equilibrium constant for HCN and HNC. *The Journal Of Chemical Physics* 117 (24), 11239-11243 (2002). doi: 10.1063/1.1521131.

[58] J. Hrabina, M. Hosek, S. Rerucha, L. Pravdova, J. Lazar, O. Cip, and Z. Pilat. Saturated Spectroscopy of HCN. 2021 Joint Conference of the European Frequency and Time Forum and IEEE International Frequency Control Symposium (EFTF/IFCS). 2021. doi: 10.1109/EFTF/IFCS52194.2021.9604272.

[59] O. Cip, A. Lesundak, T. M. Pham, V. Hucl, M. Cizek, S. Rerucha, J. Hrabina, J. Lazar, P. Obsil, R. Filip, and L. Slodicka. The compact setup for laser cooling and high-resolution spectroscopy with cold $^{40}Ca^{+}$ ions. *2018 European Frequency and Time Forum (EFTF)*. 2018. doi: 10.1109/EFTF.2018.8409077.

[60] M. Hosek, J. Hrabina, S. Rerucha, M. Cizek, L. Pravdova, and O. Cip. Saturation Spectroscopy of $H^{13}C^{14}N$ Absorption Lines. *2023 Joint Conference of the European Frequency and Time Forum and IEEE International Frequency Control Symposium (EFTF/IFCS)*. 2023. doi: 10.1109/EFTF/IFCS57587.2023.10272040.

List of abbreviations

AD	Analogue-digital converter.
ADDA	Analogue-digital digital-analogue.
AMP	Amplifier.
AOM	Acousto-optic modulator.
AR	Anti-reflective.
ATN	Attenuator.
BD	Beam-dump.
BIPM	International Bureau of Weights and Measures. *Bureau international des poids et mesures.*
BP	Band pass.
BRG	Brag grating.
BS	Beam splitter.
BSF	Beam sampler.
CGPM	General Conference on Weights and Measures. *Conférence générale des poids et mesures.*
CH	Chopper.
CIR	Circulator.
CNAM	National Conservatory of Arts and Crafts. *Conservatoire national des arts et métiers.*
CPL	Radio frequency coupler.
CTL	Continuously-tunable laser.
DBM	Double-balanced mixer.
DBPD	Double-balanced photodetector.
DDS	Direct digital synthesiser.
DFB	Distributed feedback.
DFM	Danish Fundamental Metrology.
ECSL	External cavity semiconductor laser.
EDFA	Erbium-doped fibre amplifier.

FC	Fibre coupler.
FCL	Fibre collimator.
FFT	Fast Fourier transform.
FI	Faraday isolator.
FP	Fabry-Perot.
FPC	Fibre polarisation controller.
FR	Faraday rotator.
GNSS	Global navigation satellite system.
GPIB	General purpose interface bus.
GT	Glan-Taylor.
HC-PBG	Hollow-core photonic bandgap fibre.
HWHM	Half width at half maximum.
INRIM	National Metrology Institute of Italy. *L'Istituto Nazionale di Ricerca Metrologica.*
ISI	Institute of Scientific Instruments. *Ústav přístrojové techniky.*
KTP	Potassium titanyl phosphate.
L	Lens.
LaVA	Large Volume Metrology Applications.
LD	Laser diode.
LNE	National Laboratory of Metrology and Testing. *Laboratoire national de métrologie et d'essais.*
LP	Low pass.
M	Mirror.
MIX	Radio frequency mixer.
NIST	National Institute of Standards and Technology.
NPL	National Physical Laboratory.
OFC	Optical frequency comb.
PBI	Probe beam intensity.

PBS	Polarising beams splitter.
PC	Computer.
PD	Photodetector.
PID	Proportional–integral–derivative.
PLL	Phase locked loop.
PM	Photomultiplier.
PZT	Piezo crystal.
RAM	Residual amplitude modulation.
Ref	Reference.
RF	Radio frequency.
S/N	Signal-to-noise.
SI	International System of Units. *Système international.*
SRM	Standard Reference Material.
VG	Vacuum gauge.
VOA	Variable optical attenuator.
VVA	Voltage variable attenuator.
W	Sapphire window.
$\lambda/2$	Half-wave plate.
$\lambda/4$	Quarter-wave plate.

List of symbols

a	Slope of the frequency scan.
A	Area of the pump beam.
A_m, B_m	Fourier coefficients.
B_{12}	Einstein coefficient of induced absorption.
c	Speed of light in vacuum 299792458 $m \cdot s^{-1}$.
dk_{ISI}	Uncertainty of pressure shift coefficients measured at Institute of Scientific Instruments.
dk_{SW}	Uncertainty of pressure shift coefficients published in [11].
$E_{1,2}$	Energy of the higher and lower energy levels.
f	Frequency.
f_0	Offset frequency.
$f_{1,2}$	Absorption lines central frequency.
f_{AOM}	Acousto-optic modulator nominal frequency.
f_B	Beat-note frequency.
f_{HCN}	Central frequency of the hydrogen cyanide absorption line.
f_{ISI}	Frequency of hydrogen cyanide absorption lines measured at the Institute of Scientific Instruments.
f_L	Light frequency.
f_{modul}	Modulated frequency.
f_n	Frequency of the optical frequency comb.
f_r	Repetition frequency.
f_{Rb}	Central frequency of the rubidium absorption line.
f_{SW}	Frequency of hydrogen cyanide absorption lines published in [11].
$g_{1,2}$	Statistical weight of the lower and higher energy levels.
G	Gauss profile.
I	Light intensity lowered by crossing the distance z in the absorptive medium.
I_0	Light intensity before the absorptive medium.

h	Planck constant $6.626070040 \cdot 10^{-34}\ J \cdot s$.
$\hbar$	Reduced Planck constant $1.054571800 \cdot 10^{-34}\ J \cdot s$.
k	Boltzmann constant $1.380649 \cdot 10^{-23}\ J \cdot K^{-1}$.
k_{ISI}	Pressure shift coefficients measured at Institute of Scientific Instruments.
k_{SW}	Pressure shift coefficient published in [11].
l	Length of the active laser medium.
L	Lorentz profile.
n	Integer signing the order of the comb tooth.
N	Number of modulation periods.
$N_{1,2}$	Population density of lower and higher energy levels.
N_m	Number of molecules.
P	Pump beam power.
R^*	Effective relaxation rate.
$R_{1,2}$	Relaxation rates of the lower and higher energy levels.
S	Saturation coefficient.
t	Time.
t_T	Transit time of molecules through the laser beam area.
T	Starting time of the integration.
u_c	Uncertainty of the length measurement.
$u_{f1,2}$	The uncertainty of the absorption line centre frequency $f_{1,2}$.
V	Volume.
V_g	Voigt profile.
z	Distance travelled by the light in the absorptive medium.
$\alpha(\omega)$	Absorptive coefficient.
γ	Half width at half maximum of the Lorentz profile.
γ_l	Loss coefficient, including all the losses in the interaction cavity.
δf	Uncertainty of the frequency of hydrogen cyanide absorption lines measured at Institute of Scientific Instruments.

ΔE	Broadening of the energy level.
Δf	Modulation amplitude.
ΔN	Difference in the population densities of the energy levels.
$\Delta\nu_{Cs}$	Unperturbed ground-state hyperfine transition frequency of the caesium 133 atom 9 192 631 770 Hz.
σ	Half width at half maximum of Lorentz profile.
$\sigma_{cross.}$	Absorption cross section for the particular energy transition.
ϕ	Phase difference between the modulation and the demodulation frequency.
ω	Angular frequency.
ω_0	Angular frequency of the absorption line minimum.

List of publications

M. Hosek, S. Rerucha, L. Pravdova, M. Cizek, J. Hrabina, and O. Cip. Využití kyanovodíku jako absorpčního média pro laserovou spektroskopii. *Sborník příspěvků multioborové konference LASER 58*. 2018. ISBN: 978-80-87441-24-4.

M. Hosek, S. Rerucha, L. Pravdova, M. Cizek, J. Hrabina, and O. Cip. Investigating the use of the hydrogen cyanide (HCN) as an absorption media for laser spectroscopy. *Proceedings Volume 10976, 21st Czech-Polish-Slovak Optical Conference on Wave and Quantum Aspects of Contemporary Optics*. 2018. doi: 10.1117/12.2517761.

M. Hosek, S. Rerucha, J. Hrabina, M. Cizek, and O. Cip. Measurement of the Hydrogen Cyanide Absorption Lines' Centers with the Potential for Mise en Pratique. *2021 Joint Conference of the European Frequency and Time Forum and IEEE International Frequency Control Symposium (EFTF/IFCS)*. 2021. doi: 10.1109/EFTF/IFCS52194.2021.9604261.

J. Hrabina, M. Hosek, S. Rerucha, L. Pravdova, J. Lazar, O. Cip, and Z. Pilat. Saturated Spectroscopy of HCN. 2021 Joint Conference of the European Frequency and Time Forum and IEEE International Frequency Control Symposium (EFTF/IFCS). 2021. doi: 10.1109/EFTF/IFCS52194.2021.9604272.

M. Hosek, J. Hrabina, S. Rerucha, L. Pravdova, J. Lazar, and O. Cip. Měření absorpčních spekter HCN metodami laserové spektroskopie. *Sborník příspěvků multioborové konference LASER 61*. 2021. ISBN: 978-80-87441-28-2.

J. Hrabina, M. Hosek, S. Rerucha, M. Cizek, Z. Pilat, M. Zucco, J. Lazar, and O. Cip. Absolute frequencies of $H^{13}C^{14}N$ hydrogen cyanide transitions in the 1.5-μm region with the saturated spectroscopy and a sub-kHz scanning laser. *Optics Letters* 47 (21), 5704-5707 (2022). doi: 10.1364/OL.467633.

M. Hosek, S. Rerucha, J. Hrabina, M. Cizek, L. Pravdova, and O. Cip. High-precision measurement of the center frequencies of the hydrogen cyanide (HCN) hyperfine transitions in the 1.5 μm wavelength band. *Proceedings Volume 12502, 22nd Polish-Slovak-Czech Optical Conference on Wave and Quantum Aspects of Contemporary Optics*. 2022. doi: 10.1117/12.2664209.

M. Hosek, S. Rerucha, J. Hrabina, M. Cizek, L. Pravdova, and O. Cip. Systém pro skenování spektrálních čar kyanovodíku $H^{13}C^{14}N$. *Sborník příspěvků multioborové konference LASER 62*. 2022. ISBN: 978-80-87441-31-2.

M. Hosek, J. Hrabina, S. Rerucha, M. Cizek, L. Pravdova, and O. Cip. Saturation Spectroscopy of $H^{13}C^{14}N$ Absorption Lines. *2023 Joint Conference of the European Frequency and Time Forum and IEEE International Frequency Control Symposium (EFTF/IFCS)*. 2023. doi: 10.1109/EFTF/IFCS57587.2023.10272040.

Curriculum vitae

Ing. Martin Hošek

Address:	Charbulova 23, Brno, 618 00, Czech Republic
Telephone:	+420 731 486 415
E-mail:	martin.hosek1993@gmail.com
Nationality:	Czech

Education

2018 – ongoing (graduation 2024)	Brno University of Technology, Faculty of Mechanical engineering, branch – Physical and Materials Engineering, doctorals studies, the topic of the thesis: Methods for detecting the frequency of centers of Hydrogen-Cyanine (HCN) hyperfine transitions using a tunable laser in the range 1527 nm to 1563 nm
2016 – 2018	Brno University of Technology, Faculty of Mechanical engineering, branch – Physical engineering and nanotechnology, master studies, the topic of the thesis: Comparison of quantification strategies in Laser-Induced Breakdown Spectroscopy
2013 – 2016	Brno University of Technology, Faculty of Mechanical engineering, branch – Physical engineering and nanotechnology, bachelor studies, the topic of the thesis: Study of energy transitions in laser-induced plasma
2009 – 2013	Electro-technical high school, Kounicova 16

Other education and courses

2021	Online Python Academy Engeto
2019	Freemover course (Turin, Italy) – internship – Saturated absorption spectroscopy in HCN
2017	Erasmus course (Bari, Italy) – internship – comparison of plasma created by LIBS (laser-induced breakdown spectroscopy) and NELIBS (nanoparticle enhanced laser-induced breakdown spectroscopy)
2016	Belarusian State University (Minsk, Belarus) – internship – studies of lasers

2015	Photonics-enlighten me (Brussels, Belgium) – student course – photonics optics

Work experience

2018 – 2023	Institute of scientific instruments, Czech Academy of Sciences – laboratory work on optical setup for absorption spectroscopy
2016 – 2017	Institute of scientific instruments, Czech Academy of Sciences – design of optical setup for visualisation of Rayleigh-Bénard convection by laser-induced fluorescence

Skills

Languages:	Czech – native speaker
	English – level B2, passed FCE exam
Driving licence:	B
Computer skills:	https://github.com/hrasek, Python – Online python academy Engeto, HTML, CSS, JavaScript, Matlab, Arduino, Latex, Origin, LabVIEW, Comsol, MS Windows, MS Office, internet

Interests

Chess

Floorball

Football

Key publications reprints

Research article I

Measurement of the Hydrogen Cyanide Absorption Lines' Centers with the Potential for Mise en Pratique.

M. Hosek, S. Rerucha, J. Hrabina, M. Cizek, and O. Cip. *2021 Joint Conference of the European Frequency and Time Forum and IEEE International Frequency Control Symposium (EFTF/IFCS)*. 2021. doi: 10.1109/EFTF/IFCS52194.2021.9604261.

2021 Joint Conference of the European Frequency and Time Forum and IEEE International Frequency Control Symposium (EFTF/IFCS) | 978-1-6654-3935-0/21/$31.00 ©2021 IEEE | DOI: 10.1109/EFTF/IFCS52194.2021.9604261

Measurement of the Hydrogen Cyanide Absorption Lines' Centers with the Potential for Mise en Pratique

Hosek M.*, Rerucha S., Hrabina J., Cizek M., Cip O.
Institute of Scientific Instruments of the CAS
Brno, Czech Republic
*mhosek@isibrno.cz

***Abstract*—We built a linear absorption spectroscopy setup to measure hydrogen cyanide ($H^{13}C^{14}N$) $2\nu_3$ rotational-vibrational band. The laser's frequency was locked to the minimum of the absorption line by using the 1f technique. We used a commercially available lock-in amplifier combined with a custom-made PID controller allowing for the short-term frequency stability of about 10^{-10}. The laser frequency was determined by measuring the beat-note between the laser and the optical frequency comb. The laser was locked to each absorption line for about 8 hours and the final time record allowed us to determine the absorption line central frequency with the uncertainty of about 40 kHz. This shows significant improvement compared to the data already available for HCN. Our work can potentially lead to the acceptance of HCN for Mise en Pratique (MeP), which means that laser locked to one of the HCN lines can become the official source of the one-meter unit.**

Keywords—hydrogen cyanide, linear absorption spectroscopy, optical frequency comb, frequency reference, frequency stabilized lasers, SI meter

I. Introduction

The main goal of the LaVA project (Large Volume Metrology Applications), which the presented work is part of, is to improve the metrology capability of FSI (frequency scanning interferometry) instrumentation developed at NPL (National Physical Laboratory). One of the prerequisites for this method is the gas cell and the knowledge of its absorption lines' frequencies. Currently, the absorption media used in 1.55 µm absorption band is acetylene (C_2H_2), which is recognized in the MeP for the SI meter. The main benefit of hydrogen cyanide (HCN) over C_2H_2 is its broader absorption spectrum. $^{12}C_2H_2$ has an absorption spectrum of about 25 nm broad, $^{13}C_2H_2$ about 30 nm and $H^{13}C^{14}N$ about 40 nm broad that again can improve the FSI measurement accuracy. The available data for HCN [1] does not provide comparable accuracy to C_2H_2 [2], [3] mainly due to the use of not so precise measurement methods. Concretely, authors in [1] measured the lines' positions by scanning laser frequency over the profile of HCN absorption line and fitting it by Voight profile.

We firstly reported on our progress in [4]. Here we show that with the linear absorption spectroscopy method combined with the measurement of beat-note frequency between laser and optical frequency comb the HCN's absorption lines' centers can be determined more accurately by a factor of 100 in comparison with the previous results [1].

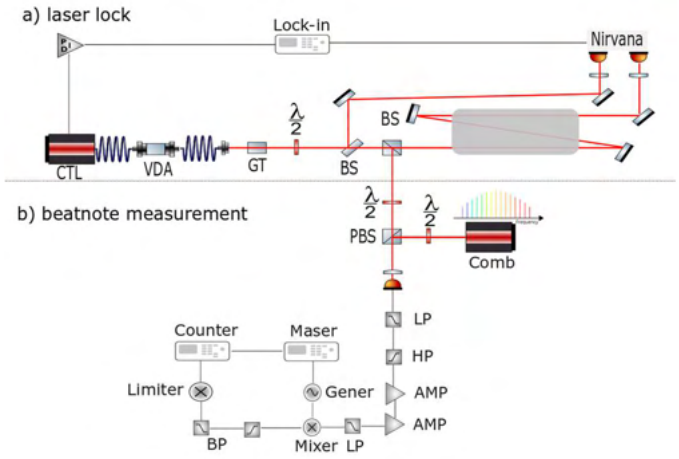

Fig. 1 Experimental setup – continuously tunable laser (CTL), voltage-driven attenuator (VDA), Glan-Taylor crystal (GT), beam splitter (BS), half-wave plate (λ/2), polarizing beam splitter (PBS), low-pass filter (LP), high-pass filter (HP), and band-pass filter (BP).

II. Methods

The laser source we used in our experiment is a continuously tunable laser (CTL), allowing the wavelength of the laser to be tuned from 1510 nm to 1630 nm, which is more than sufficient for the measurement of HCN $2\nu_3$ rotational-vibrational band that spreads from 1525 nm to 1565 nm.

The linear absorption spectroscopy setup shown in Fig. 1., consists of two distinct parts. In the first part, the laser beam goes through a voltage-driven attenuator and Glan-Taylor crystal, which ensures that laser beam power and polarization are stable during the whole measurement. The beam is then split into three parts. Two of them are used in the lock of laser frequency and the last one in the beat-note measurement, which will be described later in this paragraph. The two beams used for the laser lock hit the Nirvana balanced optical receiver. One of them goes through a commercially available 0.4 m long HCN gas cell filled to 0.4 Torr (~ 53 Pa). Windows of the cell are wedged, AR coated and fitted to the tubes at a small tilt to minimize the interference effects. The gas cell was put in a

978-1-6654-3935-0/21/$31.00 ©2021 IEEE

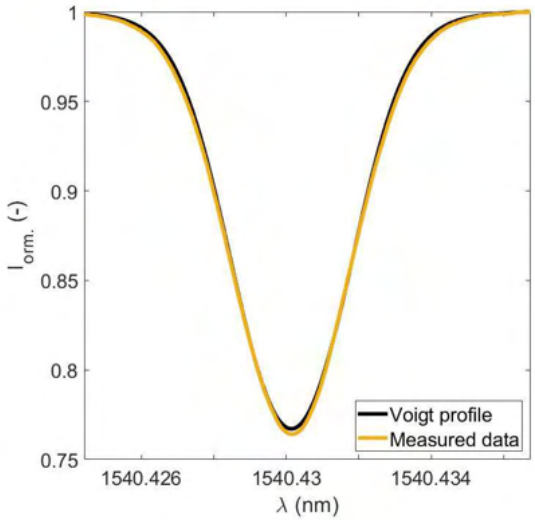

Fig. 2. Profile of the R2 absorption line.

temperature-controlling device, ensuring there are no temperature-induced changes of pressure in the cell during the measurement. We used a three-pass arrangement in order to improve the signal to noise ratio.

The signal from the Nirvana photodetector goes to the lock-in amplifier, which, combined with the PID controller, locks the laser frequency and closes the feedback loop. The lock-in amplifier referenced to active hydrogen maser produced the modulation frequency of 10 kHz and the modulation depth of about 6 MHz.

In the beat-note part of the experimental setup, the laser beam is combined with the optical frequency comb beam, and then hits the photodetector. The signal from the photodetector goes through a set of filters and amplifiers and then it is combined with the signal from the generator, which allows subtracting the modulation from beat-note. After the next filtering, the signal goes through a limiter that changes the shape of the beat-note, so it is more recognizable by a counter. The counter is referenced to 10 MHz coming from an H-maser.

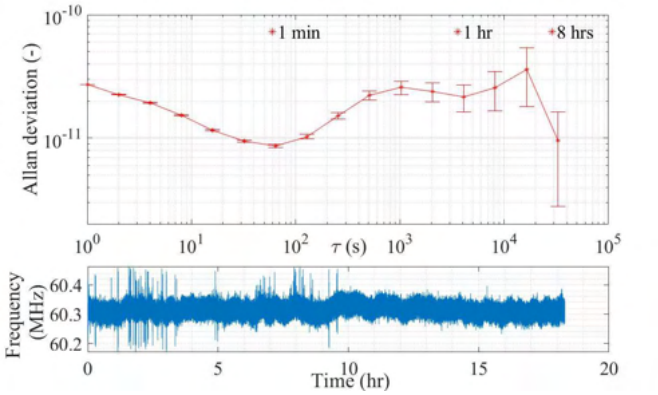

Fig. 3 Allan deviation (upper figure) calculated from the time record of laser frequency locked to R6 absorption line (lower figure).

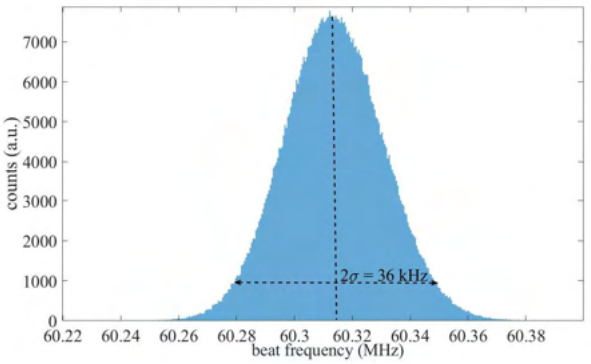

Fig.4. Histogram of frequency occurrences calculated from the laser frequency time record shown in Fig.3.

III. Results

We measured the frequency of the absorption lines' centers in the $2\nu_3$ rotational-vibrational band of $H^{13}C^{14}N$ (see line profile in Fig. 2.). All the lines were about 400 MHz broad, and the line intensity was varying from 50 % for the strongest lines down to 30 %. The main broadening mechanism is the Doppler broadening which can be eliminated by using saturated absorption spectroscopy. On the other hand, this method makes the experimental setup much more complex.

The position of every single line was measured by locking the laser frequency to its minimum and keeping it locked typically for 8 hours. The example can be seen in Fig. 3, where the length of a time record is about 18 hours. The Allan deviations show the short term stability of the laser locked to absorption line minimum in 10^{-10} order. Calculation of histogram then shows the unwanted trend in time record if there is any, and ideally, it should correspond to the Normal distribution. In our case, the histogram corresponds to the Normal distribution very well (Fig. 4), and the 2σ calculations

Table 1. Lines' centers of R branch HCN absorption line with the corresponding uncertainties.

R branch	frequency (MHz)	uncertainty (MHz)
2	194,615,893.43	0.06
3	194,697,533.81	0.06
4	194,777,994.36	0.04
5	194,857,273.35	0.04
6	194,935,369.49	0.04
7	195,012,280.18	0.04
8	195,088,004.33	0.04
9	195,162,540.03	0.05
10	195,235,885.62	0.05
11	195,308,039.52	0.05
12	195,379,000.21	0.05
13	195,448,766.29	0.04
14	195,517,335.80	0.05

Table 2. Lines' centers of P branch HCN absorption line with the corresponding uncertainties.

P branch	frequency (MHz)	uncertainty (MHz)
3	194,101,383.63	0.06
4	194,011,539.87	0.05
5	193,920,532.34	0.04
6	193,828,363.34	0.05
7	193,735,034.34	0.04
8	193,640,548.56	0.04
9	193,544,907.37	0.04
10	193,448,113.37	0.05
11	193,350,168.82	0.04
12	193,251,076.07	0.04
13	193,150,837.24	0.05
14	193,049,454.45	0.06
15	192,946,931.25	0.07

gives the uncertainty of about 40 kHz for the strongest lines.

You can see the summarizing tables with positions of absorption lines' centers in Table 1 for R branch of $2\nu_3$ rotational-vibrational band and in Table 2 for P branch. In our measurement, the most important sources of uncertainty for the positions of lines are the 2σ uncertainty of time record and the repeatability, which is more or less equal to it. Other sources of uncertainty are much less significant.

IV. Conclusion

The results described in the last section show great potential for HCN to become an alternative absorption medium to C_2H_2 in 1.5 μm absorption band (so-called C-band). All measured lines' positions, if calculated to zero pressure using pressure shift coefficients from [1], land well in the uncertainty interval of the previous results in [1] and [5].

Much work on this topic is still to be done, namely, e.g., evaluating the pressure shift coefficients of all HCN absorption lines to improve uncertainty from [1]. The results will then be compared with the same measurements done by other groups, and this set of results will hopefully lead to the application and the acceptance of HCN for MeP.

ACKNOWLEDGMENT

The work has been performed within the project 17IND03 LaVA. This project 17IND03 LaVA has received funding from the EMPIR programme co-financed by the Participating States and from the European Union's Horizon 2020 research and innovation programme. The research was also supported by projects: 19-14988S (GA CR) and CZ.02.1.01/0.0/0.0/16_026/0008460 (MEYS CR).

REFERENCE

[1] Swann,C., and Sarah G.. 2005. Line Centers, Pressure Shift, And Pressure Broadening Of 1530-1560 nm Hydrogen Cyanide Wavelength Calibration Lines. Journal Of The Optical Society Of America B 22 (8). J. Clerk Maxwell, A Treatise on Electricity and Magnetism, 3rd ed., vol. 2. Oxford: Clarendon, 1892, pp.68–73.

[2] Nakagawa, K., M. de Labachelerie, Y. Awaji, and M. Kourogi. 1996. "Accurate optical frequency atlas of the 15-μm bands of acetylene." Journal of the Optical Society of America B 13 (12). https://doi.org/10.1364/JOSAB.13.002708."

[3] Edwards, C. S., H. S. Margolis, G. P. Barwood, S. N. Lea, P. Gill, and W. R. C. Rowley. 2005. "High-accuracy frequency atlas of 13C2H2 in the 1.5 μm region." Applied Physics B 80 (8): 977-983. https://doi.org/10.1007/s00340-005-1851-0.

[4] Hosek, M, S. Řeřucha, L. Pravdova, M. Cizek, J. Hrabina, O. Cip, and P. Zemanek. 2018. "Investigating the use of the hydrogen cyanide (HCN) as an absorption media for laser spectroscopy." 21st Czech-Polish-Slovak Optical Conference on Wave and Quantum Aspects of Contemporary Optics, October: 8-. https://doi.org/10.1117/12.2517761.

[5] Gilbert, S. L. , W. C. Swann, and C. M.Wang, Hydrogen cyanide H13C14N absorption reference for 1530{1560 nm wavelength calibration|SRM 2519, Natl. Inst. Stand.Technol. (US) Spec. Publ. 260-137 (National Institute of Standards and Technology, 1998).

Research article II

Absolute frequencies of $H^{13}C^{14}N$ hydrogen cyanide transitions in the 1.5-μm region with the saturated spectroscopy and a sub-kHz scanning laser.

J. Hrabina, M. Hosek, S. Rerucha, M. Cizek, Z. Pilat, M. Zucco, J. Lazar, and O. Cip.
Optics Letters 47 (21), 5704-5707 (2022). doi: 10.1364/OL.467633.

Optics Letters

Absolute frequencies of $H^{13}C^{14}N$ hydrogen cyanide transitions in the 1.5-μm region with the saturated spectroscopy and a sub-kHz scanning laser

Jan Hrabina,[1] Martin Hosek,[1] Simon Rerucha,[1,*] Martin Cizek,[1] Zdenek Pilat,[1] Massimo Zucco,[2] Josef Lazar,[1] and Ondrej Cip[1]

[1]Institute of Scientific Instruments of the CAS (ISI), Kralovopolska 147, 61264 Brno, Czech Republic
[2]INRIM Istituto Nazionale di Ricerca Metrologica, Strada delle Cacce 91, Torino, 10135, Italy
*Corresponding author: res@isibrno.cz

Received 20 June 2022; revised 6 October 2022; accepted 12 October 2022; posted 12 October 2022; published 28 October 2022

The wide span and high density of lines in its rovibrational spectrum render hydrogen cyanide a useful spectroscopic media for referencing absolute frequencies of lasers in optical communication and dimensional metrology. We determined, for the first time to the best of our knowledge, the molecular transitions' center frequencies of the $H^{13}C^{14}N$ isotope in the range from 1526 nm to 1566 nm with 1.3×10^{-10} fractional uncertainty. We investigated the molecular transitions with a highly coherent and widely tunable scanning laser that was precisely referenced to a hydrogen maser through an optical frequency comb. We demonstrated an approach to stabilize the operational conditions needed to maintain the constantly low pressure of the hydrogen cyanide to carry out the saturated spectroscopy with the third-harmonic synchronous demodulation. We demonstrated approximately a forty-fold improvement in the line centers' resolution compared to the previous result.

https://doi.org/10.1364/OL.467633

Introduction. Two decades ago, the hydrogen cyanide (HCN) molecule emerged among spectroscopic media suitable for referencing the lasers' optical frequencies in the 1550-nm bands. It brought some interesting features as an alternative to commonly used isotopes of acetylene. The absorption lines' wavelength band is significantly wider than that of acetylene, and it particularly fits the most widely used C-band in the wavelength division multiplexing in optical fiber communications. The spectrum of HCN isotope $H^{13}C^{14}N$ $2\nu_3$ band contains more than 50 rovibrational transitions, shown in Fig. 1, useful for spectroscopic referencing the lasers' optical frequencies, provided that the absolute frequencies of the transitions are precisely determined.

The first thorough study [1] determined the frequencies of absorption line centers with the uncertainty of ≈ 15 MHz (which translates to a fraction uncertainty of 8×10^{-8}). More recent and the most exhaustive study so far [2] delivered more accurate data reaching the fraction uncertainty of 5×10^{-9} and added the characterization of a pressure-induced shift and Doppler broadening. These works used linear spectroscopy to determine the center of absorption lines, which is, however, influenced by the Doppler background. The use of saturated absorption spectroscopy can achieve a significant improvement, such as, for example, with the acetylene where the uncertainties fall below 1×10^{-11} for the $^{13}C_2H_2$ isotope [3].

The activities related to the latter study, carried out by NIST [2], might have brought the reception and recognition of HCN among the established spectroscopic media. Consequently, several commercial manufacturers started producing cells, and later on, HCN found its way to applications beyond optical communications.

In this paper, we demonstrate the feasibility of an approach to systematically measure the line centers' frequencies and other characteristics with (estimated) fractional uncertainty below 1.3×10^{-10} level. Then we present a comparison to previously published data, where our measurement revealed a systematic deviation from previous measurements.

Aims and challenges. Our effort was motivated by an application in dimensional metrology, namely the optical absolute distance measurement with frequency scanning interferometry (FSI) [5,6]. In single-wavelength interferometry, the fractional uncertainty of laser optical frequency, i.e., the ratio of the absolute uncertainty of the optical frequency (i.e., laser linewidth) to nominal optical frequency, translates to an equal uncertainty contribution in the length measurement $u_c = u_\nu/\nu$. The effect is more pronounced in the multi-wavelength absolute measurement (such as the FSI) where the uncertainties propagates (for two wavelengths) as $u_c = (u_{\nu 1} + u_{\nu 2})/(\nu_1 - \nu_2)$, i.e., the ratio of the sum of the linewidths to the difference of the optical frequencies. For example, with two lines at 1535 and 1550 nm, with uncertainty of $u_{\nu 1} = u_{\nu 2} = 1$ MHz (5×10^{-9}) used for the inference of absolute distance, would contribute 3×10^{-7} to the uncertainty of the length measurement. This uncertainty has two major components: (a) the precision of the line center resolution; and (b) the uncertainty of line center frequency. Our effort aims to tackle the latter.

Surprisingly, an atlas of precisely measured centers by the saturated absorption spectroscopy of hyper-fine hydrogen cyanide

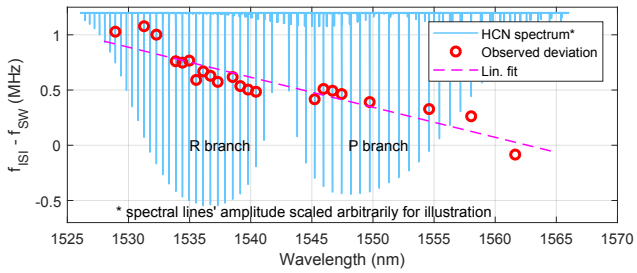

Fig. 1. Frequencies of the line centers measured with saturated spectroscopy (ν_{ISI}) compared to published data (ν_{SW}) [2]. The "HCN spectrum" shows the hydrogen cyanide $H^{13}C^{14}N$ $2\nu_3$ rotational–vibrational band spectrum obtained by scanning a tunable laser and measuring the laser intensity transmitted through an HCN cell with an interaction length of 120 cm and filled to a pressure of 267 Pa (2 Torr ±10%); the rolling ball filter [4] was used to remove the signal background.

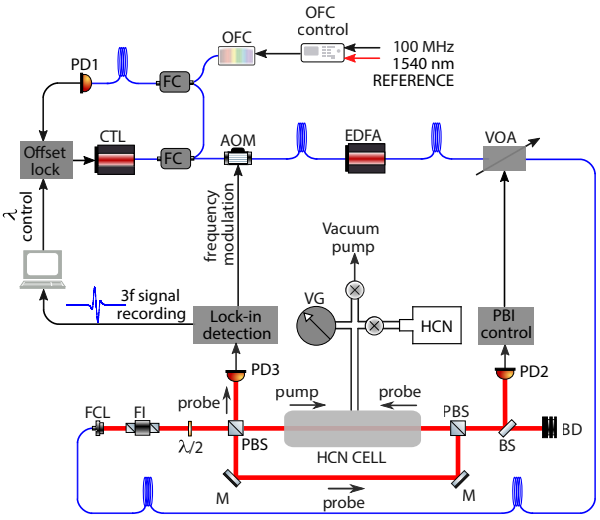

Fig. 2. Experimental arrangement. Optical frequency comb (OFC), continuously tuneable laser (CTL), Faraday isolator (FI), acousto-optical modulator (AOM), Er-doped fiber amplifier (EDFA), voltage-controlled optical attenuator (VOA), photodetectors (PD), polarizing beam splitters (PBS), mirrors (M), beam sampler (BS), beam dump (BD), vacuum gauge (VG), fiber couplers (FC), fiber collimator (FCL), probe beam intensity(PBI).

transitions was still not developed, although primary time standards [7] and optical atomic clocks [8] with relative stability higher than 10^{-16} are available now, and optical frequency combs [9] allow the transfer of such stability to any wavelength in the visible and infrared part of the spectrum. To date, "many narrow lines" have been observed in [10], which reported saturated spectroscopy using a cell placed inside a cavity to build up the necessary pump power but without determining the center frequencies. The insular measurement of the P27 line took place using a similar setup in [11], and the observation of the single R7 line's Lamb dip using an HCN-filled photonic fiber was reported in [12].

We identified a likely reason why any complex investigation did not occur: we found it challenging to maintain the HCN in stable conditions (in terms of pressure and observed line profile intensity) over a prolonged period when the HCN pressure is kept low (≈ several Pa). We attributed this effect partially to extensive adsorption and desorption of HCN molecules to gas cell walls, while we assume other effects are still present.

Methods. We developed an experimental apparatus, shown in Fig. 2, which allowed us to investigate the line centers' frequencies of HCN with high precision and absolute accuracy. Three principal parts of the setup were: (a) the widely tunable laser referenced to an optical frequency comb; (b) the vacuum system optimized for the HCN fine-resolution pressure control; and (c) the optical arrangement for saturated spectroscopy. For each investigated line, we used the precise control of the laser's optical frequency to scan over the line profile, record the amplitude profile of the third-harmonic error signal, and detect its zero crossing, which corresponds to the center frequency.

Highly coherent scanning laser. The optical setup was powered by the continuously tunable extended cavity diode laser (CTL) that features a mode-hop-free tuning range from 1510 nm to 1630 nm (CTL 1550, TOPTICA Photonics AG). The CTL's optical frequency was locked to a selected tooth of the optical frequency comb (OFC) using optical mixing and an in-house developed digitally controlled frequency offset lock, which incorporated a direct digital synthesizer (18-bit resolution) and a fast phase-locked loop unit (450-kHz bandwidth; based on AD9956 chip). This scheme allows us to precisely control the CTL's output frequency and also narrow the linewidth of the emission spectral profile from the initial ≈ 300-kHz down to the ≈ 100-Hz level. The OFC itself was optically referenced to a laser that was stabilized to an ultra-narrow linewidth optical cavity at 1540 nm. The repetition frequency of OFC (250 MHz) was disciplined by an H-maser [13]. Its absolute frequency is maintained by continuous tracking to a global navigation satellite system (GNSS) time through a time transfer receiver instrument [14](DICOM GTR50), and non-periodic comparisons with the $^{40}Ca^{+}$ ion optical clock [15]. With this arrangement, the absolute frequency of the CTL was well known with 10^{-13} accuracy and controllable down to the 10^{-15} level.

Vacuum system with pressurized absorption cell. The vacuum part of the setup consisted of the absorption cell, reservoir with HCN gas, vacuum gauge, and turbomolecular vacuum pump. The body of the 40-cm-long absorption cell was made of stainless steel equipped with a vacuum flange, enabling interconnection to the vacuum system. The cell's optical windows were made of fused silica and glued to the cell body by vacuum-compatible glue. The amount of gas could be precisely dosed by a needle valve from the reservoir filled with $H^{13}C^{14}N$ (Wavelength References, Inc.), and the pressure inside the cell was monitored with a capacitance vacuum gauge. The vacuum gauge offset was zeroed before each filling of the cell to keep the absolute scale of the gauge stable and repeatable.

To mitigate the low-pressure effects (such as the adsorption/desorption of HCN molecules to/from the cell body), the inside of the cell was activated by perfusion with ozonized air for 90 minutes, with ≈ 50 mg/h of ozone. Subsequently, the cell was filled with a 1% solution of chlorotrimethylsilane (Aldrich, >98% by GC) in methanol (Penta chemicals, p.a.) and incubated for 90 minutes at room temperature. The solution was then discarded, and the cell was thoroughly washed with pure methanol, blown dry with filtered air, and simultaneously heated to approximately 50 °C with a hot air gun.

Saturated spectroscopy setup. The investigation of the HCN absorption lines used a saturated spectroscopy optical setup. The output beam of the CTL was frequency modulated with

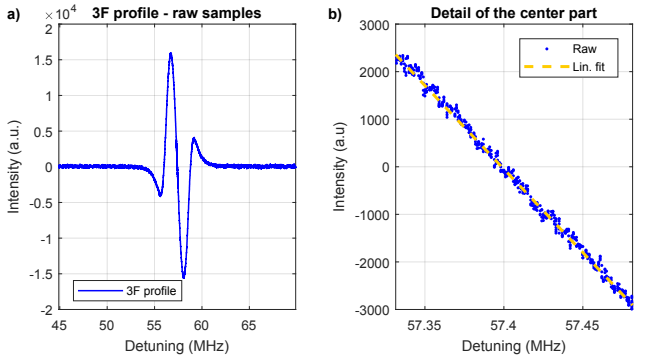

Fig. 3. (a) Third-harmonic profile of the R7 line of the $2\nu_3$ band obtained using 40-cm-long cell filled to a pressure of 1, 6 Pa and (b) the detail of the center part with an indicated linear fit.

an acousto-optical modulator/shifter (AOM) (5-kHz modulation frequency, 3-MHz FM deviation) and amplified in an Er-doped fiber amplifier (EDFA) with ≈ 200-mW output power. A voltage-controlled optical attenuator (VOA; V1550PA, Thorlabs) suppressed residual amplitude fluctuations. The laser light was fed through an optical fiber collimator and Faraday isolator into the free-space part of the optical setup, where it split on polarizing beam splitters into two counter-propagating beams: pump (≈ 120 mW) and probe (≈ 10 mW) with diameters of 2.3 mm. The probe signal from a 40-cm-long refillable absorption cell was synchronously demodulated using a digital lock-in amplifier (SRS 865, Standford Research Systems) with third harmonic detection. We would like to note that we identified the analog modulation signal as susceptible to residual offsets from zero and zero-drifts, which could cause significant shifts in the observed line centers' frequencies.

Measurement of the line centers' frequencies. Before actual measurement, the vacuum system was evacuated and then filled with HCN to the desired pressure. The laser frequency was detuned from the line profile, and the offset of the lock-in amplifier was zeroed (to suppress the residual amplitude modulation).

After preparation, the scanning sequence was commenced in the frequency range of ±12.5 MHz around the line center. We used 1-kHz steps around the central part of the profile and 5-kHz steps in the rest of the range at the rate of 100 ms/step. The intensity signal was digitized and recorded with auxiliary information (e.g., cell pressure).

From the recorded data (typical SNR ≈ 100 dB), shown in Fig. 3, we averaged the readings at individual points and (coarsely) removed any residual background caused by residual amplitude modulation and etalon effects in the optical part. We identified the third-harmonic profile's minimum and maximum, and interpolated the points around the central part to detect the zero-crossing, which corresponds to the line's center frequency.

To investigate the measurement repeatability, we ran repeated scans of the R7 line profile (arbitrarily selected) over slightly longer than a day. Then we selected and measured the profiles of 17 lines (those with convenient offset from the nearest OFC tooth), ten times each. We carried out the measurements with pressures between 1.45 Pa and 1.8 Pa.

Results and observations. The R7 line frequency recording, shown in Fig. 4(b), reveals the standard deviation of frequency determination of 0.5 kHz.

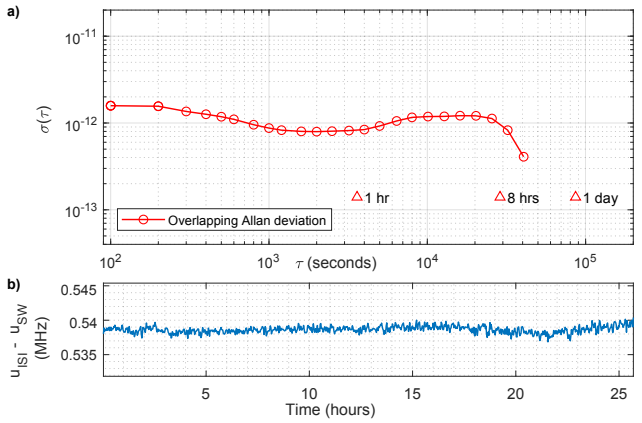

Fig. 4. (a) Overlapping Allan deviations calculated from repeated scanning over the R7 absorption line and (b) the frequency recording expressed as a coincidence of measurements with saturated spectroscopy (ν_{ISI}) and published data (ν_{SW}) [2].

Table 1. Center Frequencies of the $2\nu_3$ Band of $H^{13}C^{14}N$, Measured in a 40-cm Cell Filled to the Pressure of (1.65 ± 0.10) Pa and Interpolated to Zero Pressure[a]

Line	This work[b]	Ref. [2][c,d]	$\delta\nu$
	ν_{ISI} (Hz)	ν_{SW} (MHz)	(MHz)
R23	196080395.145 (25)	196080394.150(1154)	0.995
R18	195779623.109 (25)	195779622.061(1023)	1.048
R12	195379001.274 (25)	195379000.555(1019)	0.719
R11	195308040.399 (25)	195308039.664(1018)	0.734
R9	195162540.395 (25)	195162539.755(1016)	0.640
R8	195088004.481 (25)	195088003.897(1016)	0.584
R7	195012280.156 (25)	195012279.620(1015)	0.536
R5	194857273.056 (25)	194857272.495(1013)	0.561
R3	194697533.032 (40)	194697532.583(1012)	0.450
R2	194615892.657 (40)	194615892.235(1011)	0.422
P4	194011541.171 (25)	194011540.774(1004)	0.397
P5	193920533.536 (25)	193920533.046(1003)	0.491
P7	193735035.335 (25)	193735034.897(1002)	0.439
P10	193448113.529 (25)	193448113.185(999)	0.344
P16	192843268.251 (25)	192843267.988(992)	0.263
P20	192417282.929 (25)	192417282.740(988)	0.189
P24	191973284.118 (25)	191973284.280(1106)	-0.162

[a]Measured pressure coefficient from [2], Table 1 are considered.

[b]A general estimate of the uncertainty is stated.

[c]Calculated values from [2], table 4 are considered.

[d]The counter-intuitive slightly decreasing trend in uncertainties results from the fact the reference data are expressed as wavelength and with the precision of ≈ 0.12 MHz.

The overlapping Allan deviations, in Fig. 4(a), reach the bottom of 8×10^{-13} for $\tau \approx 1800$ s and the entire curve fits below 1.6×10^{-12}, which translates to 0.3 kHz. The frequency recording is compensated for the pressure shifts and also for slight drifts (0.05 Pa/hr) in the pressure measurement we observed during the measurement. Further investigation is needed here.

The line centers measured so far and extrapolated to zero pressure using the previously published pressure coefficients [2], displayed in Table 1, reveals approximately forty-fold improvement in the uncertainty of the center frequency determination compared to [2]. For the present data, the 25-kHz (40-kHz) uncertainty was stated uniformly. This qualified estimate took

into account uncertainty in pressure coefficients and pressure measurement (≈ 10 kHz), the observed spread of values with repeated measurement of individual lines (≈ 5 kHz), the uncertainty of the fitting function (≈ 3 kHz), residual zero-offset or profile background (≈ 3 kHz), residual offsets and drifts in the harmonic detection analog control (≈ 3 kHz), and additional (large) safety margin for potential systematic effects in, e.g., the degree of purity of HCN gas, in-homogeneous density of the HCN gas in the cell, and other phenomena unknown in this period of the research. The uncertainty was increased for lines R2, R3 (40 kHz) due to observed distortion in the profile, which we attribute to residual spectroscopic features in close vicinity of the measured line. Further investigation is required before the complete atlas will be issued. For the comparison with the previously published measurement, we used the calculated frequencies, their uncertainties, and pressure shifts from [2].

The results indicate a linear trend in the frequency deviations depending on the absorption line frequency, as shown in Fig. 1. It reveals that the present data systematically deviate from previous data toward higher frequencies. The deviation lies within the stated uncertainty for the previous data (except for the R18); nonetheless, in applications using, for instance, the frequency resolution against multiple lines, this deviation might skew the measurement results significantly. We may attribute this systematical deviation to the fact that the wavelength meter used for the measurement in [2] was referenced right at the $\lambda = 1560$ nm, where both datasets better coincide. The observed systematic deviation also might explain the HCN cell calibration issues discussed in [5].

Conclusion. We developed the widely tunable scanning laser system with sub-kHz linewidth and the absolute accuracy of 10^{-13}. In conjunction with the optical assembly for saturated spectroscopy and a vacuum system allowing for precise pressure control in the gas cell, the third-harmonic profiles of selected lines in the $H^{13}C^{14}N$ $2\nu_3$ band were measured.

We measured ≈ 30% of the lines in the spectrum of interest with an associated uncertainty down to 25 kHz ($<1.3 \times 10^{-10}$ fractional uncertainty). The precision achieved represents an approximately forty-fold improvement against previous investigations [2]. To the best of our knowledge, a systematic investigation of such an amount of individual lines by saturated spectroscopy has not been reported before. Compared to the previously published data, we generally confirmed the validity and correctness of the previous results. However, we identified a systematic deviation of the line centers' determination below the resolution of the original data.

We demonstrated a methodology allowing for further measurement of the complete spectra of interest, detailed investigation of the pressure effects, and stated the associated uncertainties. Such an outcome would hopefully be a valuable addition to the current state-of-the-art in the well-known and accepted spectroscopic references for the realization of the SI meter in the 1550-nm region. The refined spectroscopic data might help the hydrogen cyanide toward inclusion in the CIPM's *Recommended values of standard frequencies* [16] and *Mise en pratique for the definition of the SI meter* [17].

Funding. European Metrology Programme for Innovation and Research (17IND03 LaVA); Ministerstvo Školství, Mládeže a Tělovýchovy (CZ.02.1.01/0.0/0.0/16_026/0008460, CZ.1.05/2.1.00/01.0017, LO1212); Akademie Věd České Republiky (RVO:68081731).

Acknowledgments. Authors acknowledge the support from and fruitful discussion with the team from NPL, UK involved in the LaVA project (A. Lewis, B. Hughes, M. Campbell). Authors acknowledge the support with HCN-related calculations from our dear colleague Prof. Frédéric Du Burck from Laboratoire de Physique des Lasers, Université Sorbonne Paris Nord. The project 17IND03 LaVA has received funding from the EMPIR programme co-financed by the Participating States and from the European Union's Horizon 2020 research and innovation. The research used infrastructure supported by MEYS CR, EC, and CAS (LO1212, CZ.1.05/2.1.00/01.0017, RVO:68081731).

Disclosures. The authors declare no conflicts of interest.

Data availability. Data underlying the results presented in this paper are not publicly available at the time of publication but may be obtained from the authors upon reasonable request.

REFERENCES

1. H. Sasada and K. Yamada, Appl. Opt. **29**, 3535 (1990).
2. W. C. Swann and S. L. Gilbert, J. Opt. Soc. Am. B **22**, 1749 (2005).
3. C. Edwards, H. Margolis, G. Barwood, S. Lea, P. Gill, and W. Rowley, Appl. Phys. B **80**, 977 (2005).
4. S. R. Sternberg, Computer **16**, 22 (1983).
5. J. Dale, B. Hughes, A. J. Lancaster, A. J. Lewis, A. J. H. Reichold, and M. S. Warden, Opt. Express **22**, 24869 (2014).
6. B. Hughes, M. A. Campbell, A. J. Lewis, G. M. Lazzarini, and N. Kay, Videometrics, Range Imaging, and Applications XIV **10332**, 1033202 (2017).
7. R. Li, K. Gibble, and K. Szymaniec, Metrologia **48**, 283 (2011).
8. A. D. Ludlow, M. M. Boyd, J. Ye, E. Peik, and P. O. Schmidt, Rev. Mod. Phys. **87**, 637 (2015).
9. T. Fortier and E. Baumann, Commun. Phys. **2**, 153 (2019).
10. M. D. Labachelerie, K. Nakagawa, Y. Awaji, and M. Ohtsu, Opt. Lett. **20**, 572 (1995).
11. Y. Awaji, K. Nakagawa, M. de Labachelerie, M. Ohtsu, and H. Sasada, Opt. Lett. **20**, 2024 (1995).
12. J. Henningsen, J. Hald, and J. C. Peterson, Opt. Express **13**, 10475 (2005).
13. M. Čížek, L. Pravdová, T. Minh Pham, A. Lešundák, J. Hrabina, J. Lazar, T. Pronebner, E. Aeikens, J. Premper, O. Havliš, R. Velc, V. Smotlacha, L. Altmannová, T. Schumm, J. Vojtěch, A. Niessner, and O. Číp, Opt. Express **30**, 5450 (2022).
14. P. Pánek and A. Kuna, in *Proceedings of the 44th Annual Precise Time and Time Interval Systems and Applications Meeting*, (2012), pp. 301–310.
15. O. Číp, A. Lešundák, T. M. Pham, V. Hucl, M. Čížek, J. Hrabina, Š. Řeřucha, J. Lazar, P. Obšil, R. Filip, and L. Slodička, in *2018 European Frequency and Time Forum, EFTF 2018* pp. 392–394 (2018).
16. F. Riehle, P. Gill, F. Arias, and L. Robertsson, Metrologia **55**, 188 (2018).
17. R. Schödel, A. Yacoot, and A. Lewis, Metrologia **58**, 052002 (2021).